STUDY OF THERMAL PERFORMANCE AND PROPERTIES OF 1-PYRENE CARBOXYLIC-ACID FUNCTIONALIZED GRAPHENE NANOFLUIDS IN A HEAT PIPE

ALIREZA ESMAEILZADEH

FACULTY OF ENGINEERING
UNIVERSITY OF MALAYA
KUALA LUMPUR

2022

STUDY OF THERMAL PERFORMANCE AND PROPERTIES OF 1-PYRENE CARBOXYLIC-ACID FUNCTIONALIZED GRAPHENE NANOFLUIDS IN A HEAT PIPE

ALIREZA ESMAEILZADEH

THESIS SUBMITTED IN FULFILMENT OF THE REQUIREMENTS FOR THE DEGREE OF DOCTOR OF PHILOSOPHY

FACULTY OF ENGINEERING UNIVERSITY OF MALAYA KUALA LUMPUR

2022

UNIVERSITY OF MALAYA

ORIGINAL LITERARY WORK DECLARATION

Name of Candidate: ALIREZA ESMAEILZADEH

Matric No: 17013139

Name of Degree: Doctor of Philosophy

Title of Thesis ("this Work"): STUDY OF THERMAL PERFORMANCE AND PROPERTIES OF 1-PYRENE CARBOXYLIC-ACID FUNCTIONALIZED GRAPHENE NANOFLUIDS IN A HEAT PIPE.

Field of Study: Mechanics and Metal Work

 I do solemnly and sincerely declare that:

(1)   I am the sole author/writer of this Work;

(2)   This Work is original;

(3)   Any use of any work in which copyright exists was done by way of fair dealing and for permitted purposes, and any excerpt or extract from, or reference to or reproduction of any copyright work has been disclosed expressly and sufficiently and the title of the Work and its authorship have been acknowledged in this Work;

(4)   I do not have any actual knowledge, nor do I ought reasonably to know that the making of this work constitutes an infringement of any copyright work;

(5)   I hereby assign all and every rights in the copyright to this Work to the University of Malaya ("UM"), who henceforth shall be owner of the copyright in this Work and that any reproduction or use in any form or by any means whatsoever is prohibited without the written consent of UM having been first had and obtained;

(6)   I am fully aware that if, in the course of making this Work, I have infringed any copyright, whether intentionally or otherwise, I may be subject to legal action or any other action as may be determined by UM.

  Candidate's Signature   Date:

Subscribed and solemnly declared before,

  Witness's Signature   Date:

Name:

Designation:

STUDY OF THERMAL PERFORMANCE AND PROPERTIES OF 1-PYRENE CARBOXYLIC-ACID FUNCTIONALIZED GRAPHENE NANOFLUIDS IN A HEAT PIPE

ABSTRACT

A new trend in the heat pipes and successful thermosyphons application is related to nanotechnologies. Nano liquids, nanocoating, and nanocomposites invention open a new niche in the heat pipe and thermosyphon design and use. This research is carried out experimentally and analytically to investigate the thermal performance of heat pipe when functionalized graphene nanoplatelets (GNP) with 1-pyrene carboxylic acid (PCA) is utilized as a working fluid.

In this study's first stage, three influential parameters on the viscosity and thermal conductivity, including concentration, temperature, and specific surface area of nanofluid, were investigated. In the second stage, an experimental investigation was accomplished to study a sintered wick heat pipe's thermal performance using stable aqueous dispersions of noncovalently functionalized graphene nanofluids. The experiments are conducted to characterize a low-cost nanofluid and evaluate its effect on the sintered-wick heat pipe efficiency. The various parameters being investigated include different fluids, tilt angles of the heat pipe, and input powers. The result shows the enhancement of thermal conductivity of PCA-functionalized graphene nanofluids in the range of 21% and 40%. It is found that the tilt angle of heat pipe has a substantial impact on the thermal properties, which could enhance the thermal performance by 79%. The experimental results indicated that the heat pipe thermal resistance is reduced using PCA-functionalized graphene nanofluids. The reduction in thermal resistance was the best at the high heat flux.

The last stage focused on the CFD modeling of nanofluid heat transfer in the heat pipe. Numerical modeling of a heat pipe included with a phase change heat transfer was

developed to assess the effects of three parameters of nanofluid, heat pipe inclination angles, and input heating power. Distilled water (DW) and 1-pyrene carboxylic-acid (PCA)-functionalized graphene nanofluid (with concentrations of 0.06 wt%) were used as working fluids in the heat pipe. A computational fluid dynamic (CFD) model was developed to evaluate the heat transfer and two-phase flow through the heat pipe's steady-state process. It was found that inclination significantly affects the heat transfer of the heat pipe. The maximum increment of thermal performance in the heat pipe peaked at 49.4% by using the amount of 0.06 wt% of PCA-functionalized graphene as working fluids. The result associated with this comparison indicates that the highest deviation is less than 6%, consequently confirming that the CFD model was successful in reproducing the heat and mass transfer processes in the DW and nanofluids charged heat pipe. The results of the CFD simulation have good agreement between predicted temperature profiles and experimental data.

Keywords: Heat pipe, Graphene, Nanofluid, Thermal resistance, Simulation.

KAJIAN PRESTASI TERMA DAN SIFAT-SIFAT 1-PIREN CARBOXYLIC-ACID FUNGSIONAL GRAFEN CECAIR NANO DALAM PAIP HABA

ABSTRAK

Trend baru dalam penggunaan paip haba dan termosifon yang berkesan adalah berkaitan dengan nanoteknologi. Penciptaan cecair nano, nanocoatings, dan nanocomposites membuka bidang tertumpu yang baru dalam reka bentuk dan penggunaan paip haba dan termosifon. Penyelidikan yang dilakukan secara eksperimental dan analitik adalah untuk mengkaji prestasi terma paip haba apabila nanoplatelet graphene (GNP) yang bereaksi dengan asid karboksilik 1-piren (PCA) dimanfaatkan sebagai cecair kerja.

Pada peringkat pertama kajian ini, tiga parameter berpengaruh pada kelikatan dan kekonduksian terma termasuk kepekatan, suhu, dan luas permukaan nanofluid telah diselidiki. Tahap kedua, penyelidikan eksperimental telah dilakukan untuk memeriksa terma, prestasi paip haba sumbu yang disinter menggunakan penyebaran berair stabil dari cecair nano yang berfungsi secara kovalen. Eksperimen yang dijalankan adalah untuk mencirikan nanofluid kos rendah dan untuk menilai kesannya terhadap kecekapan paip haba sintered-wick. Pelbagai parameter telah disiasat yang merangkumi cecair yang berbeza, sudut kecondongan paip haba, dan daya input. Hasil dari penyiasatan itu menunjukkan peningkatan kekonduksian terma nano cairan graphene yang berfungsi PCA dalam julat 21% dan 40%. Didapati juga bahawa sudut kemiringan paip haba mempunyai kesan besar terhadap sifat terma, yang dapat meningkatkan prestasi terma sebanyak 79%. Hasil eksperimen menunjukkan bahawa rintangan haba paip haba dapat dikurangkan dengan menggunakan graphene nano cairan. Pengurangan rintangan haba adalah berkesan pada arus panas yang tinggi.

Pemodelan CFD pemindahan haba nano cairan di paip haba telah difokuskan pada peringkat akhir. Pemodelan berangka dari paip haba yang disertakan dengan pemindahan

haba perubahan fasa telah dihasilkan untuk menilai kesan tiga parameter cecair nano, sudut kecenderungan paip panas, dan daya pemanasan input. Air suling (DW) dan 1-pyrene carboxylic-acid (PCA) -fungsian graphene nanofluid (dengan kepekatan 0,06 wt%) digunakan sebagai cecair kerja pada paip haba. Model dinamik cecair komputasi (CFD) telah dihasilkan untuk menilai pemindahan haba dan aliran dua fasa melalui proses keadaan stabil paip haba. Didapati bahawa kecenderungan secara signifikan mempengaruhi pemindahan haba paip haba. Peningkatan prestasi termal secara maksimum dalam paip haba telah mencapai 49.4% apabila menggunakan 0.06% berat graphene fungsian PCA sebagai cecair kerja. Hasil yang berkaitan dengan perbandingan ini menunjukkan bahawa sisihan tertinggi adalah kurang dari 6%, dan mengesahkan bahawa model CFD berjaya menghasilkan semula proses pemindahan haba dan jisim di paip haba bermuatan DW dan nanofluid. Hasil simulasi CFD menunjukkan bahawa persetujuan yang baik antara profil suhu yang diramalkan dan data eksperimen.

Kata kunci: Paip haba, Grafen, nano cairan, Rintangan haba, Simulasi.

ACKNOWLEDGEMENTS

I would like to thank my supervisor, PROFESOR MADYA IR. DR. NIK NAZRI BIN NIK GHAZALI, for giving me the opportunity of working with his research team and creating a calm research environment. If I did not have his constant companion and excellent tolerance for the entire duration of the research period, without a doubt, I could not complete my Ph.D. program. Apart from the scientific points, I learned that to succeed in other aspects of life; I should also have unremitting efforts while being patient.

I must also thank my second and third supervisors, Dr. HENDRIK SIMON CORNELIS METSELAAR and DR. AZUDDIN BIN MAMAT, for their unlimited supports. They always were supportive and attempted to push me forward to do the higher quality of the works.

Also, heartfelt thanks are extended to my best colleague and friend, SOUDEH IRANMANESH, not only for his continued support and encouragement but also for all valuable discussions, suggestions, and help during my study.

Finally, I would like to thank the University of Malaya for financial support.

TABLE OF CONTENTS

LIST OF FIGURES

LIST OF TABLES

LIST OF SYMBOLS AND ABBREVIATIONS

Symbol

A	:	area [m^2]
c	:	total mole density [kmol/m^3]
C	:	Minimum aspect ratio
C$_{p,w}$	:	specific heat J/(kg· K)
D	:	diameter [m]: diffusion coefficient [m^2/s]
F	:	friction factor
g	:	gravitational acceleration [m/s^2]
h	:	heat transfer coefficient [W/m^2]
H	:	height [m]
h_e	:	Heat transfer coefficient (W. m^2.^{o}C^{-1})
I	:	Electrical current (A)
L	:	length [m]
k	:	thermal conductivity [W/m·K]
K	:	permeability [m^2]
ṁ	:	mass flow (kg/s)
P	:	pressure [Pa]
Q	:	Heat input power (W)
Q$_C$	:	Heat rejected at condenser (W)
R	:	Thermal resistance (^{o}C/W)
q	:	heat transfer rate [W]
t	:	thickness [m]
T	:	temperature [K]
T_e	:	Average temperature of the evaporator (^{o}C)

T_c	:	Average temperature of the condenser ($^\circ$C)
V	:	Voltage (v)
α	:	Tilted incidence
ε	:	Porosity
ρ	:	Appropriate transmittance-absorptance
$(\tau\alpha)$	:	Mass flow rate, kg/s
Φ	:	Latitude
η	:	Thermal efficiency (%)
θ	:	contact angle [rad]
μ	:	dynamic viscosity [Pa·s]

Abbreviations

Al_2O_3	:	Aluminum Dioxide
CNT	:	Carbon Nanotube
CuO	:	Copper Oxide
C.V	:	Coefficient of variation
CFD	:	Computational fluid dynamic
D	:	Diameter of the pipe
DW	:	Distilled water
DI	:	Deionized
EG	:	Ethylene Glycol
GNP	:	Graphene nanoplatelets
GO	:	Graphene Oxide
HTC	:	Heat transfer coefficient
NDG	:	Nitrogen-dropped graphene
Nu	:	Nusselt number

PDR	:	Parabolic dish reflector
PCA	:	1-pyrene carboxylic acid
PTC	:	Parabolic trough collector
PCA	:	1-pyrene carboxylic acid
Re	:	Reynolds number
SA	:	Surface area
TiO_2	:	Titanium Oxide

LIST OF APPENDICES

CHAPTER 1: INTRODUCTION

1.1   Background

Heat pipes are highly effective passive devices with effective thermal conductivity and the capability to transport a large amount of heat over considerable distances. Owing to the simplicity of design and ease of manufacture and maintenance, these devices have found applications in many areas, including solar energy systems, heat recovery systems, air conditioning systems, cooling of energy storage and electronic equipment, industrial applications, and space apparatus. Heat pipes can be designed and constructed with various cross-sectional areas and geometries ranging from 0.6 mm × 0.6 mm and 25 mm in length to 2 mm in diameter and 1 m in length or even 100 m in length. All heat pipes have an evaporator and condenser section where the working fluid evaporates and condenses, respectively. Many heat pipes also have a transport or adiabatic section, which separates the evaporator and condenser sections by an appropriate distance, intended to satisfy the heat pipe limitations and the application's design constraints. A given heat pipe may have multiple evaporators, condensers, and adiabatic sections. A working fluid usually circulates due to the influence of capillary forces in a wick. However, gravitational, centrifugal, electrostatic, and osmotic forces can also return the liquid from the condenser to the evaporator. Many novel heat pipes have been developed over recent years. These heat pipes have optimized geometries to suit specific applications, improved heat flux rate, heat transfer efficiencies, new wick structures, and working fluids. Mathematical approaches, including CFD, optimization design, and modeling, have improved the new heat pipes.

1.2   Significant of study

Heat transfer fluids such as water, ethylene glycol, Freon, and mineral oil play an important role in industrial processes such as power generation, heating, cooling processes, chemical productions, transportations, and microelectronics (Mangal, Lamba, Gupta, & Jhamb, 2010). The primary problem with solar collectors' high compactness and effectiveness is the poor heat transfer characteristics of these working fluids. An improvement in these conventional fluids' thermal conductivity is a crucial idea to improve the heat transfer characteristics(Sadri et al., 2014). Thus, the important initiative is to seek solid particles especially nano-sized particles having thermal conductivity several thousand orders higher than those of conventional fluids (Mehrali et al., 2014).

The heat pipe is a passive heat transfer device that can dissipate large amounts of heat through evaporation and a working fluid's condensation. The heat pipe components are a sealed container, a wick structure attached to the container's inner surface, and a small amount of working fluid, which is in equilibrium with its own vapor Figure 1-1.
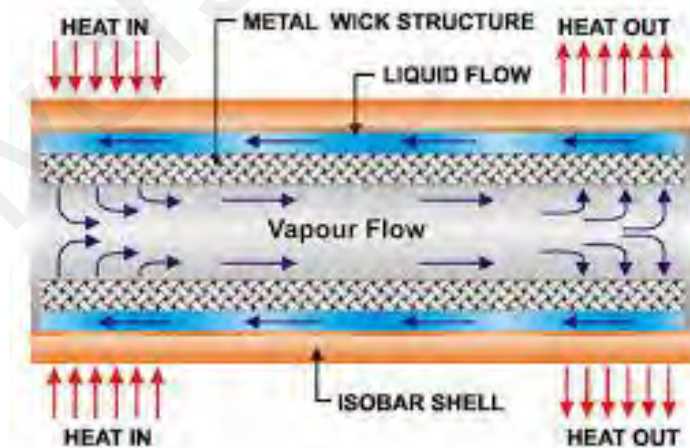
Figure 1-1: Schematic of a conventional heat pipe (Faghri, 2014).

The applied heat to the evaporator vaporizes the working fluid. The vapor is driven to the condenser by the generated pressure difference, where it releases its heat and changes its phase to liquid. The liquid is turned back to the evaporator zone by the capillary force of the wick. Since the latent heat of vaporization is usually enormous, heat pipes can efficiently transport a considerable amount of heat over a long distance with a relatively small temperature drop. While most heat pipes have cylindrical or flat shapes, they can be manufactured in various configurations for specific applications.

The effect of application of nanofluid on the efficiency of HP is examined in the current study. The HP with a sintered wick structure filled by PCA-functionalized graphene nanofluid is considered. The graphene nanofluid is functionalized with 1-Pyrene Carboxylic-Acid. Various thermocouples were applied to measure the thermo-physical attributes of the working fluids. Several parameters such as temperature distribution, thermal resistance, thermal efficiency, and overall heat transfer coefficient of the HP are examined under different tilt angles and input heat powers.

There are many CFD models to predict nanofluid heat transfer during the forced convection regime. However, it is still unclear which models can predict the nanofluid heat transfer precisely. Few numerical studies model nanofluids' heat transfer during subcooled flow boiling and conflicting results are found in the literature about boiling heat transfer enhancements or nanofluids' deterioration(Hai Wang, Qu, Sun, Kang, & Han, 2020). In this study, a CFD modeling for the operation of a sinter wick heat pipe has been used to study in detail the phenomena of heat transfer and two-phase flow.

1.3   Objectives

The main objectives of this research can be summarized as follows:

1- To develop a nanofluid with optimum thermophysical properties and new physical mechanism for thermal conductivity enhancement.

2- To analyze a cylindrical heat pipe's thermal performance with copper-sintered wick working at a different angle using Computational Fluid Dynamics (CFD) simulation.

3- To investigate the thermal efficiency enhancement of the heat pipe at different condition by using noncovalent functionalized graphene with 1-Pyrene Carboxylic Acid (PCA).

1.4   The layout of the thesis

The thesis is divided into five chapters, and the summary of each chapter is listed below:

Chapter 1 expresses the importance of the research and highlights the novelty of the current work. It also includes the problem statement and research objectives.

Chapter 2 provides an overview of heat pipe operation fundamentals. It also presents a comprehensive literature review, including numerical and theoretical heat pipe analysis and experimental studies.

Chapter 3 introduces the numerical methodology developed in this research to describe the thermal-hydrodynamic phenomena happening inside the heat pipe network. The governing equations along with boundary conditions are described, and the developed numerical procedure is delineated. Also, it presents the experimental technique used in the current work. First, it describes the general procedure for heat pipe preparation and then the procedures utilized in this research to prepare the heat pipe. Then it illustrates the experimental setup and its components.

Chapter 4 presents the results obtained from both numerical and experimental studies. First, the numerical results obtained from the steady-state simulation of the primary heat pipes are described. The effects of heat input and the radius of the primary adiabatic section on velocity, pressure, and temperature profiles are shown. Second, the experimental results are displayed, and the comparison is conducted between the numerical and experimental results.

Chapter 5 contains the interpretation of the results. The findings of the research compared with those of previous studies presented in the literature review.

Chapter 6 outlines the findings of the current work and the conclusions of the results obtained from numerical analyses and experiments

CHAPTER 2: LITERATURE REVIEW

2.1 Heat pipe overview

Some more specific heat pipe fundamentals are introduced to prepare the reader for the following chapters. Current trends and approaches to improving phase change devices' performance are summarized to give insight into advanced working fluids' potential. A brief history of the working fluids studied in this work is discussed, and the overall goals of the dissertation are outlined.

Heat pipes are one of the most effective passive heat transfer technologies (Lohrasbi, Gorji-Bandpy, & Ganji, 2017). A heat pipe transports heat by phase change of the working fluid and has a high effective thermal conductivity (several thousand times higher than copper rod (El-Nasr & El-Haggar, 1996), and an extremely low effective thermal resistance (0.05–0.4 °C/W) (Weng, Cho, Chang, & Chen, 2011). The thermo-physical properties of the working fluids significantly affect heat transfer performance of heat pipes especially in the evaporator (Gupta et al., 2018). Several conventional working fluids have shown poor heat transfer characteristics, owing to their lower thermal conductivity. Therefore, an innovative working fluid is needed to enhance the transfer performance of the heat pipes (Mousavi Ajarostaghi, Shirzad, Rashidi, & Li, 2020).

2.1.1 Principle of heat pipes

Heat pipes are one of the most efficient heat transfer devices, which move heat or thermal energy from one point to another. The operation of a heat pipe can be explained based on Figure 2-1. As shown in this figure, a heat pipe is composed of a container, which its inner wall is covered with a wick material. The heat pipe container is first evacuated and then charged with the appropriate working fluid and sealed. The wick is saturated with the working fluid's liquid phase, and the remaining volume of the chamber includes vapor. The major sections of a heat pipe are the evaporator and condenser in

contact with the heat source and the heat sinks. A heat pipe can be with or without an adiabatic section.

The received energy at the evaporator is conducted through the wall and wick structure to the liquid. Part of the liquid will be vaporized, and the vapor travels along the heat pipe to the condenser. The vapor condenses and releases its heat to the heat sink at the condenser and changes its phase to liquid. The capillary pressure of the wick structure returns the resulted liquid to the evaporator. The heat pipe continues to work as long as there is enough liquid in the wick at the evaporator section (Faghri, 1995).
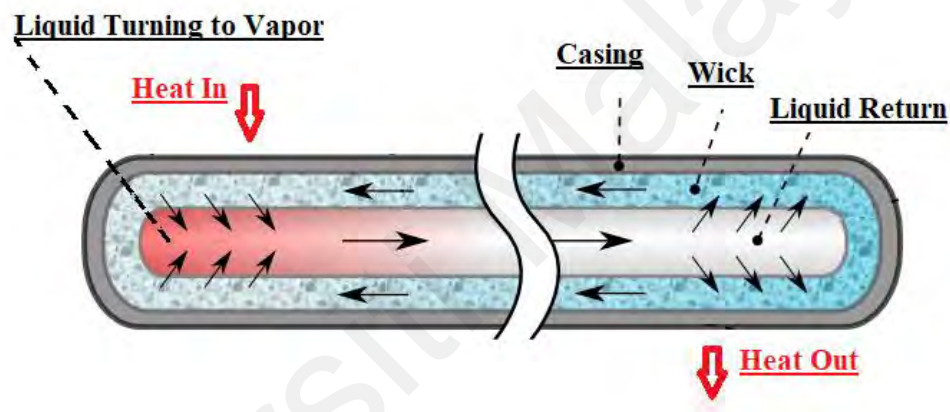
Figure 2-1: Components and principal operation of a cylindrical heat pipe.

2.1.2 Heat Transfer Limitations

During a heat pipe operation, several physical phenomena can be encountered, limiting the heat pipes' performance. These limitations can be classified as below:

Viscous limit: This limitation occurs in long heat pipes and at low operating temperatures where the inertial forces cannot dominate the losses due to the friction (Zohuri, 2011).

Sonic limit: The sonic limit happens when the vapor leaving the adiabatic section reaches sonic velocity and chokes (Zohuri, 2011).

7

Capillary limit: The capillary limit occurs when the wick structure cannot provide the required capillary pressure to circulate the liquid flow in the wick (Faghri, 1995).

Entrainment limit: High velocities of the vapor generate high interfacial shear force, which causes the droplets of liquid to be torn from the wick surface and be entrained into the vapor flowing toward the condenser section. If the entrainment becomes too great, the evaporator will dry out (Faghri, 2014).

Boiling limit: This limitation occurs in cases with high radial heat fluxes at the evaporator section when the liquid in the evaporator wick boils, and the wall temperature becomes too high. The formed vapor bubbles in the wick prevent the liquid from wetting the pipe wall and causes dry out at the evaporator in severe conditions (Faghri, 2014).

2.1.3   Wick structure

The wick structure is implemented to return the resulted liquid at the condenser back to the evaporator by providing the required capillary pressure. Tiny pores are needed at the liquid-vapor interface to provide high capillary pressure, while a large pore facilitates the wick's liquid flow (Zohuri, 2011). Various wick structures have been developed, as can be seen in Table 2-1.

Table 2-1: Typical wick design

WICK TYPE	CAPILLARY PUMPING	THERMAL CONDUCTIVITY	PERMEABILITY
Wrapped Screen	High	High	low-average
Sintered Metal	High	Average	low-average
Axial Grooves	low	High	Average-High
Open Artery	low	High	High

Three wick structure features should be taken into consideration in designing heat pipe:

Minimum capillary radius: This property is related to the pore size, and it should be small if high capillary pressures are needed.

Permeability: It is the wick resistance to the axial flow.

Effective thermal conductivity: Higher thermal conductivity leads to smaller temperature drops and the wick desired in heat pipes (Faghri, 1995).

Some wick structures are more efficient than others, while some have limitations concerning orientation and gravity.

9

The most common types of wicks that are used are as follows:

Sintered powder. Wick is made up of sintered metal powder (Figure 2-2). This process provides high power handling, low-temperature gradients, and high capillary forces for anti-gravity applications. This type of structure allows achieving very tight curves.

Figure 2-2: Sintered powder heat pipe (courtesy of Thermal core)

Screen mesh. Wick is composed of a multi-layered metal mesh (Figure 2-3). This type of wick is used in most products (e.g., CPU heat sinks) and provides readily variable characteristics in power transport and orientation sensitivity, according to the number of layers and mesh counts used.

Figure 2-3: Screen mesh heat pipe.

Grooved tube. Wick is composed of channels flowing axially on the internal wall of the pipe (Figure 2-4). The axial grooves' small capillary driving force is adequate for low power heat pipes when operated horizontally or with gravity assistance. The tube can also be bent. When used in conjunction with screen mesh, the performance can be considerably enhanced.
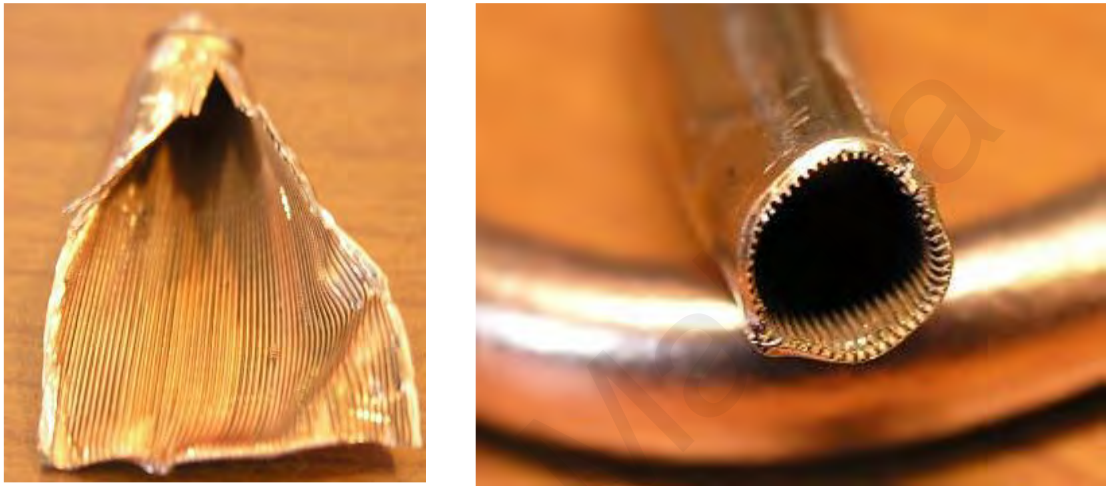
Figure 2-4: Grooved heat pipe.

2.1.4   Thin Film Evaporation

The efficiency seen in phase change heat transfer devices results from the immense heat transfer coefficients seen in thin-film evaporation, an area of research popularized (Mahdavi, 2016). The phase change at the interface does not require a significant superheat standard in nucleate pool boiling regimes described in Carey (Sharifi, Bergman, Allen, & Faghri, 2014), especially under a vacuum present in a heat pipe. However, small liquid menisci must form in the pores of heat pipe wicks where evaporation occurs. Schonberg, DasGupta, and Wayner Jr (1995) and other researchers such as Bankston and Smith (1973) determined that the extended meniscus can be separated into three regions based on the interfacial forces fluid flow shown in Figure 2-5.
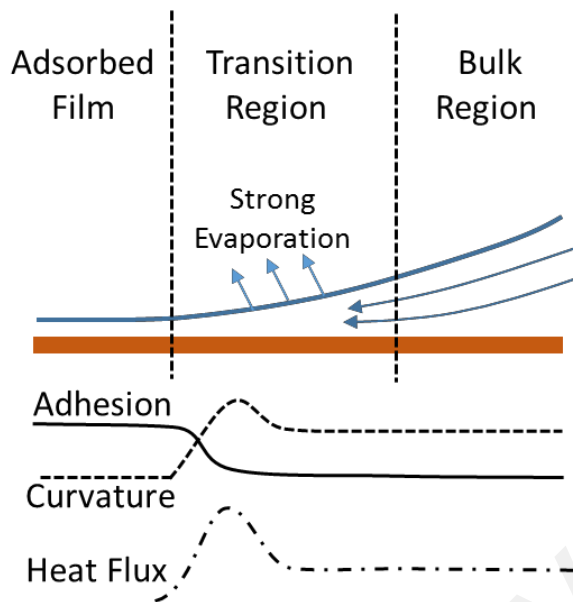
Figure 2-5: Schematic of a wetting meniscus.

The adsorbed film is a non-evaporating region where a liquid is adsorbed on the wall due to strong intermolecular forces between the solid wall and liquid molecules. In the transition region or evaporating thin-film region, the intermolecular forces are much lower. The liquid/vapor interface has a curvature that drives flow into the region. In the bulk region or intrinsic region, the intermolecular forces are negligible, and the curvature of the interface becomes constant.

Significant heat transfer coefficients are realized in the interline region due to decreased intermolecular forces and a small conductive resistance through the thin film. The transition/interline region exists over a minimal length (<1μm), but heat transfer coefficients remain high as long as the film is thin. Hao Wang, Garimella, and Murthy (2007) model thin film evaporation in a microchannel with radii ranging from 2.5 μm to 210μm. They demonstrated that a thin film (<1μm in thickness) contributes over 50% of the entire meniscus's heat transfer for the 210 μm radius channel and 97% for the 2.5 μm channel. Stephan and Busse (1992) calculated the heat transfer in a 1 mm wide trapezoidal groove by solving the conduction equation in the walls and bulk liquid. The micro-region

was found to contribute 45% to the total heat transfer. (Cheng, Dong, Thompson, & Ma, 2012) used the Galerkin method to solve conduction in a rectangular microgroove in combination with thin-film evaporation. The contribution of the thin film was investigated as a function of contact angle and superheat. For a maximum film thickness of 2 µm and a 0° contact angle, the thin film contributed over 90% of the heat transfer. The percentage dropped to 78% for a 60° contact angle. This film evaporation is an important design aspect for enhancing the evaporation efficiency in phase-change devices.

2.2   Working fluid

Nanofluids are another type of heat transfer fluid that is created by suspending nanoparticles in typical working fluids. Nanoparticle materials are typically chemically stable metals such as copper, gold, silver, and metal oxides. Numerous nanofluid studies have demonstrated the enchantments of Critical Heat Flux (CHF) in pool boiling (Wu & Zhao, 2013). These fluids were original of interest for two-phase heat transfer due to their increases, though modest, in thermal conductivity and other changes in thermophysical properties. However, many studies concluded that surface modification from nanoparticles' deposition created a much more significant enhancement through increased surface wetting and capillarity (Ahn & Kim, 2012). They concluded that significant CHF enhancement of nanofluids during pool boiling resulted from increased surface wettability and improved capillarity resulting from nanoparticles' surface deposition. The CHF of a nanofluid is enhanced by its improved ability to wet the heater surface actively, thanks to the thin nanoparticle layers (H. D. Kim & Kim, 2007).

Nanofluid, a colloidal mixture of conductive nanoparticles in the base fluid, shows higher thermal conductivity than conventional coolant and has a wide application prospect (Ajarostaghi, Zaboli, & Nourbakhsh, 2021; Ramezanizadeh, Alhuyi Nazari,

Ahmadi, & Chau, 2019). Nanofluids have also been shown to increase thermal performance in heat pipes and capillary grooves (Sureshkumar, Mohideen, & Nethaji, 2013). Liu, Li, and Bao (2010) tested CuO nanofluids' performance in inclined grooved heat pipe and achieved a 60-80% decrease in thermal resistance and doubled the dry-out power. Solomon, Ramachandran, and Pillai (2012) studied nanoparticle-coated screen wicks to delineate the effect of changes in thermophysical properties and the surface coating. A clean screen wick and a nanofluid performed the same as a screen wick coated in nanoparticles and tested in a heat pipe with DI water. Both out-performed water in thermal resistance by 40%. They concluded that all the performance enhancement was due to the wick deposition and that changes in fluid properties were negligible.

Stability is the major difficulty to nanofluid practical application. Akbari and Saidi (2019) revealed that the more stable nanofluid achieves better thermal performance, while the less stable nanofluid provides a worse thermal performance than water. Different approaches to prepare more stabilized nanofluids were used by researchers. For this purpose, stability enhancement methods and stability evaluation methods are commonly followed. In several stability improvement approaches, techniques like changing PH values, surfactant addition and ultrasonication are used. Considering nanofluids applied into heat pipes, researchers used these techniques to improve the stability of nanofluids. In various stability evaluation approaches, techniques like spectral absorbance analysis, Zeta potential, centrifugation and sedimentation method are used to evaluate the stability of nanofluids. Besides, some characterization methods like TEM, SEM and XRD are used to identify the morphology of nanoparticles.

Thermo-physical properties (especially thermal conductivity and viscosity) affect heat transfer and flow behaviour. The main parameters influencing the nanofluid properties such as particle structure, shape, size, fluid type, temperature, surfactant and

PH value etc., have been widely investigated (Yousefi, Shojaeizadeh, Veysi, & Zinadini, 2012). Besides, the preparation of a stable suspension of nanofluid is para- mount before implementing it in the application, as better stability will improve the efficiency of heat transfer equipment and reduce the size and fabrication cost of the equipment. Several results have been re- ported on various types of combinations of base fluids and nanoparticles. Figure 2-6 presents the common nanoparticles and base fluids. The conventional nanofluids either have a good rheological property or a better thermal network. Recently, hybrid nanofluid, a homogeneous mixture of two or more nanoparticles type, has gained significant attention from researchers because of its encouraging improvement in thermo-physical, thermal transfer and hydrodynamic properties (Gorji & Ranjbar, 2017; Gürbüz, Sözen, Variyenli, Khanlari, & Tuncer, 2020).
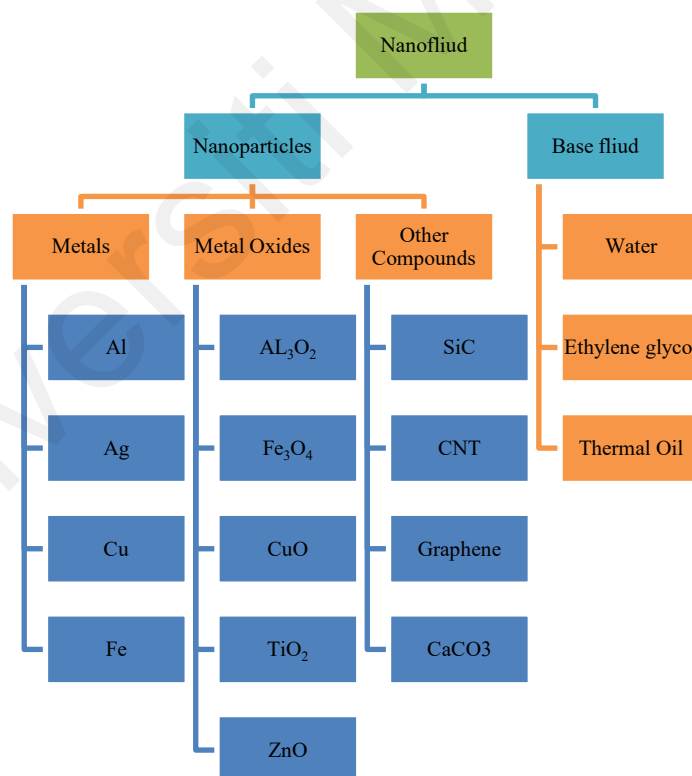
Figure 2-6: Common nanofluid and base fluid.

The application of nanofluids in heat pipes can be one of the most interesting techniques for heat transfer enhancement (M. Kaya et al., 2019; Liu & Li, 2012). A plethora of studies have reported that the nanofluids can improve the boiling thermal

transfer due to the modification of heated surface characteristics (e.g., size of cavities, surface wettability and roughness) by the nanoparticles depositing on the wall, as well as the changes of thermo-physical properties of the nanofluids (e.g., thermal conductivity and capillary force) (Duangthongsuk, Yiamsawasd, Selim Dalkilic, & Wongwises, 2013; Quan, Wang, & Cheng, 2017). Meanwhile, many attempts have been made to combine the advantages of nanofluids and heat pipes to obtain a higher heat transfer coefficient (Moradgholi, Nowee, & Farzaneh, 2018). However, the micro factors in nanofluids such as instant clustering, particle charge condition and micro motion, contribute to the complicated thermo-physical properties of nanofluids and complex heat transfer mechanisms for heat pipes (Kiseev & Sazhin, 2019). These problems lead to difficulties in obtaining accurate value and variation law, which should be determined by pre-experiments before designing the heat pipes with nanofluids, thus seriously limiting the development of nanofluids in heat pipes.

Heat pipes can be built and manufactured in various shapes based on their applications. Each application has a temperature range that the heat pipe needs to work in, and it should be included in the heat pipe design. The desired temperature range can be obtained by selecting the appropriate working fluid. Figure 2-7 shows some commonly used working fluids. The operating temperature is classified into Cryogenic, low, medium, and high temperatures (Mahdavi, 2016).
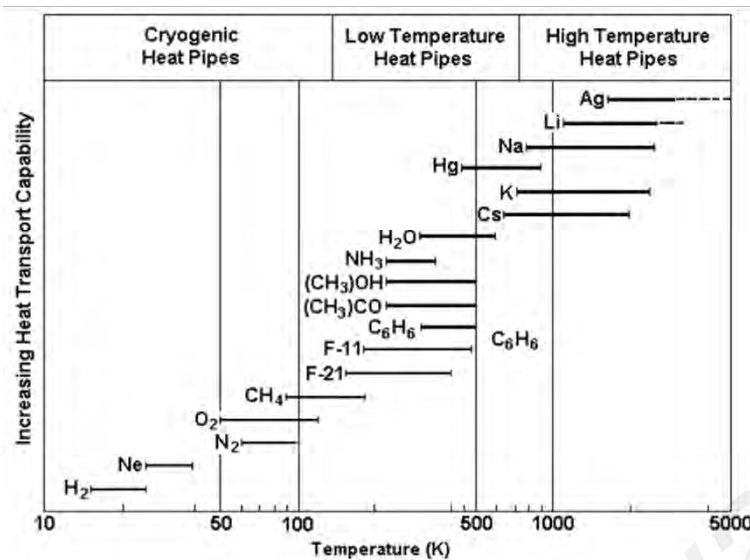
Figure 2-7: Approximate range of working fluids' applicability in the various temperature regimes (Mahdavi, 2016).

To ensure the long-life heat pipes operation, the working fluid should be compatible with the wick and container material. Table 2-2 presents the compatibility test of commonly used working fluids (Sharifi et al., 2014).

Table 2-2: Working fluid and container compatibility data (Sharifi et al., 2014).

Working Fluid	Compatible Material	Incompatible Material
Water	Stainless Steel, Copper, Silica	Aluminum, Inconel
Ammonia	Aluminum, Stainless Steel, Cold	
Methanol	Stainless Steel, Iron, Copper,	Aluminum
Sodium	Stainless Steel, Nickel, Inconel,	Titanium

2.3 Numerical and analytical heat pipe simulations

Several analytical and numerical simulations have been developed with various degrees of complexity to understanding the thermal and hydrodynamic behavior of heat pipes. Initially, the studies were focused on modeling the steady-state vapor and fluid flow dynamics in heat pipes. The steady-state laminar incompressible flow was assumed

in the investigation of different heat pipe configurations such as flat (Ooijen & Hoogendoorn, 1979), cylindrical (Bankston & Smith, 1973), the annulus (Faghri & Parvani, 1988), and disk-shaped heat pipes (Vafal, Zhu, & Wang, 1995).

Layeghi and Nouri-Borujerdi (2004) investigated the steady-state behavior of an incompressible vapor flow in a concentric annular heat pipe at both low and moderate Reynolds numbers. The evaporation and condensation were modeled as uniform flow injection and suction. They showed that several small and large recirculation zones are created at both ends of the evaporator and condenser sections by increasing the radial Reynolds number. These zones exert a shear force on returning liquid in the wick, which increases the momentum of returning flow and leads to improved performance of the heat pipe.

Numerical investigations by Do and Jang (2010) for nanofluids in a rectangular grooved heat pipe predicted over 100% improvements in overall heat transfer coefficients though they were never validated. They assumed the nanofluids produced a uniform porous coating over the evaporating section similar to the geometry modeled by J. Wang and Catton (2001) for a groove covered by a porous coating. The performance increases were also attributed to the extended evaporating area. However, a parametric study of the coating thickness revealed that careful design is necessary. The excess thickness and low thermal conductivity of the coating material can potentially cause a reduction in performance.

M.-M. Chen and Faghri (1990) presented a numerical procedure to analyze a cylindrical heat pipe's steady-state performance, including the effects of conjugate heat transfer, compressibility, and viscous dissipation. The wick region was modeled by neglecting the liquid flow inside the wick and considering pure conduction with the porous structure's effective thermal conductivity. Two-dimensional elliptic governing

equations and thermodynamic equilibrium relation for wick-vapor interface were solved for high and low-temperature heat pipes. Their results showed a fair agreement with available experimental data. In another work, Faghri and Chen (1989) performed a similar analysis, studying the effects of the flow reversal phenomenon in the condenser section and utilizing parabolic versus elliptic governing equations on the obtained results. They concluded that both types of equations lead to similar results except for conditions with high radial Reynolds number and the wick's sizeable thermal conductivity. Adopting the same procedure, Faghri, Buchko, and Cao (1991a) studied a high-temperature heat pipe with multiple heat sources. They solved two-dimensional transient mass, momentum, and energy equations in the vapor zone along with the energy equations in the wick and wall regions. The obtained numerical predictions agreed with their experimental results (Faghri, Buchko, & Cao, 1991b).

The finite element method was applied to simulate two-dimensional fluid flow and heat transfer in a cylindrical heat pipe at the steady-state condition. Linear capillary pressure variation in the radial direction was assumed and implemented to couple the liquid and vapor pressure at the interface. The wall and vapor temperature distributions' numerical results showed a good agreement with available experimental data (Thuchayapong, Nakano, Sakulchangsatjatai, & Terdtoon, 2012).

Pooyoo, Kumar, Charoensuk, and Suksangpanomrung (2014) investigated the copper-water cylindrical heat pipe with non-Darcian transport of liquid flow inside the wick and varying mass flow rate of the liquid-vapor interface. The outer wall temperature, centerline velocity magnitude, and thermal performance of the heat pipe were obtained. A numerical technique was developed to predict the effect of heat distribution on the performance of a low-temperature cylindrical heat pipe with multiple heat sources (Park, 1997).

A three-dimensional, finite element-based model is presented to study the performance characteristics of flow in a water-copper heat pipe. They considered laminar incompressible vapor flow with non-uniform heating in the evaporator area. The governing equations were simplified by neglecting the convection terms in the extended form of the Darcy equation in the wick. They also ignored the viscous dissipation and pressure works in the vapor energy equation. The results indicated that the wick material with high thermal conductivity provides a more uniform spread of the applied non-uniform heat (T. Kaya & Goldak, 2007).

Koito, Imura, Mochizuki, Saito, and Torii (2006) formulated a mathematical model to simulate the thermal fluid phenomena in a flat heat pipe made of copper. Water was considered as working fluid. They assessed the capillary pressure needed to circulate the working fluid. Besides, an experimental setup was devised to support the validation of the numerical solution.

Aghvami and Faghri (2011) studied the thermal-fluid behavior of a flat heat pipe with separate heating and cooling configurations analytically. The vapor temperature drop was expressed by using the Clausius-Clapeyron equation. The results showed that reducing the heat source's size could abase the performance of the heat pipe. It was also concluded that the evaporation and condensation are uniform only if the wall material's thermal conductivity is negligible. Shabgard and Faghri (2011) presented an analytical solution to investigate the cylindrical heat pipe's performance with multiple heat sources. They also carried out a parametric study to evaluate the wall's axial heat conduction on the heat pipe performance. It was shown that not considering wall heat conduction could bring about more than a ten percent error in the calculated pressure drop.

Three-dimensional numerical analyses were also performed for the conditions that the heating or cooling is not uniform in the third direction (T. Kaya & Goldak, 2007; Xiao & Faghri, 2008).

The transient operation of heat pipes can be classified into two categories. The first group focuses on the startup process in which the wick is initially in a frozen state, and the heat pipe core is evacuated (Tournier & El-Genk, 2003; Y. Wang & Vafai, 2000). Generally, the heat pipe startup is very complicated and involves vapor transport in free molecular and continuum flow regimes, working fluid as solid, mushy, and liquid and moving interfaces (Alizad, Vafai, & Shafahi, 2012; Y Cao & Faghri, 1993).

In the second group, the transient continuum behavior of heat pipes has been investigated. Continuum transient modeling methods can be divided into two main groups based on calculating the vapor-wick interface's condensation and evaporation rates. In the first technique, the energy balance equation is solved by applying the heat fluxes at the vapor and wick regions to obtain the evaporation mass flow rate. The condensation profile is obtained using outflow boundary conditions at the vapor core exit or with mass suction obtained from the energy-balanced equation (Yiding Cao & Faghri, 1991; Faghri et al., 1991a; Sobhan, Garimella, & Unnikrishnan, 2000). In the second group, the mass flow rate at the wick-vapor interface is calculated by the kinetic theory of gasses. The energy balance and the Clausius-Clapeyron equations are used to determine the saturation temperature at the interface. The system operating pressure was computed by enforcing overall mass balance in the vapor core (Ranjan, Murthy, Garimella, & Vadakkan, 2011; Vadakkan, Garimella, & Murthy, 2004).

Jang, Faghri, and Chang (1989) developed a first-order transient model of the vapor flow in a heat pipe. One-dimensional compressible vapor flow in a porous pipe accounting for laminar and turbulent friction coefficients was employed to simulate heat

pipe operation. Noh and Song studied the transient switching operation of the heat pipes with several heat sources. The governing equations for the water-vapor flow were described using a two-dimensional transient procedure. The wick and wall regions were simulated using the heat conduction equation. The evaporation and condensation rates were obtained from energy-balanced equations. They reported brief time needed to reach a steady-state for heat pipes with different heat source configurations (Noh & Song, 1998). Wang et al. studied the transient operation of a high-temperature heat pipe. The two-dimensional transient conduction model for the heat pipe wall and wick structure was coupled with the one-dimensional quasi-steady model for the vapor flow. The kinetic theory of gasses was implemented to calculate the mass flow rates at the wick-liquid interface (C. Wang et al., 2013).

2.4   Experimental investigations

Experimental studies on heat pipes have been done to investigate various parameters on heat pipes' thermal performance. These studies are classified into different groups studying the heat pipe operating conditions (Senthilkumar, Vaidyanathan, & Sivaraman, 2012), type of the wick structure (Solomon et al., 2012), working fluid type, or the geometry of the heat pipe (J.-S. Chen & Chou, 2015; Seo, Bang, & Lee, 2016).

They suggest using nanofluids as working fluids, which can significantly develop heat pipes' thermal performance (Asirvatham, Nimmagadda, & Wongwises, 2013). Numerous scientists have studied the effects of nanoparticle characteristics and concentrations on heat pipes' thermal performance for several operating conditions and base fluids (Kang, Wei, Tsai, & Huang, 2009). researchers report that the dispersion of nanoparticles in the working fluid seriously rallies the heat pipe's heat transfer capacity and thermal performance (Teng, Hsu, Mo, & Chen, 2010). Furthermore, dry-out conditions are

enhanced by using nanofluids in a heat pipe (Venkatachalapathy, Kumaresan, & Suresh, 2015). Investigations of the various types of nanoparticles (including CuO, Al_2O_3, TiO_2, ZnO, CNT) usable in heat pipes demonstrate that, when the concentration of nanoparticles in the distilled water (DW) increases, the wall temperature of the heat pipe decreases under various heat loads (Sadeghinezhad et al., 2016). According to the researcher, when a nanofluid is used as a working fluid in a heat pipe, the evaporator section's surface temperature is reduced by up to 7 °C (Kumaresan, Venkatachalapathy, Asirvatham, & Wongwises, 2014).

Peyghambarzadeh, Shahpouri, Aslanzadeh, and Rahimnejad (2013) explored the effect of various working fluids on the performance of a heat pipe's dual-diameter. They used water, methanol, and ethanol as working fluid and reported that higher heat transfer coefficients are obtained for water and ethanol compared to methanol. Recently, water based nanofluids have gained interest in heat pipe working fluid instead of conventional working fluid due to their higher thermal conductivity. Many studies have been done exploring the effects of different nanofluids on heat pipe performance (Hajian, Layeghi, & Sani, 2012; Kole & Dey, 2013; Menlik, Sözen, Gürü, & Öztaş, 2015).

It is imperative to select a proper working fluid in the heat pipe of a closed-loop heat exchanger that functions based on phase transition (Shafieian, Khiadani, & Nosrati, 2019). To select a suitable operating fluid, one must pay attention to many parameters that could affect its performance. Nanofluid use has proved to be a high potential option (Naemsai, Kammuang-lue, Terdtoon, & Sakulchangsatjatai, 2019) for this purpose. Homogeneous suspensions of nanoparticles in oil or distilled water form nanofluids, effective in heat exchanging due to their improved thermal transfer due to enhanced thermal conductivity (Hai Wang et al., 2020). In contrast, heat pipes' function relies on a phase change thermal transmission (Chu, Bai, Cui, Nie, & Diao, 2020). Thus, heat pipes'

associated physical mechanism varies from the usual heat exchangers, relying only on one phase. Extensive research has been accomplished to evaluate the nanofluids' thermal efficiency in heat pipes (Bahmanabadi, Faegh, & Shafii, 2020). Heat transfer coefficient, thermal performance, and heat pipe's wall temperature are among the standard functional specifications that the examinations were conducted accordingly. These studies have tried to explore the different nanofluid characteristics (K. M. Kim, Jeong, Kim, & Bang, 2015). Mousa (2011), worked on the heat delivery efficiency of a thermosyphon filled with graphene acetone nanofluid, and it was claimed that the improvement of thermal resistance up to 70.3% could be achieved. This study also noted that the overall heat transfer coefficient rose by 61.25% in the evaporator section. In another study on oscillating heat pipe, with 1% diamond nanofluid, the temperature variation between the evaporator and condenser was found to decrease from 40.9°C to 24.3°C. Fe_2O_3 kerosene nanofluid, as examined by Goodarzi, Rashidi, and Basiriparsa (2012), revealed that a 16% increment in thermal delivery of the heat pipe is achievable. Furthermore, Ghanbarpour, Nikkam, Khodabandeh, Toprak, and Muhammed (2015) found an 11% enhancement in the heat pipe's thermal conductivity with Ag nanofluid. The thermal efficiency of TiO_2 alcohol nanofluid was evaluated by Naphon, Assadamongkol, and Borirak (2008). They established that the heat pipe's thermal performance could improve by 80 % at 0.1% volume. Most recent research about the heat pipe systems shown that proper functioning fluid selection should be taken into account to have good performance and efficiency increment of heat pipes (Sadeghinezhad et al., 2020). It was found that the thermal efficiency of the thermosyphon using the 2% (v) (SiC) nanoparticles was 1.11 times that of pure water, and the maximum efficiency occurs for the 3% (Al2O3) nanoparticle concentration with an input power of 300 W (Hoseinzadeh, Heyns, Chamkha, & Shirkhani, 2019).

Tsai et al. (2004) considered a gold nanofluid and reported thermal resistance assortments between 0.17 and 0.215 °C/W. They also found that the total thermal resistance of heat pipes filled by nanofluids is lower than when the DW is the working fluid. Research has been reported for various types of heat pipes, including grooved, screen meshed, and sintered, to regulate the effect of varying working fluid (Jiang, Tang, Wu, Zhou, & Jiang, 2014; Teng et al., 2010). Kang, Wei, Tsai, and Yang (2006) considered a heat pipe's thermal performance using an Ag nanofluid and indicated that that nanofluid is suitable for cooling devices with high heat fluxes. Ma et al. (2006) investigated a pulsating heat pipe filled with a diamond nanofluid and achieved a thermal resistance of 0.03 °C/W at 336 W input power. Naphon et al. (2008) examined a TiO_2/alcohol nanofluid for a heat pipe and compared it to heat pipes using alcohol and DW as working fluids. Those authors focused on the effects of heat flux, nanofluid concentration, filling ratio (the percentage of the heat pipe volume filled by the working fluid), and tilt angle (inclination angle of heat pipe relative to the horizontal position) on the thermal performance of the heat pipe. They established that the thermal efficiency of the heat pipe was notably enhanced at a 66% filling ratio, a tilt angle of 45° and a nanofluid concentration of 0.1 vol%. Lin, Kang, and Chen (2008) investigated the effects of heating power, nanofluid concentration, filling ratio of the heat pipe and tilt angle on the thermal efficiency of an Ag/water heat pipe. Their research showed that the highest thermal efficiency and temperature difference between the condenser and the evaporator sections occurs at a 60% filling ratio and a 85 W heat input rate, and that the surface temperature is reduced by 7.79 °C and thermal resistance reached 0.092 °C/W com- pared to the case with DW as the working fluid. Table 2-3 summarizes the heat pipe tests reported in the literature.

Table 2-3: Literature's summary of the heat pipe experiments

Researcher	Working fluid	Concentration(vol%)	Heat pipe	Thermal performance improvement (approximate)
Do, Ha, and Jang (2010)	Al_2O_3/water	1, 3	Copper (D: 4 mm)	65%
Kole and Dey (2013)	Cu/water nanofluid	0.0005, 0.005, 0.05, 0.5	Copper (D: 10 mm, L: 300	15%
Septiadi, Putra, Juarsa, Putra, and Sahmura (2013)	TiO_2, Al_2O_3/water nanofluid	1, to 5	Copper (D: 6, 8, 10 mm, L: 200, 300, 400 mm)	24%
P.-Y. Wang, Chen, Liu, and Liu (2012)	CuO/water nanofluid	0.5,1.0,1.5,2.0	Copper (D: 8 mm, L: 350 mm)	40%
Naphon et al. (2008)	Ti/alcohol nanofluid	0.01, 0.05, 0.1, 0.5	Copper (D: 15 mm, L: 600	11%
Kumaresan et al. (2014)	CuO/water nanofluid	0.5, 1.0, 1.5	Copper (D: 12 mm, L: 330	30%
Kang et al. (2009)	Ag/water nanofluid	0.001, 0.01, 0.1	(D: 6 mm, L: 200 mm)	35%
K. M. Kim et al. (2015)	SiC/water nanofluid	0.01, 0.1	Stainless steel 316L (D: 19 mm, L: 1000 mm)	46%

De Schampheleire, De Kerpel, Deruyter, De Jaeger, and De Paepe (2015) investigated

the effects of novel wick material composed of metal fibers on a water copper's thermal

operation heat pipe. The fiber mesh heat pipe thermal resistance was compared to those of heat pipes with screen mesh and sintered wick. They also studied the effects of thickness and porosity of the wick material (De Kerpel, De Schampheleire, Steuperaert, De Jaeger, & De Paepe, 2016). Kempers, Ewing, and Ching (2006) studied the effects of mesh layers and fluid loading on water-copper heat pipes' performance. They concluded that the heat pipe's maximum heat transfer increased as many mesh layers were used for the wick. Franchi and Huang (2008) examined the enhancement in a heat pipe's thermal performance resulting from a composite wick. The wick was fabricated from a porous structure composed of fine nickel metal powder sintered onto layers of coarse pore copper mesh. More studies can be found focusing on the wick type and characteristics effects on heat pipes performance (Khalili & Shafii, 2016; Li et al., 2016).

In a review, Plawsky et al. (2014) noted the ultimate goal was to improve both the overall heat transfer coefficient and liquid transport capability. Combinations of different structures, or composite wicks, were investigated as a method of increasing capillary pressures and permeability to promote liquid flow while creating geometry favorable for thin-film evaporation. Various wick structures have been combined, such as grooves, sintered particles, screens, and meshes (Deng, Tang, Huang, Lu, & Yuan, 2013; Franchi & Huang, 2008; Li, He, & Zeng, 2013). Specific liquid transport structures or arteries have also been implemented to directly reduce the length of liquid needed to travel (Hwang et al., 2011; Min, Hwang, & Kaviany, 2009)

Grooves with a sintered layer have been investigated several times by (Khrustalev & Faghri, 1996; Vasil'ev, Grakovich, Rabetskii, & Tulin, 2012). J. Wang and Catton (2001) modeled a triangular groove with a sintered layer and found that the increase in the evaporative surface area increased the overall heat transfer coefficient up to six times. As

mentioned before, grooves significantly benefit from the increased evaporative surface area due to lack of wetting on the top of the fin.

Others have investigated the use of wick structures with pore size distributions at two different length scales (Cai & Chen, 2012; Reilly, 2013; Vadnjal & Catton, 2006). The tiny pores provide capillary pressure and area for thin-film evaporation while taking advantage of the large pores' lower flow resistance. Semenic and Catton (2009) studied the dry-out behavior of sintered bi-porous wicks in a vapor chamber. They found the large pores aided in vapor transport out of the wick while opening the tiny pores in the interior for evaporation.

Micro- and Nano-structured surfaces have also been a significant research area (Plawsky et al., 2014). The implemented geometries are simple, consisting of pin fin arrays, posts, nano-wires, and nanotubes (Ranjan, Garimella, Murthy, & Yazawa, 2011; Ranjan, Patel, Garimella, & Murthy, 2012). The structures are designed to be on the thin-film region's order, vastly increasing the thin film area and reducing the overall thermal resistance. Nano-structures are limited by permeability but have been successfully combined with larger structures as a composite wick (Weibel, Kim, Fisher, & Garimella, 2013).

Nanostructures show great potential for enhancing traditional wicking structures for heat pipes. Cost, reliability, and manufacturing capabilities are still obstacles to implementation. Cleveland, Moghaddam, and Orazem (2014) estimated that materials used for nano-fabrication could erode heavily in di-ionized water, eliminating any long-term use.

In the current study, the effect of PCA-functionalized graphene nanofluid on the heat pipe performance is examined by functionalizing the GNP with 1- Pyrene Carboxylic-

Acid. The heat pipe with a sintered wick structure filled by PCA-functionalized graphene nanofluid is considered. Various thermocouples were applied to measure the thermo-physical attributes of the working fluids. Temperature distribution, thermal efficiency, thermal resistance, and overall heat transfer coefficient of the heat pipe are examined under different tilt angles and input heat powers. Besides, a CFD modeling for the operation of a sinter wick heat pipe has been used to study in detail the phenomena of heat transfer and two-phase flow. According to the literature, there has been no research on sintered wick heat pipes filled with PCA-functionalized graphene nanofluids.

CHAPTER 3: METHODOLOGY

3.1   Introduction

This chapter is aimed at providing a detailed description of methods and procedures in this study. In order to achieve the objectives, this study has been divided into four sections. The preparation of nanofluid is described in the first section, followed by an investigation of thermophysical properties. The second section numerical simulation of a cylindrical heat pipe with a copper-sintered wick is used to analyze the thermal performance. The third step is focused on instantiation of accurate performance measurement of heat pipe using Noncovalently functionalized graphene with 1-pyrene carboxylic acid (PCA). The last section Evaluating the characteristics of deposits on the wick surface that contribute to performance enhancement. A flowchart of the experimental and analytical step is presented in Figure 3-1.

Section 1
- Preparation of nanofluid
- Characterization of nanofluid (XRD, FTIR and Thermal conductivity analysis)

Section 2
- Problem definition
- Heat pipe physical properties and key parameters
- Numerical analysis and solution procedure

Section 3
- Heat pipe preparation
- Evacuation and charging
- Experimental set up and test procedure
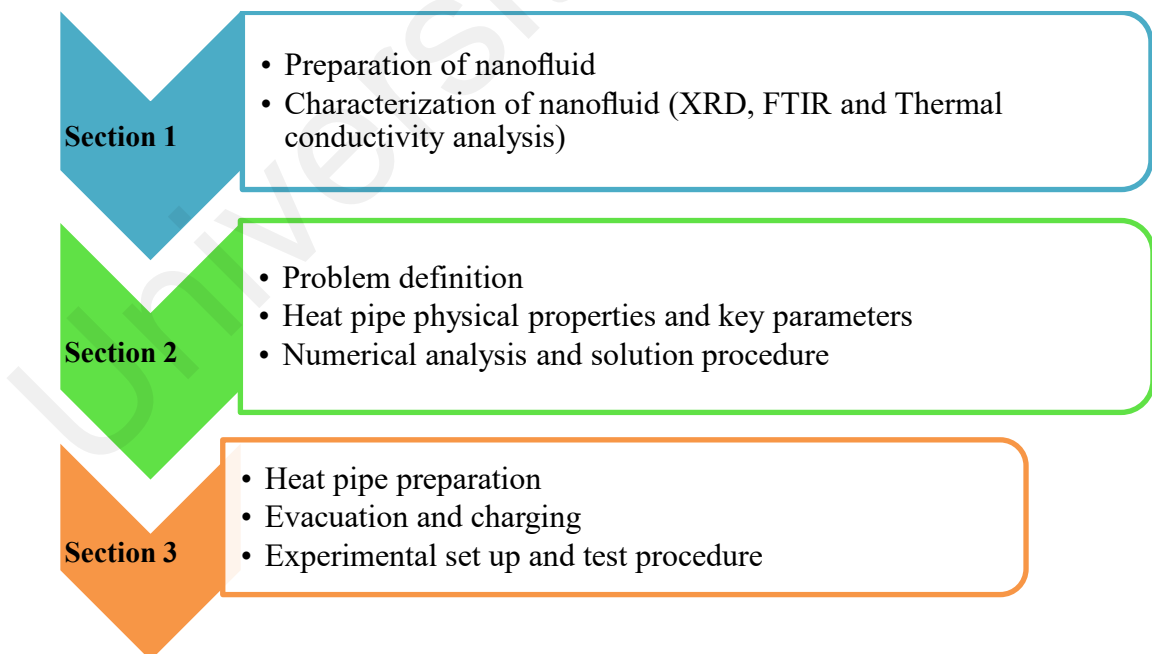
Figure 3-1: Study procedure flow Chart

3.2　Development of nanofluid

In this study, the nanofluid at volume concentrations of 0.01, 0.02, and 0.04, and 0.06 wt% with three steps.

3.2.1　Preparation of nanofluid

1-pyrene carboxylic acid (PCA), graphene nanoplatelets (GNP), ethanol, and distilled water (DW) have been utilized for the preparation of PCA-functionalized graphene nanofluids. PCA-functionalized graphene dispersions were prepared by sonicating a mixture of graphite powder (Aldrich, particle size <45 μm) and 1-pyrene carboxylic acid (Aldrich, 98%) in 50 mL methanol for 45 min with a Branson® 5510 bath sonicator. To this solution, 200 mL of distilled water was added (stage 1 of the process, see Figure 3-2), and sonication was continued for a day. The dispersion was then allowed to settle overnight (stage 2, Figure 3-2). Centrifuge with 10000 rpm was used for 20 minutes, then the clear supernatant liquid was poured away, and freshwater was added. The clear supernatant liquid was poured away, and distilled water was added. The solution was then sonicated for an additional two hours, resulting in a stable purplish-grey dispersion that does not show any significant precipitation at stage 3 when left on a lab benchtop for weeks. (stage 3, Figure 3-2).
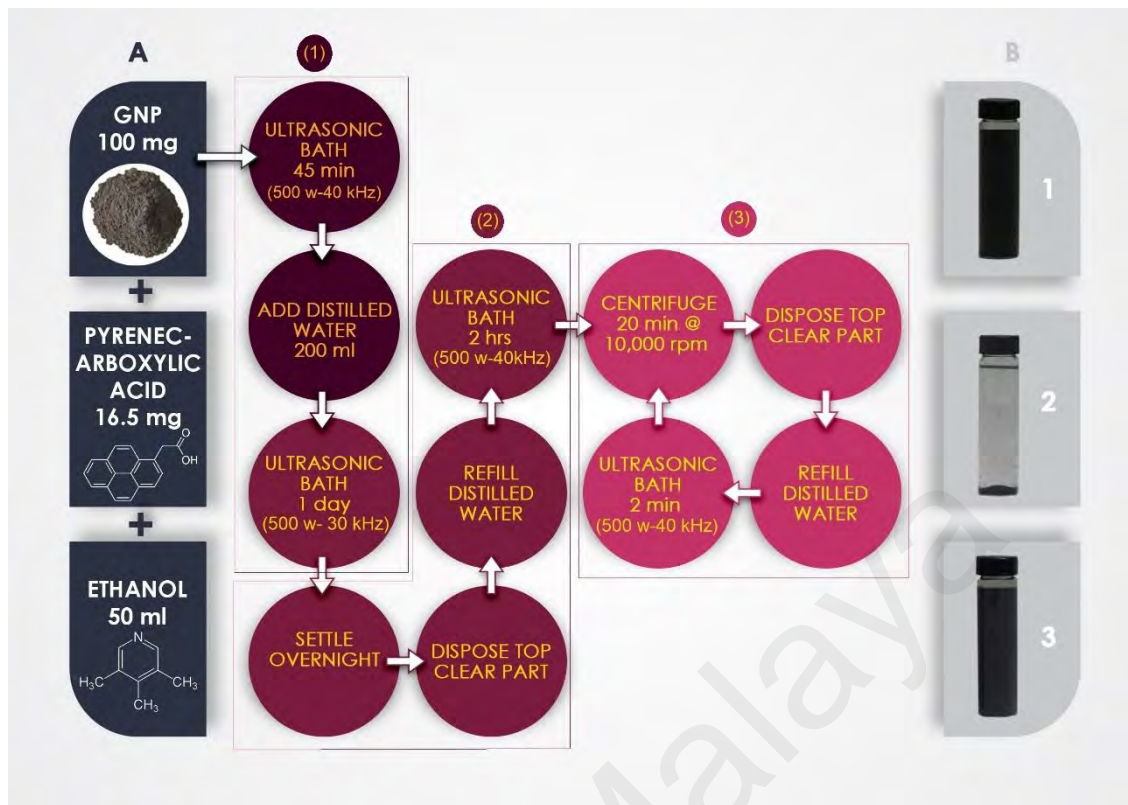
Figure 3-2: (a) Preparation procedure of the nanofluids (b) stages of preparation.

3.2.2 Characterization of nanofluid

Morphological characterization of the Functionalize GNP and the suspension was done using a scanning electron microscope (Semenic & Catton) from LEO 1530 FE-SEM Carl Zeiss, Germany. Before dispersion, the as-received filler's morphology was observed using SEM, and the quality of the GNPs was studied using Brucker AXS – D8 Advance X-ray diffractometer (XRD).

FTIR studies of these adsorbents help identify various PCA forms present in the GNP.

The nanosheets dispersion is a significant process and needs special attention. The stable homogeneous PCA-functionalized graphene nanofluids were prepared by a two-step method. Figure 3-3 shows the photograph of four typical samples of PCA-

functionalized graphene nanofluids at their concentration after three months, and it can be observed that there is practically no sediment at the bottom of the container.

Figure 3-3: Nanofluid concentrations for sedimentation test

A KD2 Pro device (Decagon Devices, USA) has been utilized to measure nanofluids' thermal conductivity. In this device, the transient hot-wire method is employed (Figure 3-4). The KS-1 sensor with 60 mm long and 1.27 mm diameter made of stainless steel is used for thermal conductivity measurement. This sensor was interpolated into a vessel filled with nanofluid located in a stable temperature bath. The sensor operates as a line heat source.
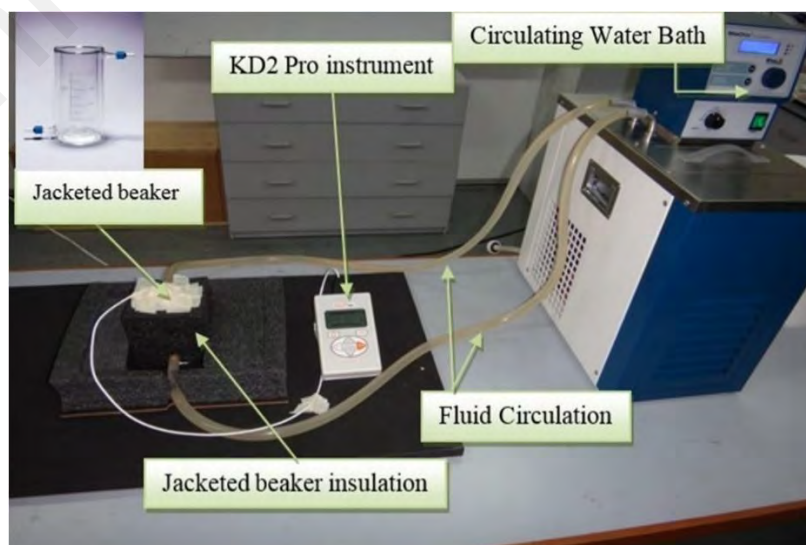
Figure 3-4: Setup for thermal conductivity measurement.

In nanofluids' thermophysical properties, the viscosity is a significant property that governs the quality of heat transfer fluid. Therefore, the numerous thermal applications of nanofluid are affected by it and cooling systems and heat exchangers. Based on a 1% error rate, by an effect of temperature, by an Anton Paar rheometer (Physica MCR 301, Anton Paar GmbH, Austria). Before using the nanofluids, it was calibrated with the distilled water.

3.3 Numerical analysis

3.3.1 Problem definition

The flowing fluid and heat transfer into the heat pipe is a complex process. In consequence, the efficiency of a thermal CFD simulation depends on many factors. The creation of the model geometry and its integration in a physical domain, grid generation, and choice of a suitable numerical computing scheme are significant factors determining the simulation process's success level. The main steps of the performed studies are described in the following paragraphs.

3.3.2 Heat pipe physical properties and critical parameters

The system configuration is shown in Figure 3-5a. The unit consists of a heat pipe network, a cooling system, and a heat engine. The thermal energy received from the heat engine on the evaporator surface is transferred to the liquid in the wick the liquid phase changes to vapor. The vapor is driven through the adiabatic part due to the generated pressure difference. The vapor leaving the adiabatic section towards the main condenser is like a jet. The vapor jet strikes the main condenser surface and spread out radially while its phase changes to a liquid and releases its heat to the heat engine via a condenser. The heat dissipation to the heat engine is simulated by attaching a heat absorber with high thermal conductivity to the primary condenser. Vacuum insulation is considered as the adiabatic boundary condition in mathematical modeling.
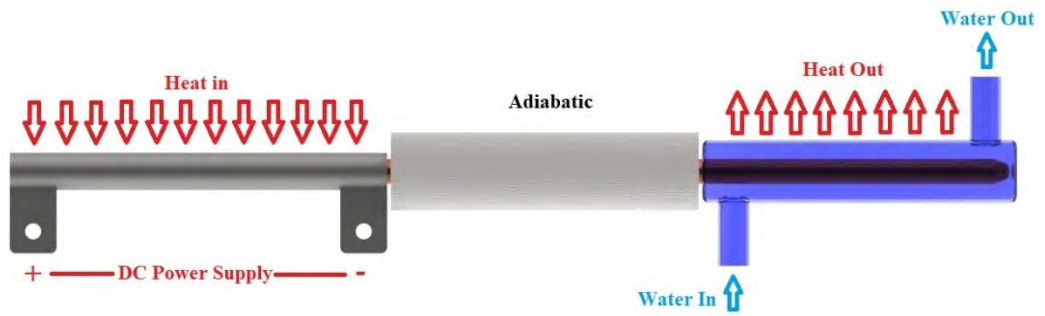
(a)

(b)

Figure 3-5: The heat pipe network's schematic integrated with (a) cooling system unit and a heat engine, (b) vapor jet strikes in heat pipe.

The thermophysical properties of the vapor chamber material and working fluid are tabulated in Table 3-1. The coolant water temperature and the heat transfer coefficient on the condenser are 298 K, and 400 W/m^2 K. Table 3-1 shows the working fluid's thermophysical properties, wick structure, and wall. Two sides of the heat pipe wall considered to be the wick.

Table 3-1: Thermophysical properties of the heat pipe material and working fluid.

Copper wall/wick	Thermal conductivity	387.6 W/m K
	Specific heat	381 J/kg K
	Density	8978 kg/m^3
	Thermal conductivity of the wick	40 W/m K
Water	Thermal conductivity	0.6 W/m K
	Specific heat	4182 J/kg K
	Density	1000 kg/m^3
	Viscosity	1.05 mPa-s
Water vapor	Thermal conductivity	0.026 W/m K
	Specific heat	2014 J/kg K
	Density	0.01 kg/m^3
	Viscosity	0.00849 mPa-s
Water/vapor	Latent heat of vaporization	2446.36 kJ/kg
PCA-functionalized graphene nanofluid with 0.06 wt%	Viscosity	1.23 mPa-s
	Density	1025 kg/m^3
	Specific heat	4210 J/kg-K
	Thermal conductivity	0.79 W/m-K

3.3.2.1   Effect of gravity in the heat pipe

In this work, heat pipe experiments depending on gravity because gravity is one of the phenomena which affects the heat transportability of the heat pipe. In heat pipe technology is gravity on the one side positive when ensuring the circulation of the working fluid in gravity heat pipe (GHP) (thermosiphon) and on the other side negative when act opposite the capillary action in the wick heat pipe (WHP). This study was focused on the influence of working position on heat transfer ability of heat pipe. It was realized with the various working positions in the range from vertical to horizontal with the sequence of the inclination angle about 30° (see Figure 3-6).
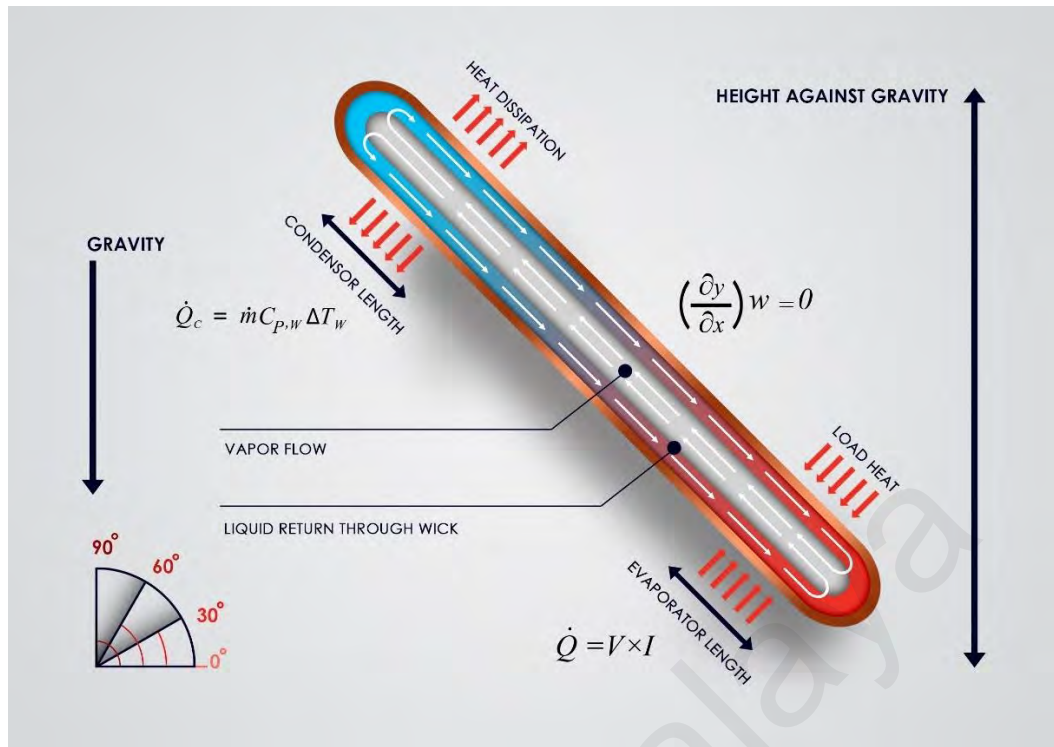
Figure 3-6: Schematic of the working position and heat transfer ability of heat pipe

It has been implicit that the condenser is chilled by water, as claimed by the experimental procedure. Hence, a convection heat transfer coefficient was demarcated as a boundary condition on the condenser's wall. The conforming heat transfer coefficients have been considered with the formula (Ghosh et al., 2012).

$$h_c = \frac{Q_c}{2\pi r L_c (T_{c.av} - T_\infty)} \tag{3-1}$$

where Q_c is the rate of heat transfer from the condenser, $T_{c.av}$ is the average condenser temperature, L_c is the condenser height, r is the pipe radius, T_∞ is the average temperature of the condenser cooling water and h_c is the condenser heat transfer coefficient. Figure 3-6 shows the boundary conditions applied to the computational model.

3.3.3   Geometry Modeling

Figure 3-7 shows the 2D & 3D geometrical configuration of the model for CFD simulation. The proportions of this geometry have been chosen as same as the dimensions of the experimental setup used. The length of 100 mm has been taken for evaporator, adiabatic, and condenser sections of the heat pipe. The wall and wick structure are copper material. DW DI   water and PCA-functionalized graphene nanofluid are considered as working fluid.
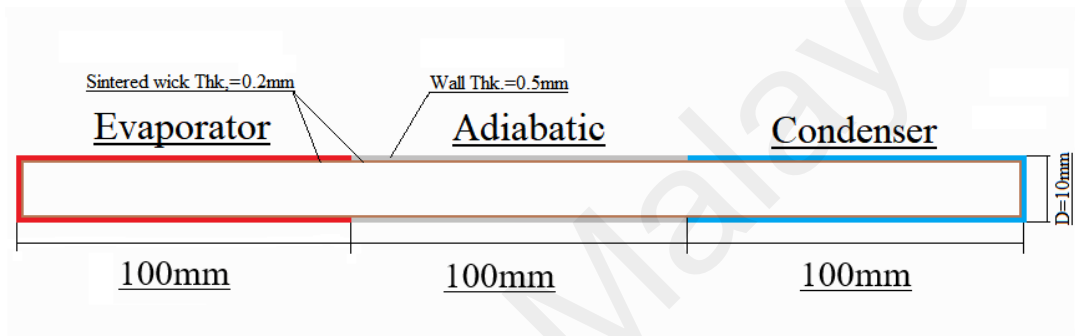
Figure 3-7: Geometry modeling of the heat pipe

3.3.4   Mesh generation

ANSYS Meshing was adopted to generate the meshes. A mapped meshing method with a Quadrilateral element was used to mesh the surface bodies. Finer grids are applied in the wall, wick, and central condenser regions. The computational meshes for vapor and wick-wall regions in the main condenser are shown in Figure 3-8 for the heat pipe.
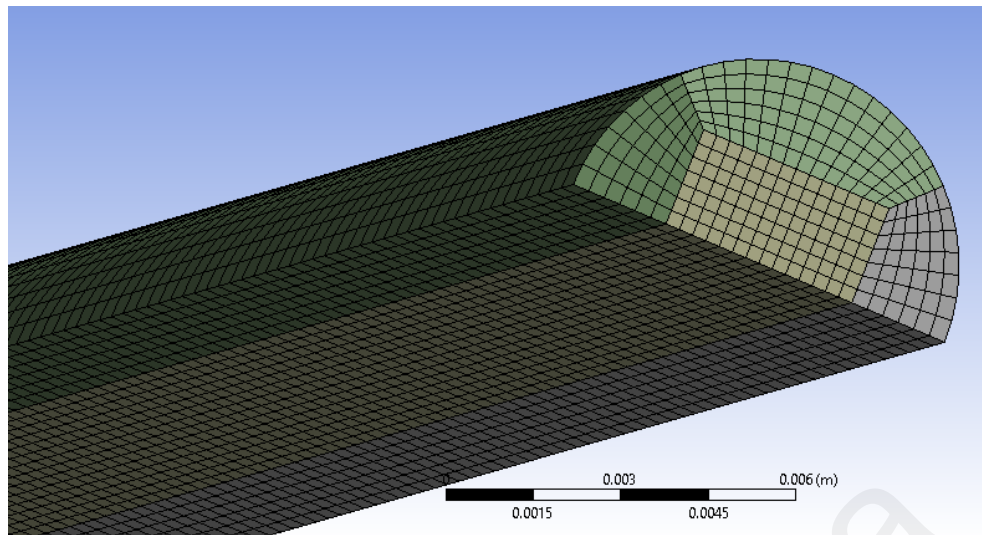
Figure 3-8: Generated mesh for heat pipe

The cupper was chosen as the wick and wall materials due to its compatibility with nanofluid. Screen mesh was selected as the wick structure. The mesh screens' key parameters are the wire diameter (d) and mesh number (N). Other parameters of the wick material, such as porosity and permeability, can be derived by the following equations (Faghri, 1995):

$$\varepsilon = 1 - \frac{1.05\pi N d}{4} \tag{3-2}$$

$$K = \frac{d^2 \varepsilon^3}{122(1 - \varepsilon)^2} \tag{3-3}$$

The effective thermal conductivity of the wick material is calculated by following equation (3-4) in which k_l is the thermal conductivity of the nanofluid and k_c is the thermal conductivity of copper.

$$k_{eff} = \frac{k_l[(k_l + k_c) - (1 - \varepsilon)(k_l - k_c)]}{(k_l + k_c) + (1 - \varepsilon)(k_l - k_c)} \tag{3-4}$$

The calculated properties of the wick are presented in Table 3-2.

Table 3-2:Physical properties of the wick structure

Wick type	Screen mesh
Number of mesh, N	120000
Porosity, ε	0.65
Permeability, K	5.4 x 10^{-9} m^2

Numerous meshes are assessed to remove the mesh sensitivity and reduction of the calculation's requirement. The grid study of the results is checked by growing the mesh numbers.

3.3.5   Boundaries condition

It can be said that determining the boundaries conditions is one of the most basic and most important stages of numerical solution simulation, which is adjusted in ANSYS-FLUENT 19.00.

Due to the symmetry of geometry and flow, we consider the symmetry level as a boundary condition at the heat pipe centerline. The computational domain consists of a solid zone; representing the heat pipe and a fluid zone; representing the heat pipe's liquid. The outer pipe wall is divided into three regions with different boundary conditions. The outer surface of the evaporator region is subjected to a heat flux boundary condition. The heat flux corresponds to the varying heat input of 40, 60, 80, 100, and 120 W is imposed on the evaporator surface. The condenser is exposed to a convective boundary condition, and the temperature was fixed at 20 C°. The middle of the heat pipe, an adiabatic zone, is subjected to zero heat flux boundary conditions.

3.3.6   Governing Equations

Before writing the governing equations, the succeeding assumptions have been used.

- Body forces are negligible.

- Vapor and liquid flows are turbulent and incompressible.

- The volume is an average of the liquid's density in the wick is reformed to preserve liquid mass and contain the variations in vapor and liquid mass correctly through the transient operational conditions.

- The vapor is saturated at t = 0 (time).

- Thermophysical properties are supposed constant, excluding the vapor density, which is calculated from the working pressure.

Surface tracking technique of the VOF model applied to the fixed Eulerian mesh. This method consists of two-volume fractions of α_l and α_v which represent the location of liquid and vapor and interface in computational cells. When $\alpha_v = 0$ the liquid phase occurs, and the vaper phase happen only where $\alpha_v = 1$. Generally, the liquid-vapor interface detects in the cell wherever $0 < \alpha_v < 1$. The volume fractions of all phases sum up in each control volume.

$$\alpha_v + \alpha_l = 1 \tag{3-5}$$

The continuity equation of volume fraction for both phases can provide interface tracking between the phases. The following equation indicates phase q.

$$\frac{1}{\rho_q}\left[\frac{\partial}{\partial t}\left(\alpha_q \rho_q\right) + \nabla.\left(\alpha_q \rho_q \vec{v}_q\right) = S_{\alpha_q} + \sum_{p=1}^{n}\left(\dot{m}_{pq} - \dot{m}_{qp}\right)\right] \tag{3-6}$$

The mass transfer from phase q to phase p shows by $\dot{m}_{qp}$ and $\dot{m}_{pq}$ present the mass transfer from p to q. The void fraction represents by α and ρ signify the density as well. The basis term on the right side of this equation is S_{α_q} which equals zero.

The equation of momentum is as follows:

$$\frac{\partial}{\partial t}(\rho \vec{v}) + \nabla.(\rho \vec{v} \vec{v}) = -\nabla p + \nabla.\left[\mu\left(\nabla_{\vec{v}} + \nabla_{\vec{v}^T}\right)\right] + \rho \vec{g} \tag{3-7}$$

In this study, the flow was a three-dimensional, incompressible, and turbulent K-ε model. The governing equations consist of mass conservation, momentum conservation, energy equation, and equations for kinetic energy K and its depreciation rate ε.

$$p' = p + \frac{2}{3}\rho k + \frac{2}{3}\mu_{eff}\frac{\partial U_k}{\partial x_k} \tag{3-8}$$

$$\mu_{eff} = \mu_t + \mu \tag{3-9}$$

p' is defined as the corrected pressure. Also μ_t is the turbulence viscosity.

The turbulent K-ε model equations:

$$\frac{\partial}{\partial xj})\rho k U_i = \frac{\partial}{\partial xj}[(\mu + \frac{\mu_t}{\sigma_k})\frac{\partial K}{\partial xj}] + G_k + Y_m - \rho\varepsilon \tag{3-10}$$

$$\frac{\partial}{\partial xj})\rho\varepsilon U_i) = \frac{\partial}{\partial xj}[(\mu + \frac{\mu_t}{\sigma_\varepsilon})\frac{\partial\varepsilon}{\partial xj}] + c_{1\varepsilon}\frac{\varepsilon}{K}G_k - c_{2\varepsilon}\rho\frac{\varepsilon^2}{K} \tag{3-11}$$

G_k Refers to the generation of turbulent kinetic energy due to the average velocity gradient. Also, the expression Y_m represents the contribution of velocity fluctuations in a turbulent flow. Also, $c_{1\varepsilon} = 1.44$ and $c_{2\varepsilon} = 1.92$ has been chosen constant coefficients according to the Fluent Program Guide.

Also, σ_k and σ_ε represent pyrantel numbers of turbulences for k-ε that are considered as follows:

$\sigma_k = 1, \ \sigma_\varepsilon = 1.3$

The viscosity of the turbulence μ_t is also calculated according to k-ε values as follows:

$$\mu_t = \rho\ C_\mu\ \frac{k^2}{\varepsilon} \tag{3-12}$$

Constant C_μ also, we considered it as 0.09.

The governing equations of vapor core, wick, and wall regions are as follows:

3.3.6.1 Vapor region

The conservation of mass and momentum equations and the energy equation for vapor can be written as:

Continuity:

$$\frac{1}{r}\frac{\partial}{\partial r}(\rho r v) + \frac{\partial}{\partial z}(\rho u) = 0 \tag{3-13}$$

r- momentum:

$$\frac{1}{r}\frac{\partial}{\partial r}(\rho r v v) + \frac{\partial}{\partial z}(\rho v u) \tag{3-14}$$

$$= -\frac{\partial p}{\partial r} + \frac{\mu}{r}\frac{\partial}{\partial z}\left[r\left(\frac{\partial v}{\partial r} + \frac{\partial u}{\partial z}\right)\right] + \frac{\mu}{r}\frac{\partial}{\partial r}\left[r\left(2\frac{\partial v}{\partial r} - \frac{2}{3}(\nabla.\vec{v})\right)\right] - 2\mu\frac{v}{r^2} + \frac{2}{3}\frac{\mu}{r}(\nabla.\vec{v})$$

z- momentum:

$$\frac{\partial}{\partial z}(\rho u u) + \frac{1}{r}\frac{\partial}{\partial r}(\rho r u v) \tag{3-15}$$

$$= -\frac{\partial p}{\partial z} + \frac{\mu}{r}\frac{\partial}{\partial z}\left[r\left(2\frac{\partial u}{\partial z} - \frac{2}{3}(\nabla.\vec{v})\right)\right] + \frac{\mu}{r}\frac{\partial}{\partial r}\left[r\left(\frac{\partial u}{\partial r} + \frac{\partial v}{\partial z}\right)\right]$$

where,

$$\nabla.\vec{v} = \frac{1}{r}\frac{\partial}{\partial r}(rv) + \frac{\partial}{\partial z}(u) = 0 \tag{3-16}$$

Energy:

$$cp\left(\frac{1}{r}\frac{\partial}{\partial r}(\rho rvT) + \frac{\partial \rho uT}{\partial z}\right) \tag{3-17}$$

$$= k\left[\frac{1}{r}\frac{\partial}{\partial r}\left(r\frac{\partial T}{\partial r}\right) + \frac{\partial^2 T}{\partial z^2}\right] + u\frac{\partial p}{\partial z} + v\frac{\partial p}{\partial r} + \mu\varphi$$

Where % is the viscous dissipation and is defined as:

$$\varphi = 2\left[\left(\frac{\partial v}{\partial r}\right)^2 + \left(\frac{v}{r}\right)^2 + \left(\frac{\partial u}{\partial z}\right)^2\right] + \left(\frac{\partial v}{\partial z} + \frac{\partial w}{\partial r}\right)^2 - \frac{2}{3}\left(\frac{1}{r}\frac{\partial}{\partial r}(rv) + \frac{\partial u}{\partial z}\right)^2 \tag{3-18}$$

Equation of state:

The compressibility effect is included by using the ideal gas equation. The vapor density can be obtained from the following equation:

$$p = \rho R_g T \tag{3-19}$$

3.3.6.2 Liquid region

Based on (Yiding Cao & Faghri, 1991), the wick's liquid flow has a negligible effect on heat pipes' temperature distribution and can be ignored. The governing equation can be written as:

$$k_{eff} = \left[\frac{1}{r}\frac{\partial}{\partial r}\left(r\frac{\partial T}{\partial r}\right) + \frac{\partial^2 T}{\partial z^2}\right] = 0 \tag{3-20}$$

Where k_{eff} is the effective thermal conductivity of the wick structure (Faghri, 1995).

3.3.6.3 Wall region

The heat conduction equation governs the heat transfer through the heat pipe wall:

$$k_w \left[\frac{1}{r} \frac{\partial}{\partial r} \left(r \frac{\partial T}{\partial r} \right) + \frac{\partial^2 T}{\partial z^2} \right] = 0 \qquad (3\text{-}21)$$

Where w states to the wall material.

3.3.7   Solution method

The simulation was conducted using ANSYS-FLUENT V-19. Two different geometries were created for solid (wall and wick) and vapor core regions using ANSYS Design Modeler. In this study, to model and simulate water and steam flow simultaneously, it is necessary to solve the flow in a two-phase (VOF) model. In such a way, the vapor phase and water phase are placed in distinct boundaries, and the effect of volumetric forces such as gravity leads to this formation of flow. At the beginning of the solution, the filling ratio is 40 percent of the heat pipe volume. The pressure-based solver is used for uncompromising flow and low speeds. However, the Density-based solver is used for overcurrent and high-speed currents. Due to the incompressibility of the flow, a pressure-based solver is used for this study.

3.4 Experimental Design

In this section, a description of the main components of the experimental setup is presented.

3.4.1 Heat pipe preparation

3.4.1.1 Cleaning and deoxidizing

All materials used in the heat pipe should be cleaned. Cleaning ensures that the working fluid will wet the materials thoroughly. It also prevents foreign objects from presenting in the working fluid during heat pipe operation.

3.4.1.2 Container degreasing

Once the machining of the heat pipe container and fabrication of the wick is completed, a procedure should remove oil and grease waxes and other drawing compounds by ethanol.

3.4.1.3 Leak detection

Leak detection should be done by pressurizing the heat pipe container with dried nitrogen gas and covering the outer surface with a soap solution. If the leak is present, the bubble will appear in the gaps.

3.4.2 Evacuation and charging

Before charging, the heat pipe should be evacuated to remove non-condensable gasses. Removal of free gasses is done by using a vacuum pump. Removal of absorbed gasses requires evacuation of the heat pipe at an elevated temperature. For this reason, the heat pipe should be evacuated at a temperature more significant than the operating

temperature. The heat pipe should be first pumped down at the ambient temperature. After completion of this stage, the charging fluid should introduce into the heat pipe.

### 3.4.3 Test procedure and experimental system

To assess the heat pipe's thermal efficacy, a standard test system encompassing the experimental sector, heating section, cooling section, an adjustable angle table, and Graphtec data logger (midi logger gl220) a computer unit was used, as shown in Figure 3-9.

Figure 3-9: Schematic of the mounting platform with the changeable tilt angle.

To measure of thermal efficacy of a heat pipe, a standard test system encompassing the experimental sector, heating section, and cooling section, a movable table with adjustable angle, data logger, and a computer unit were used, as illustrated in Figure 3-10. At the first, heat pipes are discharged with employing the vacuum pump followed by filling by a sufficient quantity of DW and PCA-functionalized graphene nanofluids. The heat pipe was then divided into three equal parts: condenser, evaporator, and adiabatic sections. Teflon end closures and acrylic tubes were used for the condenser section of the heat pipe. The condenser section loop is coupled with a flow sensor (Omega) and peristaltic dispensing pump (Longer pump) to distribute cooled water from a chilled circulating bath (DATHAN-brand ® Digital Precise Refrigerated Bath Circulator).
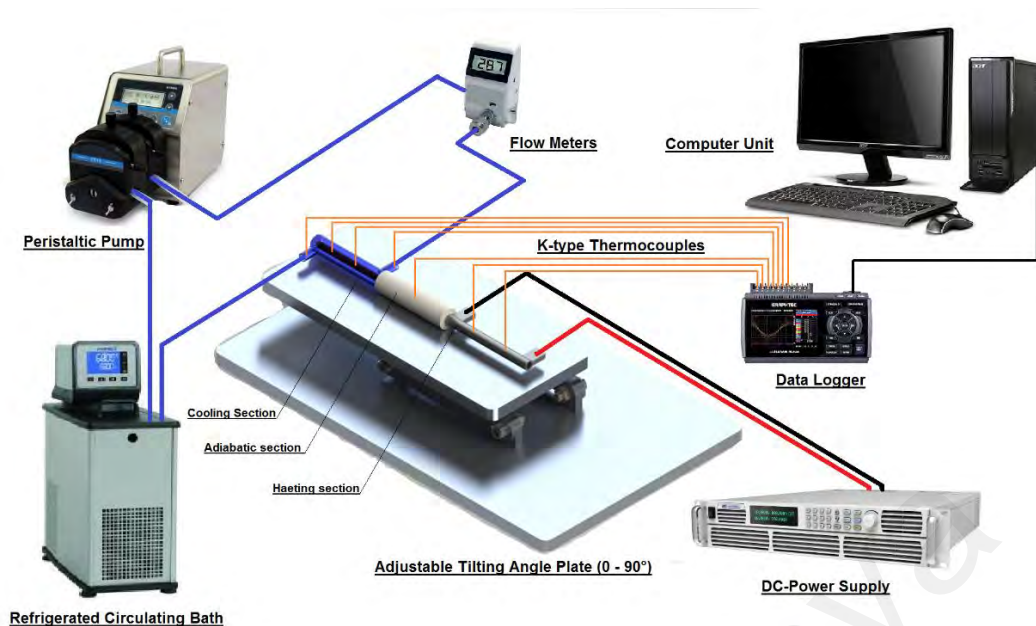
Figure 3-10: Schematic view of the experimental test rig.

Sintered wick heat pipe with a length of 300 mm, an outer diameter of 10 mm, and a wall thickness of 0.5 mm was used in this experiment. The copper heat pipe is supplied by Shenzhen Maoye Electronics Co (Shenzhen, China). Figure 3-11 illustrated a schematic of the heat pipe system used in the experiment. Five self-adhering K-type thermocouples have been positioned at the heat pipes' surfaces, consisting of two thermocouples for the evaporator, two thermocouples for the condenser, and one for adiabatic sections. This arrangement could help to measure the heat pipe surface temperature. Thermocouple calibration was conducted before the experiments., Thermocouples were linked with the Graphtec data logger (midi logger GL220) to record and monitor the thermocouple temperature.
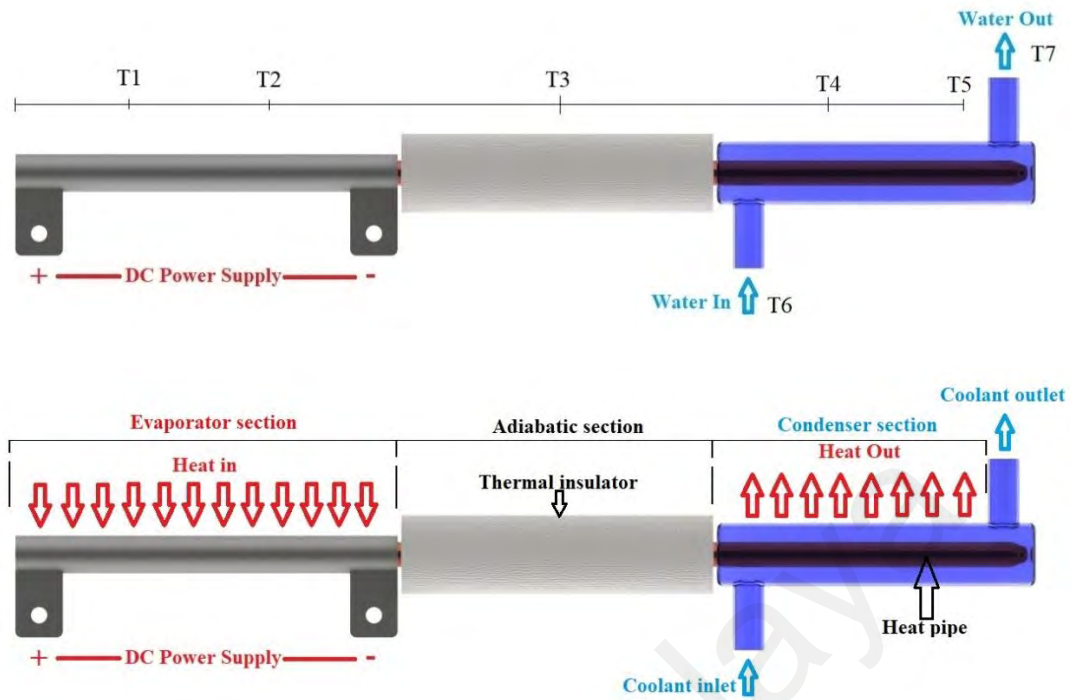
Figure 3-11: Cross-section of the experimental test section and thermocouples position.

The heat pipe's condenser segment comprises an acrylic tube and has Teflon end closures (see Figure 3-11). This section loop is prepared with a peristaltic dispensing pump (Longer pump) and flow sensors (Omega) to circulate chilling water. Two K-type thermocouples (Omega) are used to measure the condenser section's inlet and outlet temperatures (Figure 3-11). DC power supply (KEYSIGHT Technologies) was used to heat the evaporator section. The whole heat pipe system was wrapped with a few layers of ceramic fiber to avoid any loss of heat to the environment (Figure 3-12). Earlier running the experiment, the heat pipes are initially evacuated by a vacuum pump and then filled with equal amounts of nanofluids.
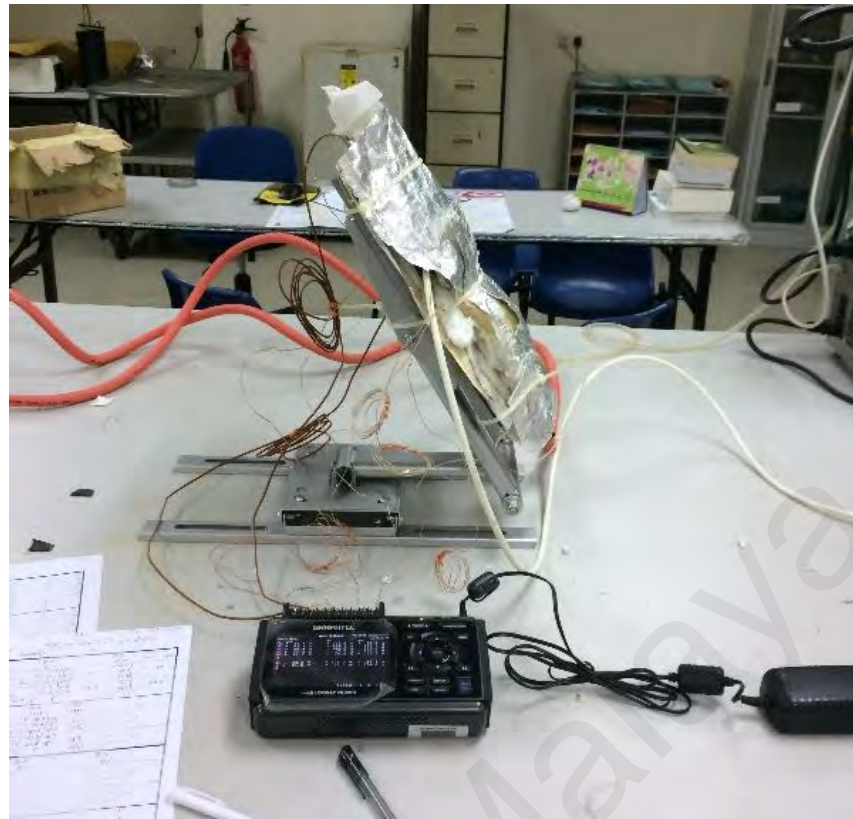
Figure 3-12: The experimental test section.

3.4.4 Data reduction

To examine the thermal efficiency, thermal resistance, and overall heat transfer coefficient of the heat pipe, an aqueous PCA-functionalized graphene nanofluid with a diverse concentration range from 0.01 to 0.06 mass% 40% filling ratio was used. The input temperature of cold water was maintained at 20 °C in the condenser section with a 400 ml/min flow rate. A variable angle holder table was utilized to modify the heat pipe tilt angle.

Additionally, the vapor temperature reductions through the evaporator section and into the adiabatic sector due to the vapor pressure and smaller temperature gradient in the vapor region. In the evaporator section of the heat pipe, the vapor and the fluid temperatures are lower than the heat pipe's external wall temperature. In contrast, in the condenser section, the inner wall surface temperature is lower than the outer surface. This

means that the evaporator's inner wall surface temperatures and the condenser should calculate the heat transfer coefficients. Nevertheless, the radial thermal resistance of the copper heat pipe wall and the copper sintered wick is meager ($\sim 10-3$ °C W) (Ghanbarpour et al., 2015), therefore the surface temperature measurements can be used with satisfactory accuracy in calculating the thermal resistance and thermal performance. The overall thermal resistance of heat pipes accounts for various resistances associated with the temperature drop between the two ends of the heat pipe (condenser and evaporator section). Recorded temperatures from heat pipe were named as evaporator temperature $T_e = (T_1 + T_2)/2$, $T_{vap} = T_3$, and $Tc = (T_4 + T_5)/2$ (Ghanbarpour et al., 2015). The heat pipe thermal resistance is calculated as:

$$R = \frac{T_e - T_a}{\dot{Q}} \tag{3-22}$$

$$\dot{Q} = V \times I \tag{3-23}$$

Where, T_e and T_c represent the average temperature of the evaporator and condenser section, respectively. Moreover, $\dot{Q}$ represents the heat input power regulated by Voltage (V) and amperage (I).

Heat transfer coefficient for evaporator can be defined as:

$$h_e = \frac{\dot{Q}}{A_e \Delta T} \tag{3-24}$$

$$\Delta T = T_e - T_{vap} \tag{3-25}$$

ΔT is the temperature change among the heat pipe's surface and the vapor temperature, and Tvap is the saturated steam temperature, which can be measured from the adiabatic section's surface.

The ratio of heat removal in the condenser to that of the heat supplied in the evaporator is called as thermal efficiency of the heat pipe, which is given by:

$$\eta = \frac{\dot{Q}_c}{\dot{Q}} = \frac{\dot{m} C_{p,w} \Delta T_w}{V \times I} \qquad (3\text{-}26)$$

Qc represents the amount of heat received in the condenser section. The other parameters such as $\dot{m}$, $C_{p,w}$, and ΔT_w are the mass flow rate, specific heat, and cooling water temperature growth.

Finally, the heat pipe effective thermal conductivity is given by:

$$k_{eff} = \frac{L_{eff}}{A_{CT} R} \qquad (3\text{-}27)$$

$$L_{eff} = 0.5 L_e + L_{ad} + 0.5 L_c \qquad (3\text{-}28)$$

L_e, L_{ad} and L_c are length of evaporator, adiabatic and condenser section which needed to calculate the L_{eff} (effective length of heat pipe). The suspicion of the estimated parameters is assessed depending on the precision of the tools. All the test tools are recalibrated, and the vulnerability outcomes are shown in Table 3-3, with the most extreme value recorded for each situation.

Table 3-3: The rate of uncertainty ranges for selected heat pipe system factors.

Factor	Error/%
Temperature	0.2
Length of the heated section	2.3
The diameter of the heat pipe	2
Heat input	3.3
Heat flux	3.2
Thermal resistance	4.1
Heat transfer coefficient	3.5

3.4.5   Uncertainty analysis

Based on the accuracy of the instruments, the uncertainties of the measured parameters are estimated. All devices are recalibrated, and the uncertainty rate is given in Table 3-3, with the maximum value listed in each case.

The temperature reading was measured using K-type thermocouples with (0.05% rdg + 0.3 °C), and 0.5% rdg for the uncertainty measurement of power readings, the critical source of uncertainty for the R was calculated. Table 1 shows that the maximum uncertainty parameter linked with the propagation of uncertainties was around 4.1% in the experimental work, a fair value in engineering applications (Churchill & Bernstein, 1977).

3.4.6   Heat pipe's performance analysis

The experimental study's opportunity is to examine the effect of nanofluids on the performance of the heat pipe. Including thermal fluid systems, entropy generation in a heat pipe is produced primarily by heat transfer across a finite temperature difference between the two ends of the heat pipe and frictional losses in the flow of the working fluid.

The heat pipe performance investigation can be calculated as follows (Annamalai & Ramalingam, 2011):

$$Performance = \frac{\dot{Q}_c}{T_c} - \frac{\dot{Q}}{T_e} \tag{3-29}$$

Tc and Te are the entropy rates accompanying the condenser's heat transfer rates and the heat source, respectively.

There is a linear relation between irreversibility and the amount of lost work during the operation associated with the heat pipe performance (Maheshkumar & Muraleedharan, 2011). The significant factors on improvement of heat pipe performance are:

1. The temperature difference between the cold and hot section
2. The temperature drops in the vapor flow section.
3. Frictional losses are related to liquid and vapor phases.

CHAPTER 4: RESULTS

4.1   Introduction

This chapter covers the result of this research's three objectives; First, the result of nanofluid characterization. Second, the development of a heat pipe model is used to analyze the fluid dynamics and heat transfer of water and working fluids. Third, the performance measurement of heat pipe using Non-Covalently functionalized graphene with 1-pyrene carboxylic acid (PCA) has been discussed. Besides, development was needed to implement the GNP deposits' characteristics for performance enhancement of heat pipe.

4.2   Nanofluid characterization result

Figure 4-1 indicates the thermal conductivity of PCA-functionalized graphene nanofluids concentration at a different temperature measured by a transient hot-wire method (KD$_2$ Pro). The results show that the thermal conductivity increased between 21% to 40% as concentration and temperature were increased.
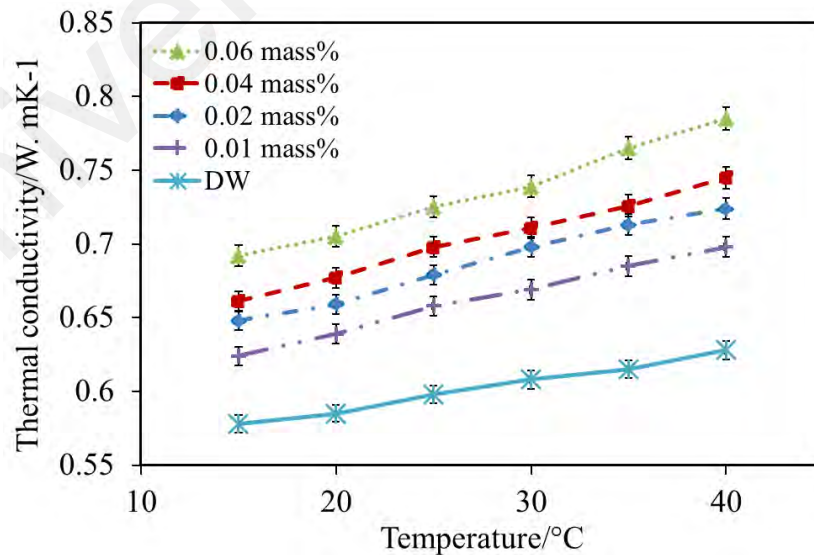
Figure 4-1:The ratio of thermal conductivity for PCA-functionalized graphene nanofluids.

Viscosity is a significant property that governs the quality of heat transfer. Therefore, it is vital to have a proper nanofluid viscosity in numerous thermal applications. Figure 4-2 indicates the viscosity at various concentrations for PCA-functionalized graphene nanofluids.
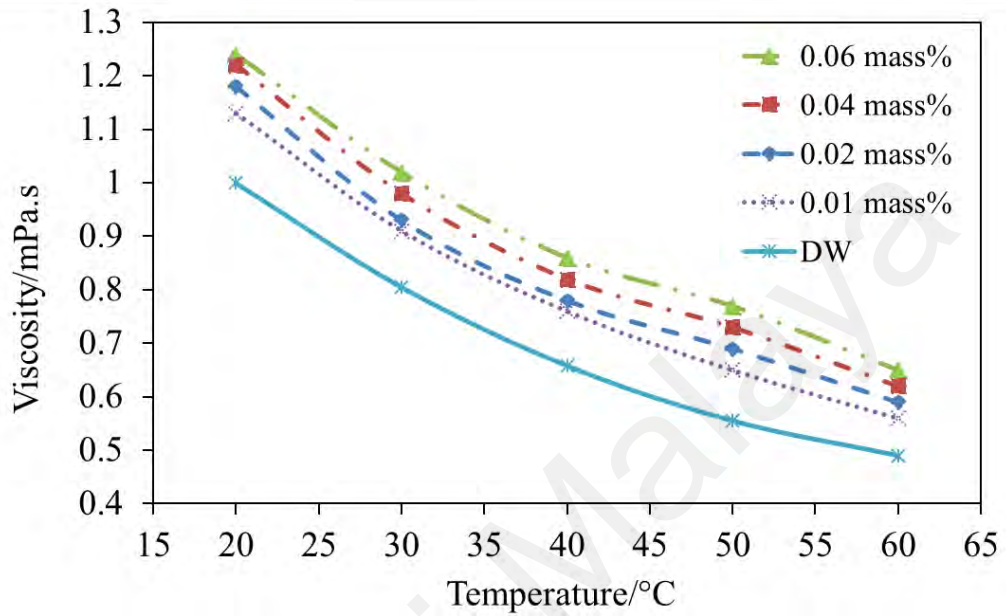
Figure 4-2: Viscosity of PCA-functionalized graphene nanofluid.

Figure 4-3 illustrates the morphology and microstructure of PCA-functionalized graphene using a field emission scanning electron microscope (FESEM) from LEO 1530 FESEM (Carl Zeiss, Munich, Germany). The porous and uniform structures of the PCA-functionalized graphene can be seen in this figure.
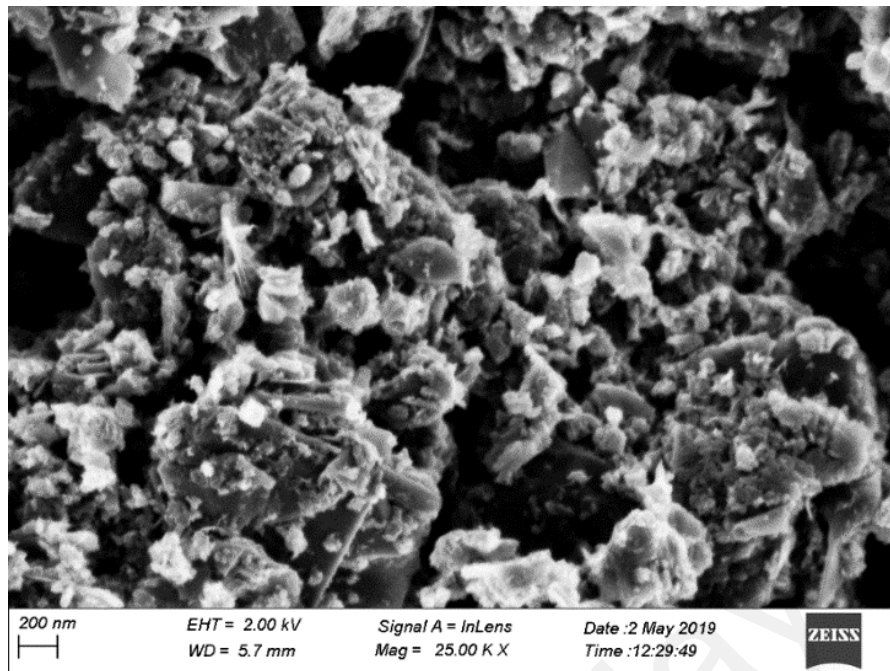
Figure 4-3: FESEM image of PCA-functionalized graphene.

X-ray powder diffraction (XRD) is a rapid analytical technique primarily used for phase identification of a crystalline material and can provide information on unit cell dimensions. The GNP 500 and Functionalize GNP's analyzed material is finely ground, homogenized, and average bulk composition is determined (Figure 4-4).
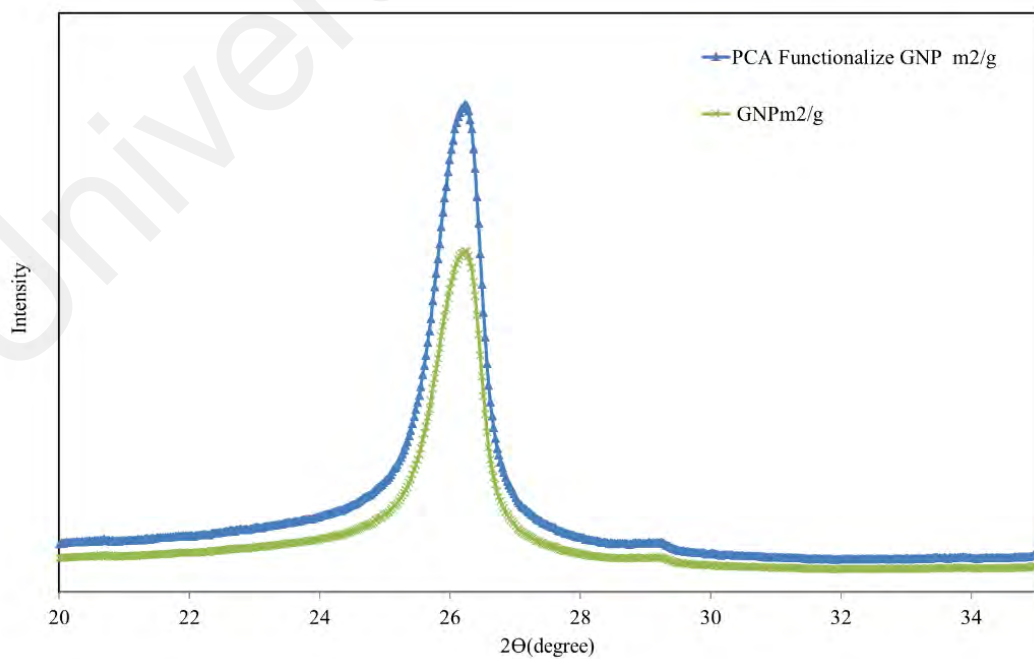
Figure 4-4: XRD patterns result of the GNP and Functionalize GNP

X-ray diffraction study shows the presence of PCA and GNP as significant phases. The presence of the above minerals was further confirmed by FTIR analysis (see Figure 4-5).
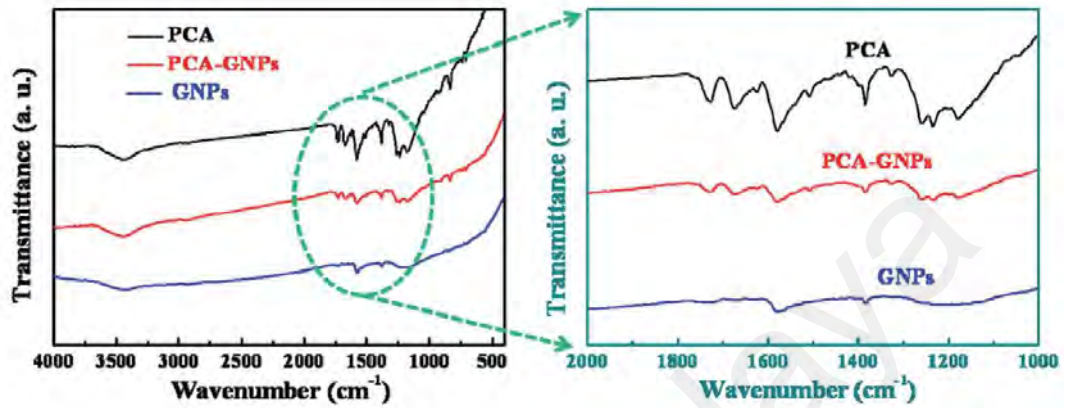
Figure 4-5: FTIR spectra of PCA, GNPs.

4.3   Numerical Results

In this section, first, the results of the heat pipe fill with distilled water are presented. The effects of heat input and gravity are investigated on the heat pipe surface temperature, volume fraction, velocity magnitude. Second, the results for the case that filled up heat pipe with nanofluid.

4.3.1   Mesh Dependency Test

The existing meshing tool in Ansys is used to construct the computational mesh. A structured mesh based on a rectangular grid is used throughout the domain (Figure 3-8). A grid independence test was performed for the tube using water as working fluid to analyze the effects of grid size on the results. Table 4-1 shows the evaluation of the dependence of results on the mesh. The grid study of the results is checked by growing the mesh numbers. These results show the maximum and average temperature on the evaporator and condenser of the heat pipe occupied with DW and working at $\theta=90°$ and

120 W heat input. The results show that 2.2 x 10⁵ cells are appropriate for obtaining satisfactory results. The grids were concentrated near the walls due to a thin layer of liquid near there. The initial row, growth factor, and the number of rows of the shaped boundary layer are 0.03, 1.3, and 8, correspondingly. The corresponding changes are less than 1% in terms of the average heat transfer coefficient by comparing the mesh configurations. Therefore, the first grid case has been adopted to obtain an acceptable compromise between computational time and accuracy.

Table 4-1: The grid study results.

Number of elements	Average temperature on evaporator sections (°C)	Maximum temperature on evaporator sections (°C)	Average temperature on condenser sections (°C)	Maximum temperature on condenser sections (°C)
110991	77.1	79.3	44.8	45.9
155910	77.9	79.7	45.7	47.1
210510	78.9	80.3	46.8	47.8
225229	79.7	80.1	47.2	47.6
290519	79.8	80.1	47.3	47.8

4.3.2   Temperature distribution of simulation

After performing various simulations for the twenty existing methods in this study, some of the results are presented as schematic results in-phase and flow contour in the following figures. Figure 4-6 shows the predicted wall temperature distribution from the evaporator section to the condenser in different working angles and 40 W power input.
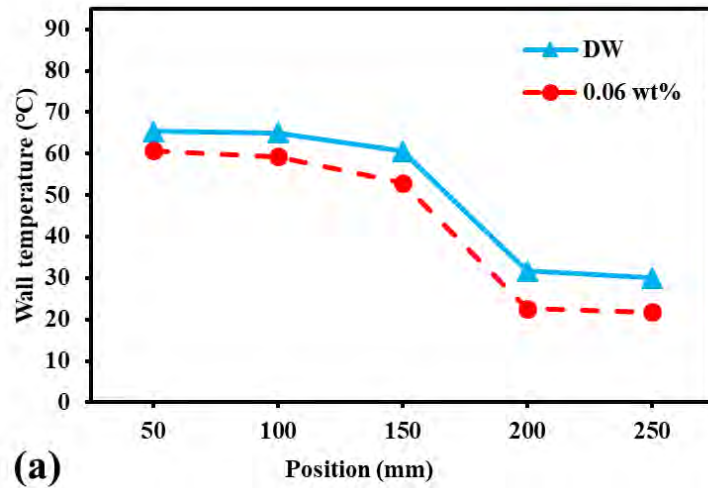
(a)
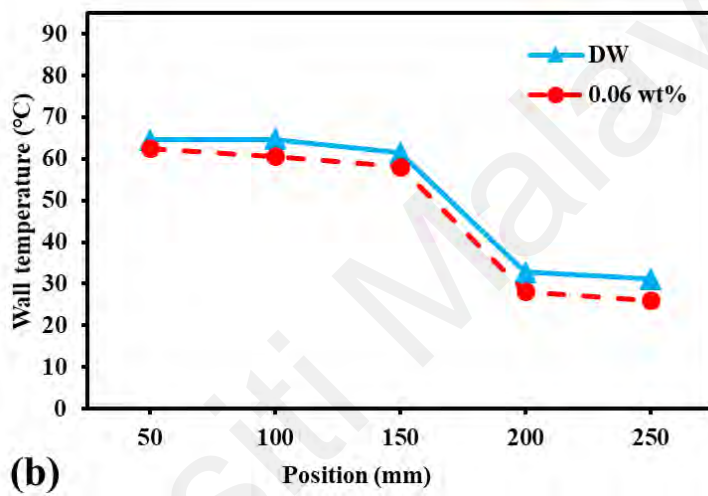
(b)

(c)
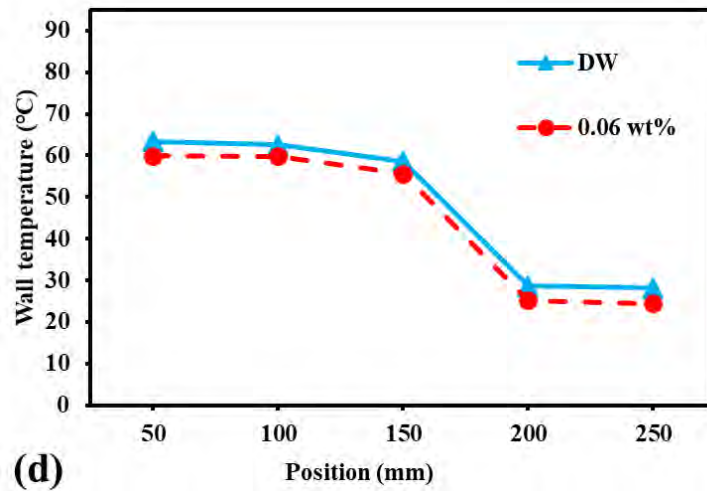
Figure 4-6: Distribution of surface temperature along heat pipe with a DW and 0.06 wt% PCA-functionalized graphene working fluid for heat input of 40W and four tilt angles (θ): (a) 0°, (b) 30°, (c) 60°, (d) 90°.

4.3.3 Flow visualization of CFD simulation results

Due to density difference, the vapor's movement from the heating section to the cooling section could typically happen. The cooling section's return to the heating section is because of the gravity and force of capilla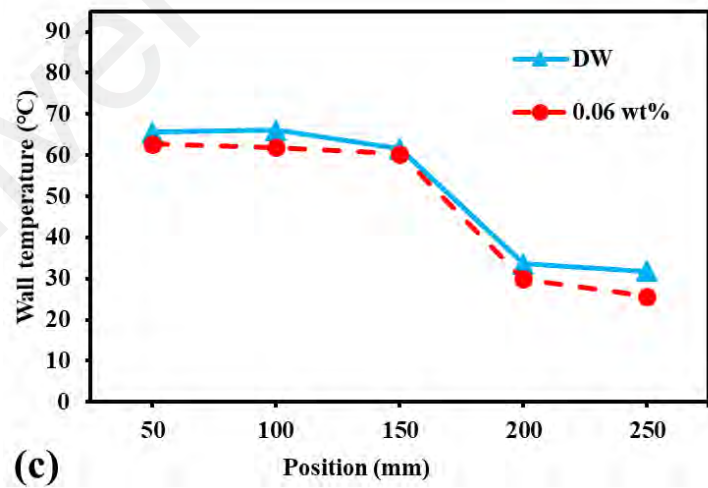ry action in the wick structure. Changing the heat pipe orientation from 0° to 90° remarkably increased the flow of liquid to the evaporator section due to the gravitational impact. This causes a decrease in the heat transfer in the outward direction and increases the heat pipe's thermal resistance. Figure 4-7 shows gravity's effect on the centerline of the heat pipe that changes the volume fraction of vapor in various heat inputs. The differences in volume fraction amongst the evaporator and the condenser sections steadily grow, increasing the heat input rate from 40 W to 120 W. The blue color indicates the minimum volume of vapor in the condenser section that could explain the return of working fluid from the condenser to the evaporator section. Due to gravity, fluid returns through the bottom line of the heat pipe, as shown in Figure 4-7.
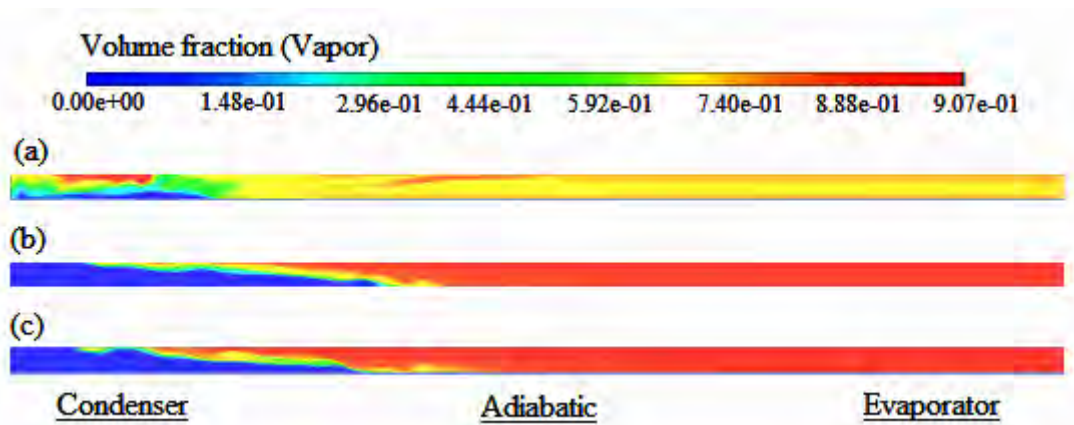
Figure 4-7: Volume fraction of vapor in 0 º title angle effected by heat input a)40 W, b)80 W, c)120 W.

Similarly, Figure 4-8 illustrated the mixture's velocity magnitude at 80 W and 120 wheat input. The velocity is higher at the top of the heat pipeline, as the liquid phase flows at the bottom line of the heat pipe and return from the condenser section to the evaporator section. Correspondingly, it is detected that the velocity grows with the increase in the heat input.
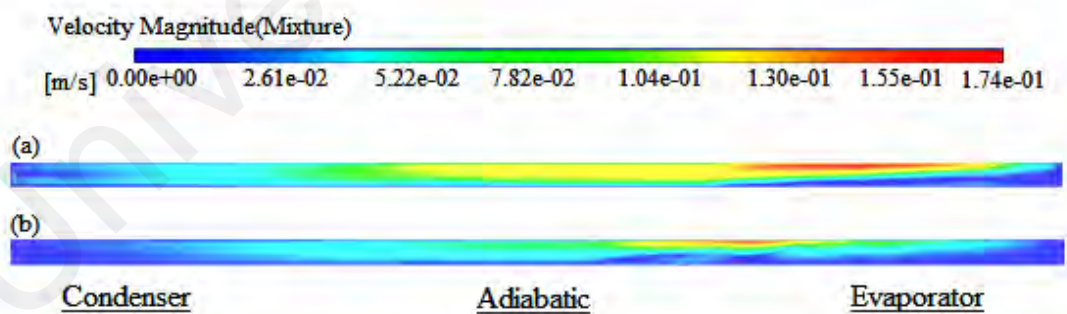
Figure 4-8: Velocity magnitude in 0º title angle effected by a)80W, b)120W.

The vapor volume is slightly more than the water volume when the temperature and the title angle increase (Figure 4-9). The liquid phase of working fluid moving from the condenser to the adiabatic section due to the gravity force.
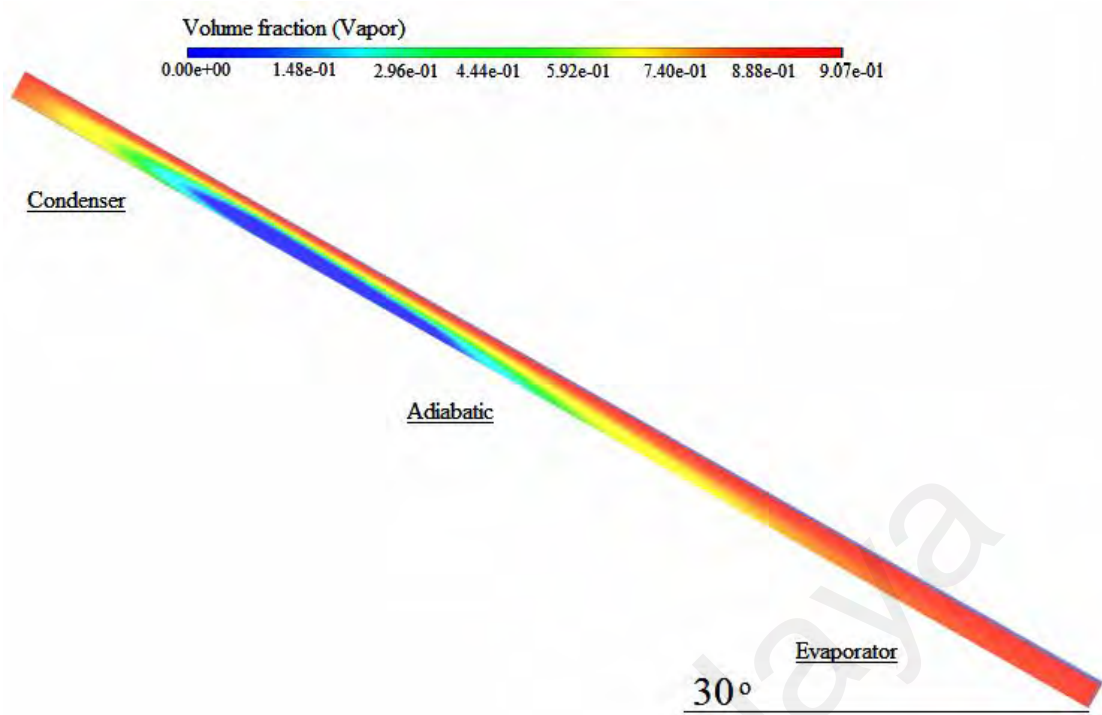
Figure 4-9: Volume fraction of vapor in 30 º title angle effected by 120 W.

Figure 4-10 indicated the velocity magnitude contours in the vapor chamber for 30 degrees and heated by 120 W, and the maximum fluid velocity is 0.174 m/s. It shows that velocity is zero at the start of the evaporator end, slowly grows towards the top of the adiabatic section and develops maximum at the beginning of adiabatic, and remains sustained along the adiabatic, and regularly decreases becomes zero at the condenser.
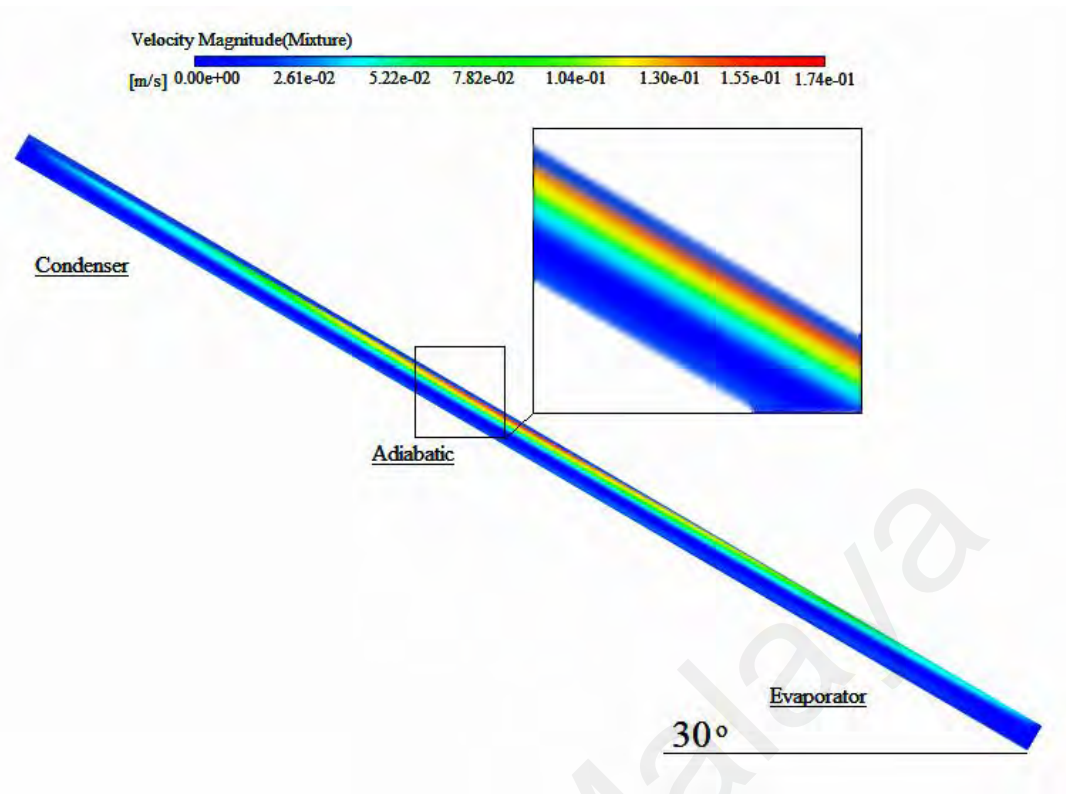
Figure 4-10: Velocity magnitude in 30 ° title angle effected by 120W.

.
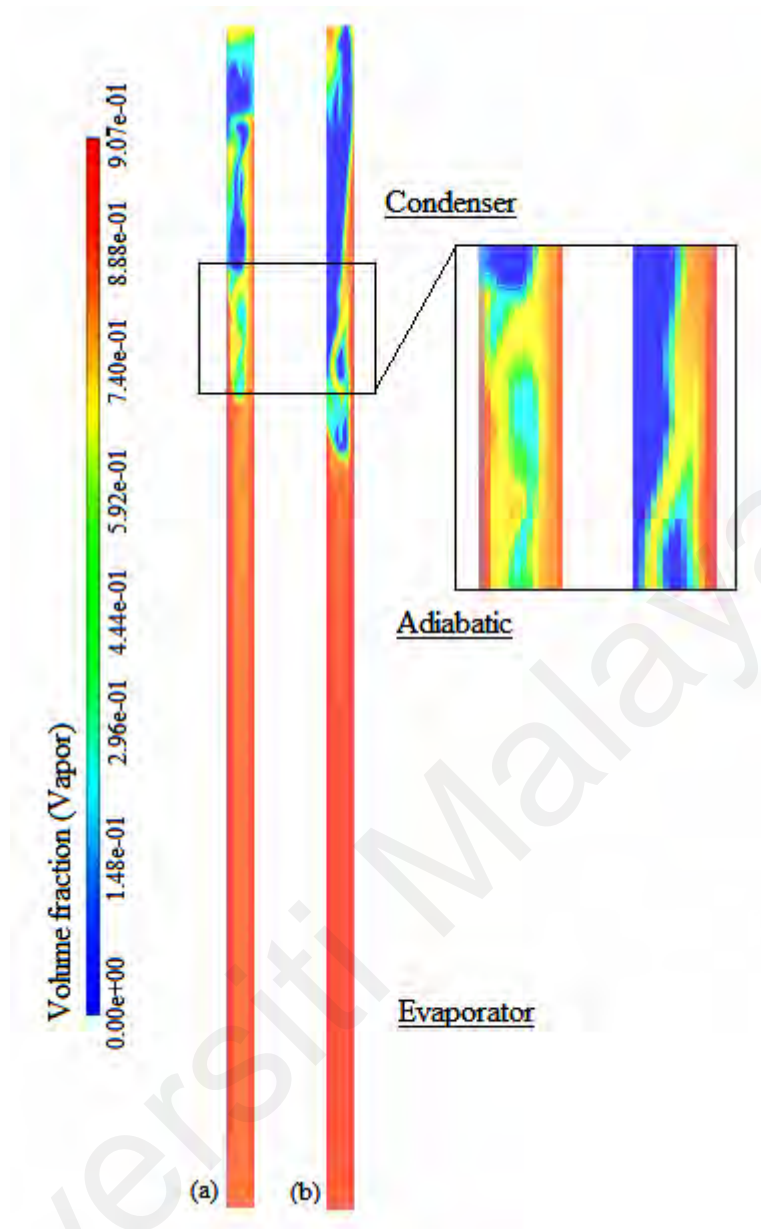
Figure 4-11: Volume fraction of vapor in 90 °title angle effected by heat input a)120 W, b)80 W.

In Figure 4-11, the volume fraction of vapor in 90° by heat pipe at working input power in the range 80–120 W. According to the volume fraction profile, the liquid phase is more on the condenser section. The gravity provides the maximum support to the liquid phase for simply return to the evaporator section at this angle. Results indicate that the heat pipe can transfer heat at any working position beside the horizontal position.

4.4   Experimental Result

4.4.1   Thermal Studies

The experimental investigations carried out a preliminary test through sintered heat pipes until they achieved the evaporator's dry-out conditions to determine their performance. Figure 4-12 a–d are shown the distributions of temperature at the outer surface of the heat pipe filled with DW as the reference working fluid for various tilt angles ($\theta = 0°, 30°, 60°, 90°$). The outer surface temperatures affect the heat transport's performance and capacity for the heat pipe that could be enhanced via a careful choice of a working fluid, heat pipe design, and incline angle. Due to the gravity effect on the working fluid, the temperature of the outer surface is minor at vertical ($\theta = 90°$) position than horizontal ($\theta = 0°$) position, as seen in Figure 4-12. The differences in temperature amongst the evaporator and the condenser sections steadily grow with developing the rate of heat input.

(a)

(b)

(c)
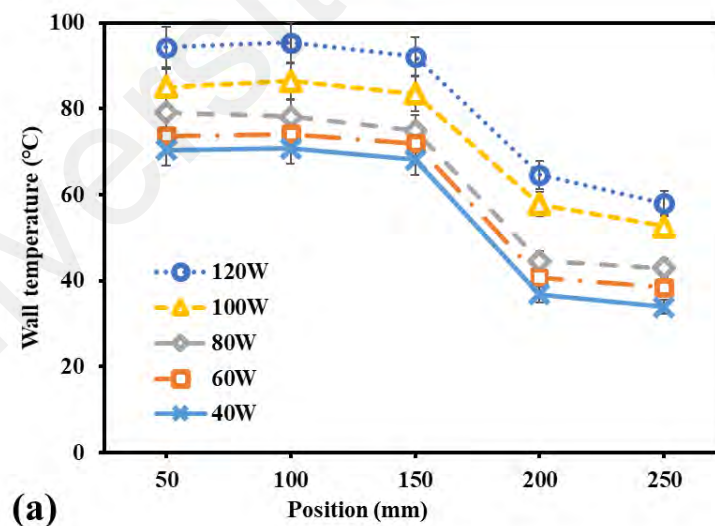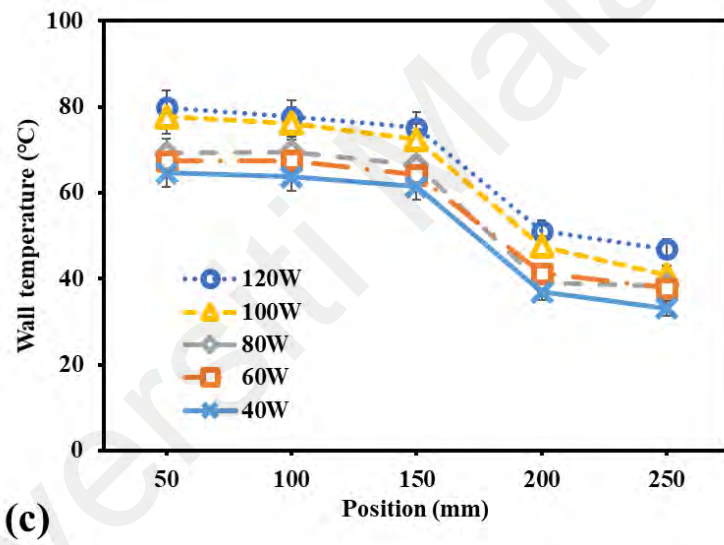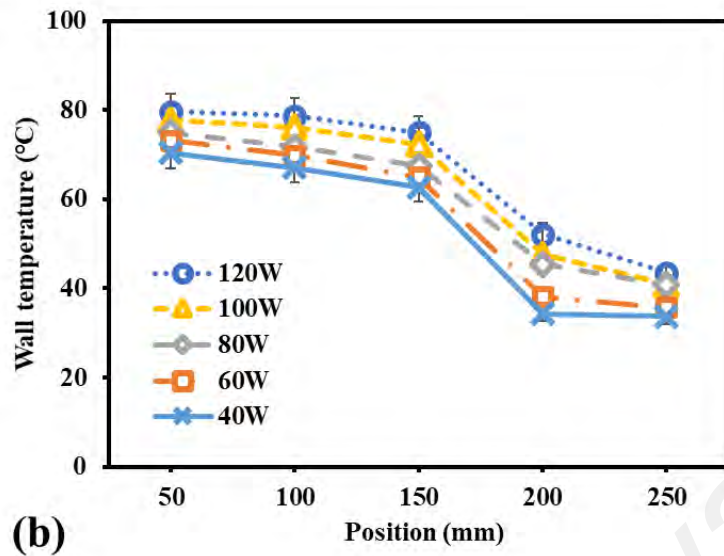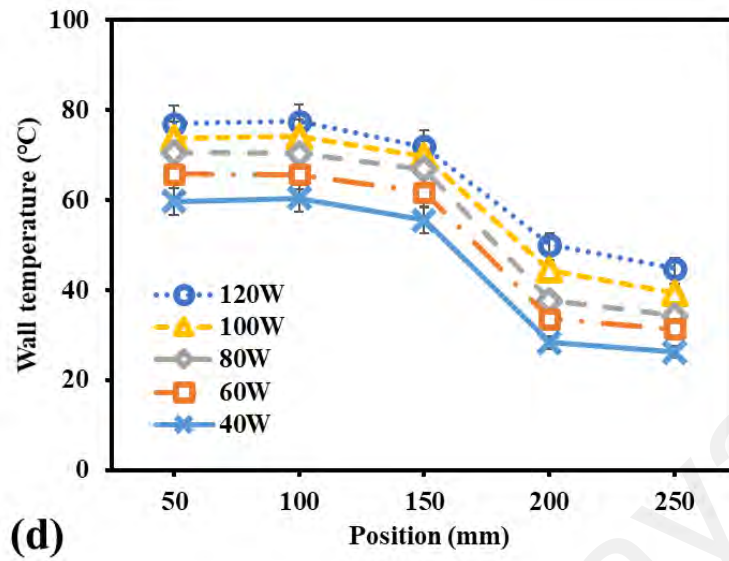
Figure 4-12: Average of distributions of temperature at the outer surface of the heat pipe that filled by distilled water (DW) for several heat power inputs and inclined angles (θ): (a) 0°, (b) 30°, (c) 60°, (d) 90°.

In the second part, a thermal performance study of heat pipes was carried out using different PCA-functionalized graphene nanofluids concentrations. Figure 4-13 illustrates the distribution of surface temperature for an input power of 40 W. The results show that the temperature of the outer wall surface varies for various PCA-functionalized graphene concentrations. It shows that the temperature difference between PCA-functionalized graphene nanofluid (concentrations of 0.06 mass%) and DW at the evaporator section is approximately 10 °C for an angle of θ = 0°. However, the temperature difference drops to 5.2 °C for θ = 90°.
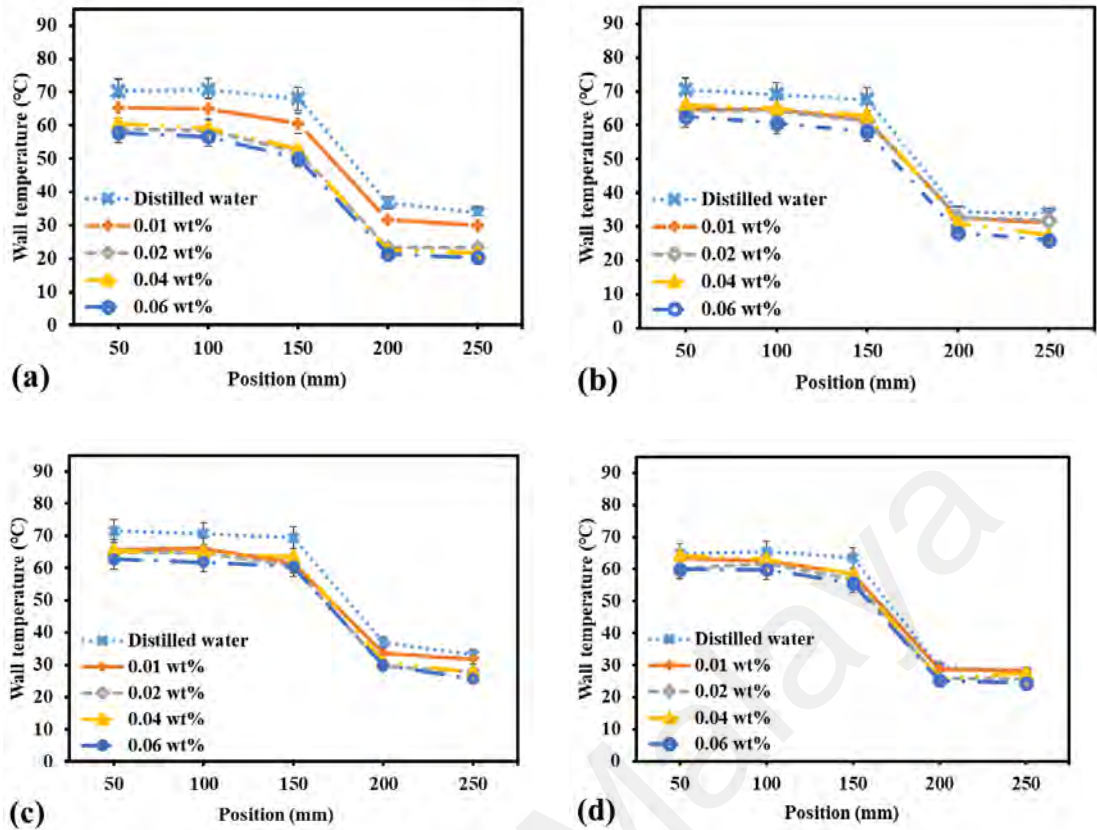
Figure 4-13: Effect of PCA-functionalized graphene nanofluid concentration on the distributions of temperature at the outer wall surface with a heat power input of 40W and tilt angles: (a) 0°, (b) 30°, (c) 60°, (d) 90°.

Figure 4-14 shows a representative result from tests held under different conditions. The dissimilarity of the temperature amongst evaporator and condenser sections at the outer surface temperature decreases to 30.5 °C with 40 W input power, 0.06 wt% concentration and $\theta = 90°$ (Figure 4-14 c) associated to the example of a DW working fluid; the temperature drops to 25 °C (Figure 4-14 a), at same input power. Furthermore, dry out conditions could be observed for the heat pipe working with DW at an input power of 120 W(Figure 4-14 b); on the other hand, the heat pipes with PCA-functionalized graphene nanofluids still working at the same input power (Figure 4-14 d). The dry-out condition occurs when the working fluids block by the bubbles to return to the evaporator section during the high heat flux. Furthermore, in the case of using DW with power input of 120W, HP evaporator reaches to close to 100 ^{o}C and works in a dry-out risk condition

(Figure 4-14 b). This condition usually occurs once the liquid and steam inside the HP are blocked at the condenser section and could not return to the evaporator. It is generally due to the high heat flux at the evaporator section and the boiling limit of working fluids (Mousa, 2011). In the similar heat input, the HP with 0.06% of nanofluid works properly without dry-out risk (Figure 4-14 d). However, the dry-out phenomenon could happen at any greater input power than the limitation of HP.

(a)

(b)
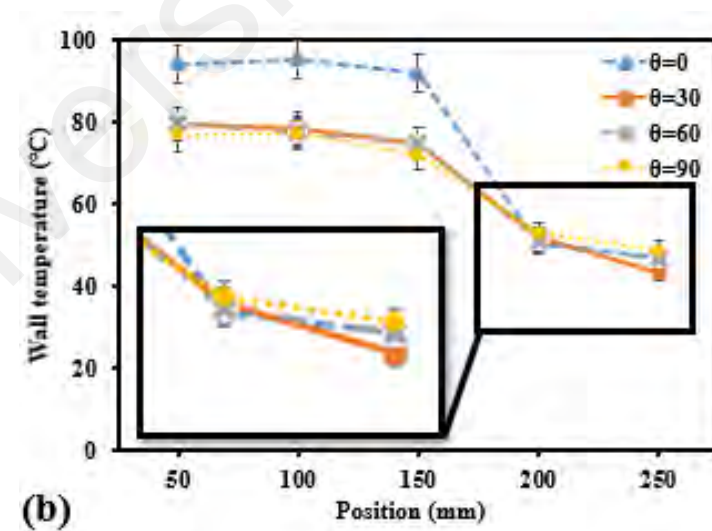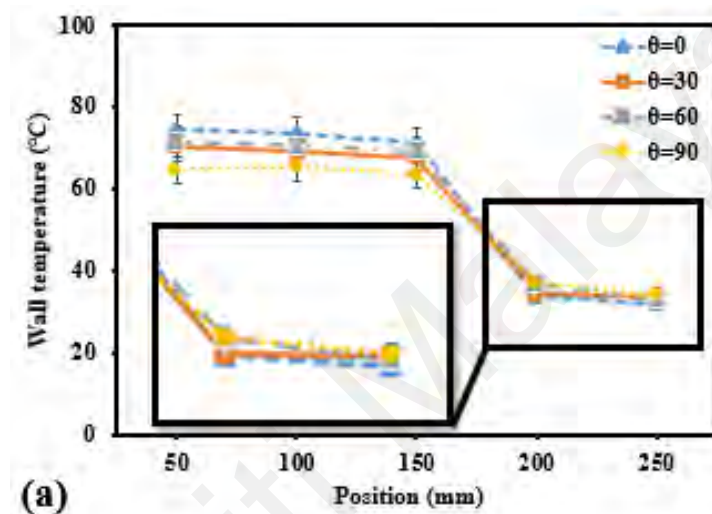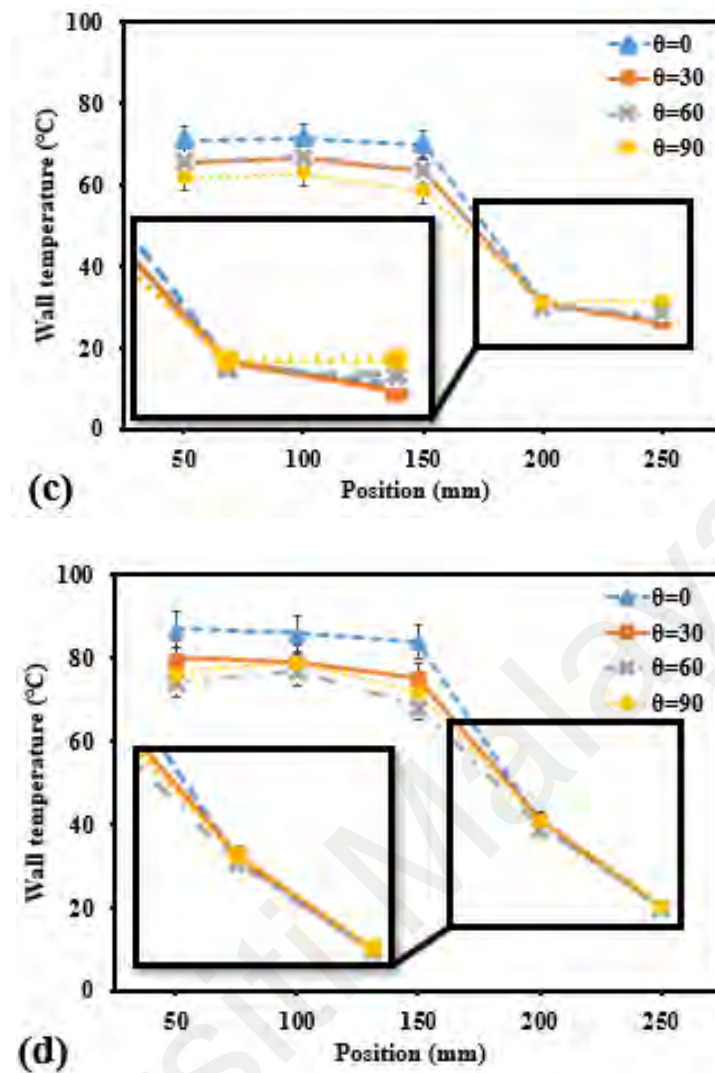
Figure 4-14: Average of distributions of temperature at the outer surface of heat pipe with a DW and 0.06 wt% PCA-functionalized graphene in different tilt angles, healing inputs; (a) DI-water, 40 W, (b) DI-water, 120 W, (c) 0.06 wt% PCA-functionalized graphene, 40 W, (d) 0.06 wt% PCA-functionalized graphene, 120 W.

4.4.2 Thermal efficiency of the heat pipe

Several heat inputs of 40, 60, 80, 100, and 120W were applied to estimate the heat pipe's thermal efficiency filled by PCA-functionalized graphene nanofluids besides DW. Figure 4-15 demonstrates the consequence of heat input on the thermal efficiency of the heat pipe for several tilt angles and various working fluids. The thermal efficiency rises with heat input since, at more extraordinary heat powers, the thermal resistance is minor.

In this example, the produced vapor bubbles freely burst through their fabrication due to contact with nanoparticle surfaces.
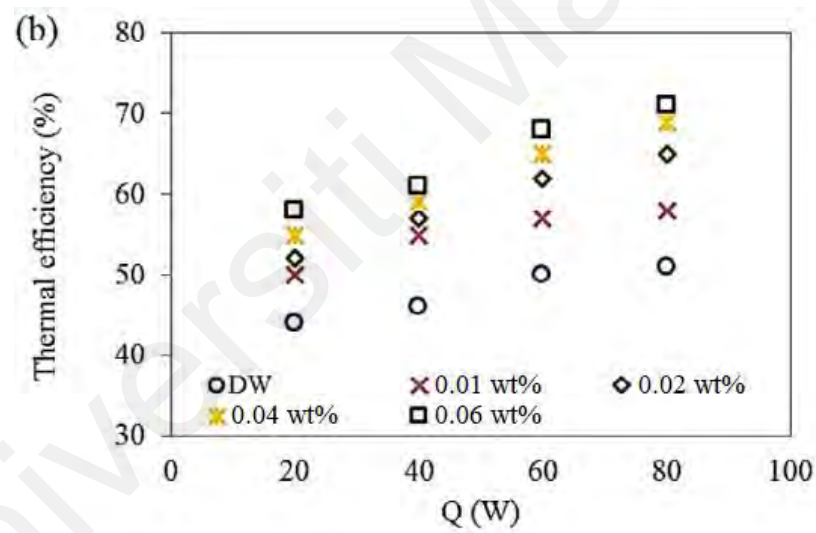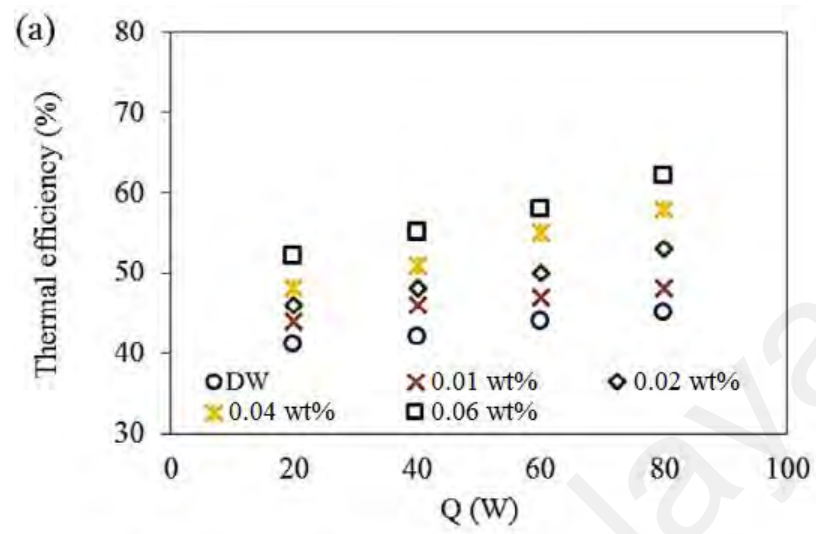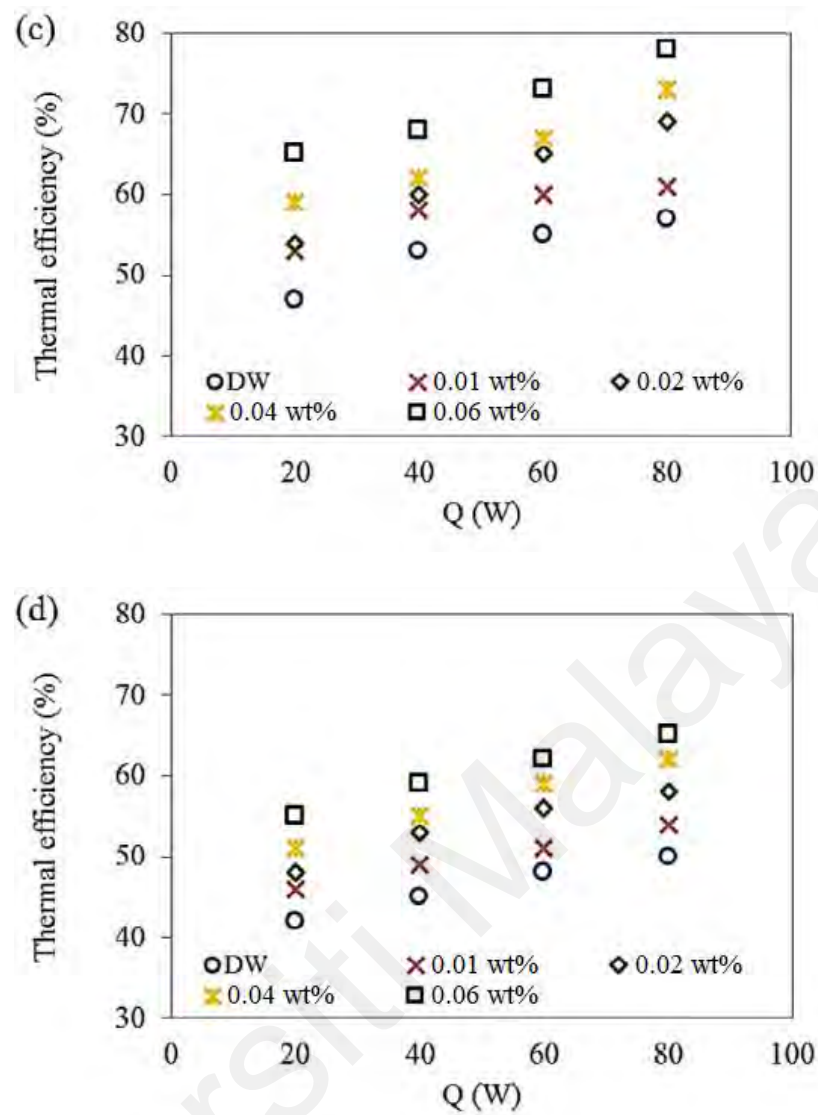
Figure 4-15: Thermal efficiency of heat pipe concerning heat input rate for four tilt angles (θ): (a) 0°, (b) 30°, (c) 60°, (d) 90°.

4.4.3   The thermal resistance of heat pipe

An evaluation of the total thermal resistance of PCA-functionalized graphene nanofluids at various concentrations and DW as working fluid is presented in Figure 4-16 with several power heat inputs. The thermal resistance of heat pipes is decreased with the enrichment of power input mostly. Instead, the thermal resistance drops significantly once the concentration of PCA-functionalized graphene increases. It is remarkable to remark that base fluids first have an excellent thermal conductivity to reduce the thermal

resistance, which was similarly performed again in PCA-functionalized graphene nanofluids at 0.01 wt% compared to an example at 0.06 wt% as shown in Figure 4-16.
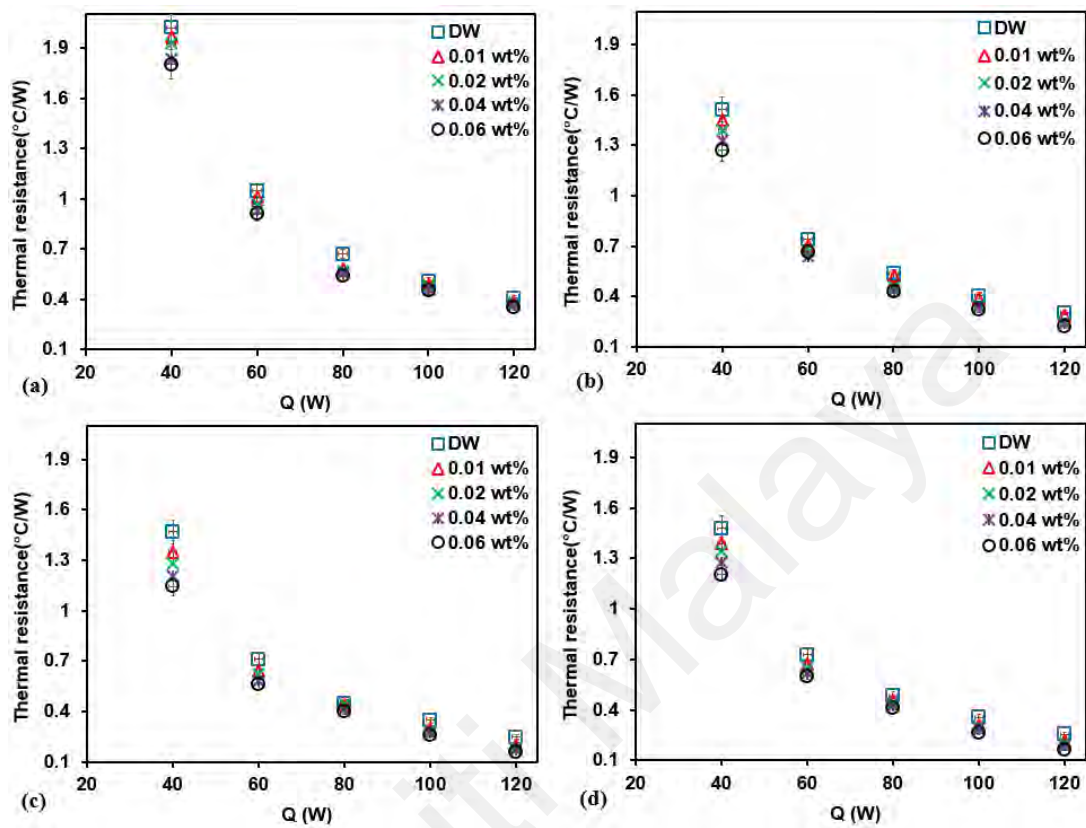
Figure 4-16: Effect of concentration of PCA-functionalized graphene nanofluid on the thermal resistance in different title angles of; (a) 0°, (b) 30°, (c) 60°, (d) 90°.

4.4.4   Heat transfer coefficient analyses

The overall heat transfer coefficient of heat pipe for DW and PCA-functionalized graphene nanofluid at several weight concentrations and various input heat powers were demonstrated in Figure 4-17, that shows the heat transfer coefficient growths with tilt angle and heat flux. Clearly, it illustrated that the tilt angle and heat flux have a significant influence on heat transfer coefficient. The most considerable improvement of heat transfer coefficient for the distilled water working fluid happens in $\theta = 90°$ and the heat flux of 38.4 kW/m^2, as shown in Figure 4-17 a.
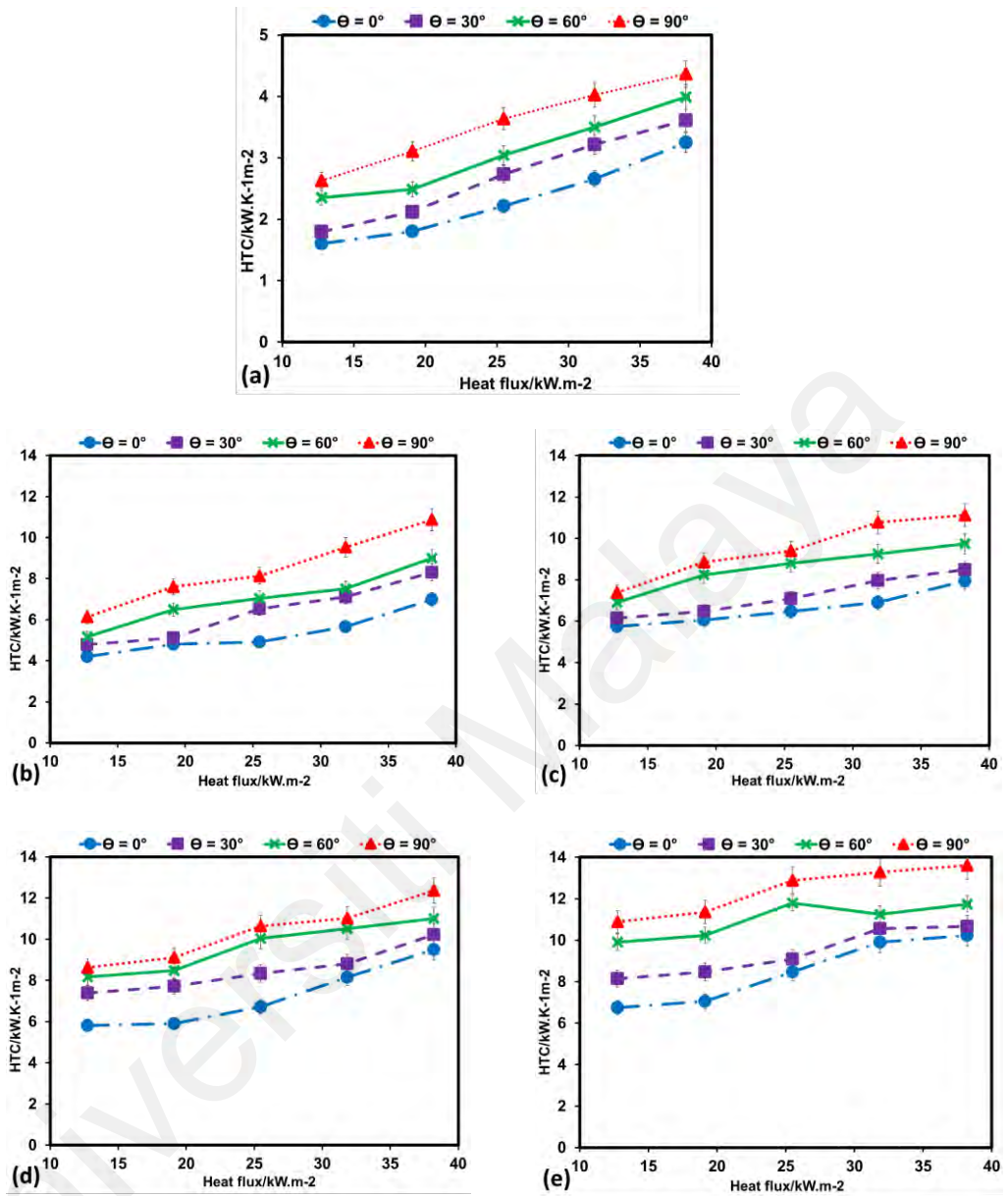
Figure 4-17: Incline angle effect on heat transfer coefficient in different working fluids; (a) DW, (b) 0.01 wt%, (c) 0.02 wt%, (d) 0.04 wt% , (e) 0.06 wt% .

4.5   Validation of CFD predicted results with experimental data

Figure 4-18 shows the comparison of numerical to experimental results for the heat pipe wall surface temperature. The heat input to the heaters was set to 100 W, and the tilt angle was set at 0 degrees. However, the heat removed by cooling water at the condenser section was calculated as 92.4 W with a discrepancy of ±14.5%. As shown in Figure 4-18, a good agreement is obtained among the simulation and experimental results.
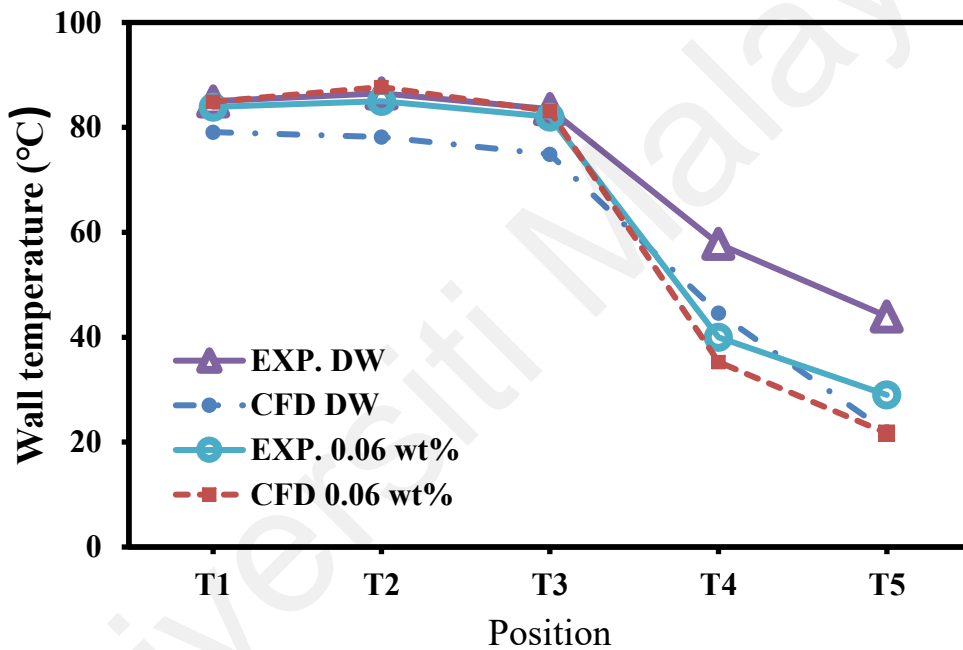
Figure 4-18: Comparison of numerical to experimental results at 0 degrees and 100W heat input condition.

CHAPTER 5: DISCUSSION

5.1   Nanofluid characterization

An accurate selection of working fluid conditions potentially promises to accomplish the HP with the highest performance at minimum diameters. Figure 4-1 indicates the thermal conductivity enhancement due to concentration change from 0.04 to 0.06 mass% is relatively higher than when it is changed from 0.02 to 0.04% mass%. The key mechanism for thermal conductivity improvement with rising temperature is attributed to the Brownian motion of the nanoparticles suspended in the base fluid (Fang et al., 2016). The possible reason for this variation could be the increased colloidal movement of nanoparticles at 0.06 mass%. The thermal conductivity improvement due to an increase in temperature is noteworthy. The results show that the thermal conductivity increased between 21% to 40% as concentration and temperature were increased (temperature range from 15 °C to 40 °C). The improvement in thermal conductivity with temperature is more workable in PCA-functionalized graphene nanofluids compare to the DW. Consequently, it confirms that the temperature has a significant impact on the growing thermal conductivity of nanofluid.

It could be observed in Figure 4-2 that the viscosity decreases for all concentrations with the increase of temperature. The result recommended that the nanofluid exhibited Newtonian behavior, and the viscosity of nanofluid reduced with temperature growing. Interestingly, there is not much variation in nanofluid viscosity, having 0.01 and 0.06 mass% nanoparticles, which indirectly assists in increasing the heat transfer rate. The viscosity of PCA-functionalized graphene nanofluids is decreased between 5 and 50% as the temperature increased from 20 °C to 60 °C. The friction and flowing resistance of fluids is enhanced by increasing PCA-functionalized graphene concentration, which eventually causes an increase in viscosity.

A noticeable thermal conductivity enhancement of hybrid nanofluids compared to normal nanofluids has been reported. However, the complex heat transfer and rheological mechanisms of hybrid nanofluids have not been sufficiently understood. So far, several types of hybrid nanoparticles have been investigated, such as: Al2O3/CNT, Cu–TiO2, CNT-Au and many more. Each nanoparticle presents its characteristics. The selection of nanoparticles is significant for the thermal conductivity and stability of hybrid nanofluids. This is because the combination of nanoparticles with better stability, but low thermal conductivity and better thermal conductivity might improve the thermal conductivity and stability of nanofluids. However, what nanomaterials and what proportion will contribute to the hybrid nanofluid exhibiting the best thermal performance is not yet clear.

After the nanofluid preparation, PCA would be bound to the graphene due to the $\pi - \pi$ connections between the pyrene moiety of PCA and the carbon rings of graphene. The dispersion of the GNPs in the solution improves by bounding between the GNP and the PCA. We can test the strength of this bounding by washing with DW. The PCA decorated GNPs experienced washing with DW and centrifugation for numerous rounds, and the content of PCA in the supernatants and the GNPs were analyzed. Figure 3-2 B shows that the color of supernatants fades willingly from dark to complete colorlessness representing an apparent decree of suspended GNPs in the supernatant with the number of washing cycles. Figure 4-5 shows the FTIR results that there was enough PCA agreement in the precipitated phase of the GNPs after washing cycles. Consequently, the measurements on both the supernatants and precipitates indicate that PCA can be bound to GNPs, forming a PCA–GNPs complex stable in an aqueous environment.

The stability of nanofluids is critical to maintaining the constant thermal performance of nanofluids and heat transfer performance of systems applied with nanofluids. The agglomeration tendency and sedimentation of nanoparticles increase with time, thus

thermal performance decreases with time. Numerous researches have focused on improving the stability, but the results are still undesirable. In addition, the effects of surfactant on thermo-physical performance (thermal conductivity and viscosity) of nanofluids are ambiguous. Some researchers report that although surfactants can improve the dispersion, they also cause the increment in viscosity and decrement in thermal conductivity. Others report that some surfactants improve the dispersion and thermal conductivity and increase viscosity only slightly and even present drag reduction.

5.2   Numerical Analysis

Numerical results associated with performance improvement of the heat pipe are discussed in this section.

The governing Equations (3-5) to (3-21) were numerically solved by considering all of the boundary and primary conditions. Heat power input sat at 40 W and 120 W. The preliminary pressure and temperature of the domain are presumed as 3778 Pascal and 20°C, separately (Soleymaniha, Amiri, Shanbedi, Chew, & Wongwises, 2018). The coolant fluid temperature or the free stream (T_c) is implicit as 20°C. For DW and 0.06 wt% PCA-functionalized graphene in the absence of the deposition of nanoparticles, the effective thermal conductivity of the wick is found to be 1.11 and 1.78 W/m-K, respectively. The adequate temperature difference between the heat source and the evaporator and the heat sink from the condenser is proportional to the system's overall heat transfer rate (Churchill & Bernstein, 1977). Figure 4-6 shows the predicted wall temperature distribution from the evaporator section to the condenser in different working angles and 40 W power input. The temperature difference between 0.06 wt% PCA-functionalized graphene nanofluid concentrations and DW at the evaporator section is approximately eight °C for an inclined angle of $\theta = 0°$. However, the temperatures of the

outer surface of the heat pipe occupied by PCA-functionalized graphene nanofluid for similar settings and an incline angle of $\theta = 90°$ are 4.1 ° C lower than while used DW as the working fluid.

The result associated with this comparison is shown in Figure 4-18 as well as the deviation. as claimed by this figure, the highest deviation is lesser than 6%, and therefore the numerical procedure is valid. The source of error can be attributed to the following factors:

- The temperatures at the condenser section measured by the surface thermocouples might be affected.
- The water flowing in the cooling jacket.
- The non-uniformity in the wick thickness.

5.3 Experimental Analysis

In the application of nanofluids in heat pipes, the main tasks include no appropriate standard for selecting the nanofluids in heat pipes, lack of comprehension of the time-dependent property of heat pipes charged with nanofluids and application of nanofluids in heat pipes restricted in terms of technology, economic and environment.

Comparing data in Figure 4.12 and Figure 4.13, the influences of concentration on the temperature are important than the input power's impact. With the enhancement of PCA-functionalized graphene nanofluid concentration, the temperature tends to drop, leading to thermal performance enhancement. Furthermore, all the wall points' steady temperatures show that the heat pipe was activated effectively at this amount of input power. This difference of temperature drops as incline angle modifications from $\theta = 90°$

to $\theta = 30°$ and then escalations as incline angle drops further to $\theta = 0°$. It shows that the gravity and wick capillary action toughly affect the outer surface temperature distribution.

The results indicate that the highest thermal efficiency of 79% was accomplished for the 0.06 wt% of PCA-functionalized graphene nanofluids at the power of 120 W and 60° tilt angle, demonstrating almost 49% enrichment compared to the DW at similar operational settings (Figure 4-15). Additionally, as the weight concentration of PCA-functionalized graphene nanofluids rises, the amount of thermal efficiency improved. It could be endorsed to the higher thermal conductivity of nanofluids with greater weight concentration of PCA-functionalized graphene nanofluids. Commonly, a higher grade of thermal efficiency (concerning input power) was achieved for all water-based nanofluids and deionized water at minor heat inputs in association with the greater input power (Thompson, Ma, & Wilson, 2011). Correspondingly, the input heat power improvement increases the heat pipe's thermal efficiency, though the growing trends to be contingent on the concentrations.

Additionally, Figure 4-16 indicates that gravity has a significant influence on thermal resistance. The outcomes have shown that the overall thermal resistance at 90° was lower than that at 0° for all the cases. Gravitational force is an actual parameter of the heat pipe's performance, as shown in Figure 4-16. The heat pipe's thermal resistance is located to its lower value at a vertical tilt angle in cooperation with PCA-functionalized graphene nanofluid and DW. The gravity effect has a critical influence on the thermal resistance of the heat pipe. This force is a fundamental parameter that affects the efficiency of the heat pipe. Figure 4-16 c shows the minimum value of the thermal resistance accrue at 60° degree for both working fluid.

Adding PCA-functionalized graphene to the distilled water raises the heat transfer coefficient of the heating section. The escalations of nanofluid concentration and heat flux

improved the heat transfer coefficient. From Figure 4-17 b to e, the most significant enrichment in the overall heat transfer coefficient was achieved using PCA-functionalized graphene nanofluid at 0.06 wt%. Furthermore, the gravity force expressively disturbs the heat transfer coefficient of the evaporator, while heat transfer coefficient escalation with incline angle from $\theta = 0°$ to $\theta = 90°$. Since different heat pipes have different structure characteristics, it is imperative to compare the heat transfer effect and mechanism of nanofluids in different types of heat pipes. The application of nanofluids in heat pipes can be divided into three categories based on working fluid reflux power, such as conventional heat pipe, pulsating heat pipe, and closed two-phase thermosyphon. In this section, the application of conventional nanofluids in heat pipes (conventional heat pipe, closed two-phase thermosyphon and pulsating heat pipe) is discussed. Some typical studies about the thermal conductivity of conventional nanofluids are summarized in Table 5-1.

Table 5-1: Comparison of applying conventional nanofluid in heat pipes.

Type of heat pipe	Type of nanofluids	Parameters affecting thermal behaviors						Maximum reduction of Thermal resistance
		Concentration	Thermal conductivity (W/m.K)	Viscosity (mPa.s)	Input power/w	Inclination	Filling ratio	
Sintered heat pipe (Sadeghinezhad et al., 2020)	DS-GNP/water	2vol%-5vol%	0.62–0.73	0.50–1.07	20–120	0–70	30%–60%	26.4%
Sintered heat pipe (Vijayakumar, Navaneethakrishnan, & Kumaresan, 2016)	CuO/water and Al_2O_3/water	0.5–1.5 wt%	0.613–0.645	0.36–0.88	10–160	0–90		26.4%
Sintered heat pipe (Wan et al., 2015)	Cu/water	1-2 wt%			25–150			21.7%

Helically-micro-grooved heat pipe (Aly, Elbalshouny, Abd El-Hameed, & Fatouh, 2017)	Al_2O_3/water				10–65	0–90	20%–80%	18.2%
Horizontal micro-grooved heat pipe (Yang, Liu, & Zhao, 2008)	CuO/water	0.5 wt%-2 wt%			10–100			39%
Micro-grooves heat pipe (Liu et al., 2010)	CuO/water	1 wt%	0.61–0.78	0.81–0.85		0–90	50%	50%
Mesh wick heat pipe (Mousa, 2011)	Al_2O_3/water	0.25 vol%-1.5vol%			10–60		20%–90%	40%

CHAPTER 6: CONCLUSION

A comprehensive investigation was carried out to understand the behavior of application of functionalized nanofluids at various concentrations ranging from 0.01 to 0.06 mass%, different tilt of HP and different heat input. The HPs' outer surface temperature was used to calculate thermal resistance, thermal efficiency, and the HP's overall heat transfer coefficient. The experiments and CFD results show how gravity affects gravity's heat transportability and wick heat pipe type at changing working position. The methodical experiments achieve the extreme surface temperature, efficiency, thermal resistance, and heat transfer coefficient of the heat pipe. following conclusions were made in this work:

1. The enhancement ranges of nanofluids' thermal conductivity are considered between 21% and 40% for the PCA-functionalized graphene nanofluid concentrations.

2. The viscosity of PCA-functionalized graphene nanofluids is decreased between 5 and 50% as the temperature is amplified from 20 °C to 60 °C which recommended that the nanofluid exhibited Newtonian behavior, and the viscosity of nanofluid reduced with temperature growing.

3. For the Inclination angle, larger values of angle amplified the gravity initiating a massive temperature reduction of the condenser, providing an exceptional return of the liquid working fluid from the condenser to the evaporator. A tilting angle of θ=90° produces the most excellent performance in every sample, emphasizing the significance of gravitational forces.

4. The Numerical Simulation of the heat pipe, heat transport limitations show that the critical limitations influencing the heat transfer ability of wick heat pipe are entrainment limitation, capillary limitation, and boiling limitation.

5. The result associated with comparison of the experimental data and the numerical technique claimed lower than 6% of deviation which validate the numerical data.

6. Results of the concentration of nanoparticles in the working fluid significantly influence the heat transfer. The extreme thermal efficiency of 79% was accomplished for the 0.06 wt% of PCA-functionalized graphene nanofluids at the power of 120 W, demonstrating nearly 49.4% improvement as associated with the DW at similar conditions.

7. The primary enrichment of the overall heat transfer coefficient was achieved using PCA-functionalized graphene nanofluid at 0.06 wt%.

As a result, the presence of PCA-functionalized graphene nanofluids decreased the thermal resistance and amplified the heat transfer coefficient of the heating section and potentially could lead to decrease its size for the same operating conditions.

6.1 Opportunities for future works

To tackle the above conclusions, further opportunities for future research and development are identified and these are outlined below:

1. Opportunities in the properties of nanofluid

Given the current development status and challenges, the solutions for the properties of nanofluids are outlined as, exploring the thermo- physical properties of nanofluids and establishing unified standards, improving the stability of nanofluids, and investigating the heat transfer mechanism and characteristics of hybrid nanofluids.

2. Improving the stability of nanofluids

The stability of nanofluids is crucial to the long-term performance of heat pipes charged with nanofluids. More research is needed to explore the effect of surfactants on nanofluids.

3. Opportunities in the application of nanofluids in heat pipes

Given the current development status and challenges, the solutions for the application of nanofluids in heat pipes are outlined as, using advanced nanoparticles and conducting more systematic investigations, focusing on the nanoparticle deposition layer and life expectancy of heat pipes, and developing the heat pipes charged with nanofluids in technical, economic and environmental aspects.

4. Developing the heat pipes charged with nanofluids in technical, economic and environmental aspects

Before thermal systems applied with heat pipes and nanofluids transform from small-scale experiments to large-scale industrial production, the reliability of thermal systems must be evaluated in technical, economic and environmental aspects. Unified technical and evaluation standards should be formulated to promote mass production of heat pipes charged with nanofluids. More attention should be paid on low-cost production techniques which could provide great thermal performance of nanofluids. In addition, natural non-toxic and non- polluting nanoparticles are encouraged for the investigation, and green technologies should also be developed for preparation of nanoparticles or nanofluids.

REFERENCES

Aghvami, M., & Faghri, A. (2011). Analysis of flat heat pipes with various heating and cooling configurations. *Applied Thermal Engineering, 31*(14-15), 2645-2655.

Ahn, H. S., & Kim, M. H. (2012). A review on critical heat flux enhancement with nanofluids and surface modification. *Journal of Heat Transfer, 134*(2), 024001.

Ajarostaghi, S. S. M., Zaboli, M., & Nourbakhsh, M. (2021). Numerical evaluation of turbulence heat transfer and fluid flow of hybrid nanofluids in a pipe with innovative vortex generator. *Journal of Thermal Analysis and Calorimetry, 143*(2), 1583-1597.

Akbari, A., & Saidi, M. H. (2019). Experimental investigation of nanofluid stability on thermal performance and flow regimes in pulsating heat pipe. *Journal of Thermal Analysis and Calorimetry, 135*(3), 1835-1847.

Alizad, K., Vafai, K., & Shafahi, M. (2012). Thermal performance and operational attributes of the startup characteristics of flat-shaped heat pipes using nanofluids. *International Journal of Heat and Mass Transfer, 55*(1-3), 140-155.

Aly, W. I., Elbalshouny, M. A., Abd El-Hameed, H., & Fatouh, M. (2017). Thermal performance evaluation of a helically-micro-grooved heat pipe working with water and aqueous Al2O3 nanofluid at different inclination angle and filling ratio. *Applied Thermal Engineering, 110*, 1294-1304.

Annamalai, S. A., & Ramalingam, V. (2011). Experimental investigation and CFD analysis of a air cooled condenser heat pipe. *Thermal Science, 15*(3), 759-772.

Asirvatham, L. G., Nimmagadda, R., & Wongwises, S. (2013). Operational limitations of heat pipes with silver-water nanofluids. *Journal of Heat Transfer, 135*(11), 111011.

Bahmanabadi, A., Faegh, M., & Shafii, M. B. (2020). Experimental examination of utilizing novel radially grooved surfaces in the evaporator of a thermosyphon heat pipe. *Applied Thermal Engineering, 169*, 114975.

Bankston, C., & Smith, H. (1973). Vapor flow in cylindrical heat pipes. *Journal of Heat Transfer, 95*(3), 371-376.

Cai, Q., & Chen, Y.-C. (2012). Investigations of biporous wick structure dryout. *Journal of Heat Transfer, 134*(2), 021503.

Cao, Y., & Faghri, A. (1991). Transient two-dimensional compressible analysis for high-temperature heat pipes with pulsed heat input. *Numerical heat transfer, 18*(4), 483-502.

Cao, Y., & Faghri, A. (1993). A numerical analysis of high-temperature heat pipe startup from the frozen state. *Journal of Heat Transfer, 115*(1), 247-254.

Chen, J.-S., & Chou, J.-H. (2015). The length and bending angle effects on the cooling performance of flat plate heat pipes. *International Journal of Heat and Mass Transfer, 90*, 848-856.

Chen, M.-M., & Faghri, A. (1990). An analysis of the vapor flow and the heat conduction through the liquid-wick and pipe wall in a heat pipe with single or multiple heat sources. *International Journal of Heat and Mass Transfer, 33*(9), 1945-1955.

Cheng, P., Dong, J., Thompson, S., & Ma, H. (2012). Heat transfer in the bulk and thin film fluid regions of a rectangular micro groove. *Journal of Thermophysics and Heat Transfer, 26*(1), 108-114.

Chu, S., Bai, F., Cui, Z., Nie, F., & Diao, Y. (2020). Experimental investigation on thermal performance of a heat pipe pressurized air receiver. *Applied Thermal Engineering, 165*, 114551.

Churchill, S., & Bernstein, M. (1977). A correlating equation for forced convection from gases and liquids to a circular cylinder in crossflow.

Cleveland, C., Moghaddam, S., & Orazem, M. E. (2014). Nanometer-scale corrosion of copper in de-aerated deionized water. *Journal of The Electrochemical Society, 161*(3), C107-C114.

De Kerpel, K., De Schampheleire, S., Steuperaert, H., De Jaeger, P., & De Paepe, M. (2016). Experimental study of the effect of felt wick porosity on capillary-driven heat pipes. *Applied Thermal Engineering, 96*, 690-698.

De Schampheleire, S., De Kerpel, K., Deruyter, T., De Jaeger, P., & De Paepe, M. (2015). Experimental study of small diameter fibres as wick material for capillary-driven heat pipes. *Applied Thermal Engineering, 78*, 258-267.

Deng, D., Tang, Y., Huang, G., Lu, L., & Yuan, D. (2013). Characterization of capillary performance of composite wicks for two-phase heat transfer devices. *International Journal of Heat and Mass Transfer, 56*(1-2), 283-293.

Do, K. H., Ha, H. J., & Jang, S. P. (2010). Thermal resistance of screen mesh wick heat pipes using the water-based Al2O3 nanofluids. *International Journal of Heat and Mass Transfer, 53*(25-26), 5888-5894.

Do, K. H., & Jang, S. P. (2010). Effect of nanofluids on the thermal performance of a flat micro heat pipe with a rectangular grooved wick. *International Journal of Heat and Mass Transfer, 53*(9-10), 2183-2192.

Duangthongsuk, W., Yiamsawasd, T., Selim Dalkilic, A., & Wongwises, S. (2013). Pool-boiling heat transfer characteristics of Al2O3-water nanofluids on a horizontal cylindrical heating surface. *Current Nanoscience, 9*(1), 56-60.

El-Nasr, A. A., & El-Haggar, S. (1996). Effective thermal conductivity of heat pipes. *Heat and Mass Transfer, 32*(1), 97-101.

Faghri, A. (1995). *Heat pipe science and technology*: Global Digital Press.

Faghri, A. (2014). Heat pipes: review, opportunities and challenges. *Frontiers in Heat Pipes (FHP), 5*(1).

Faghri, A., Buchko, M., & Cao, Y. (1991a). A study of high-temperature heat pipes with multiple heat sources and sinks: Part I—Experimental methodology and frozen startup profiles. *Journal of Heat Transfer, 113*(4), 1003-1009.

Faghri, A., Buchko, M., & Cao, Y. (1991b). A Study of High-Temperature Heat Pipes With Multiple Heat Sources and Sinks: Part II—Analysis of Continuum Transient and Steady-State Experimental Data With Numerical Predictions. *Journal of Heat Transfer, 113*(4), 1010-1016.

Faghri, A., & Chen, M.-M. (1989). A numerical analysis of the effects of conjugate heat transfer, vapor compressibility, and viscous dissipation in heat pipes. *Numerical heat transfer, 16*(3), 389-405.

Faghri, A., & Parvani, S. (1988). Numerical analysis of laminar flow in a double-walled annular heat pipe. *Journal of Thermophysics and Heat Transfer, 2*(2), 165-171.

Fang, X., Chen, Y., Zhang, H., Chen, W., Dong, A., & Wang, R. (2016). Heat transfer and critical heat flux of nanofluid boiling: a comprehensive review. *Renewable and Sustainable Energy Reviews, 62*, 924-940.

Franchi, G., & Huang, X. (2008). Development of composite wicks for heat pipe performance enhancement. *Heat Transfer Engineering, 29*(10), 873-884.

Ghanbarpour, M., Nikkam, N., Khodabandeh, R., Toprak, M. S., & Muhammed, M. (2015). Thermal performance of screen mesh heat pipe with Al2O3 nanofluid. *Experimental thermal and fluid science, 66*, 213-220.

Ghosh, S., An, X., Shah, R., Rawat, D., Dave, B., Kar, S., & Talapatra, S. (2012). Effect of 1-pyrene carboxylic-acid functionalization of graphene on its capacitive energy storage. *The Journal of Physical Chemistry C, 116*(39), 20688-20693.

Goodarzi, M., Rashidi, M. M., & Basiriparsa, A. (2012). Analytical and numerical solutions of vapor flow in a flat plate heat pipe. *Walailak Journal of Science and Technology (WJST), 9*(1), 65-81.

Gorji, T. B., & Ranjbar, A. (2017). Thermal and exergy optimization of a nanofluid-based direct absorption solar collector. *Renewable Energy, 106*, 274-287.

Gupta, M., Singh, V., Kumar, S., Kumar, S., Dilbaghi, N., & Said, Z. (2018). Up to date review on the synthesis and thermophysical properties of hybrid nanofluids. *Journal of cleaner production, 190*, 169-192.

Gürbüz, E. Y., Sözen, A., Variyenli, H. İ., Khanlari, A., & Tuncer, A. D. (2020). A comparative study on utilizing hybrid-type nanofluid in plate heat exchangers with different number of plates. *Journal of the Brazilian Society of Mechanical Sciences and Engineering, 42*(10), 1-13.

Hajian, R., Layeghi, M., & Sani, K. A. (2012). Experimental study of nanofluid effects on the thermal performance with response time of heat pipe. *Energy Conversion and Management, 56*, 63-68.

Hoseinzadeh, S., Heyns, P. S., Chamkha, A., & Shirkhani, A. (2019). Thermal analysis of porous fins enclosure with the comparison of analytical and numerical methods. *Journal of Thermal Analysis and Calorimetry, 138*(1), 727-735.

Hwang, G., Fleming, E., Carne, B., Sharratt, S., Nam, Y., Dussinger, P., . . . Kaviany, M. (2011). Multi-artery heat-pipe spreader: Lateral liquid supply. *International Journal of Heat and Mass Transfer, 54*(11-12), 2334-2340.

Jang, J. H., Faghri, A., & Chang, W. S. (1989). Analysis of the transient compressible vapor flow in heat pipe: National Aeronautics and Space Administration, Cleveland, OH (United States ….

Jiang, L.-l., Tang, Y., Wu, H.-y., Zhou, W., & Jiang, L.-z. (2014). Fabrication and thermal performance of grooved-sintered wick heat pipe. *Journal of Central South University, 21*(2), 668-676.

Kang, S.-W., Wei, W.-C., Tsai, S.-H., & Huang, C.-C. (2009). Experimental investigation of nanofluids on sintered heat pipe thermal performance. *Applied Thermal Engineering, 29*(5-6), 973-979.

Kang, S.-W., Wei, W.-C., Tsai, S.-H., & Yang, S.-Y. (2006). Experimental investigation of silver nano-fluid on heat pipe thermal performance. *Applied Thermal Engineering, 26*(17-18), 2377-2382.

Kaya, M., Gürel, A. E., Ağbulut, Ü., Ceylan, İ., Çelik, S., Ergün, A., & Acar, B. (2019). Performance analysis of using CuO-Methanol nanofluid in a hybrid system with concentrated air collector and vacuum tube heat pipe. *Energy Conversion and Management, 199*, 111936.

Kaya, T., & Goldak, J. (2007). Three-dimensional numerical analysis of heat and mass transfer in heat pipes. *Heat and Mass Transfer, 43*(8), 775-785.

Kempers, R., Ewing, D., & Ching, C. (2006). Effect of number of mesh layers and fluid loading on the performance of screen mesh wicked heat pipes. *Applied Thermal Engineering, 26*(5-6), 589-595.

Khalili, M., & Shafii, M. (2016). Experimental and numerical investigation of the thermal performance of a novel sintered-wick heat pipe. *Applied Thermal Engineering, 94*, 59-75.

Khrustalev, D., & Faghri, A. (1996). Enhanced flat miniature axially grooved heat pipe. *Journal of Heat Transfer, 118*(1), 261-264.

Kim, H. D., & Kim, M. H. (2007). Effect of nanoparticle deposition on capillary wicking that influences the critical heat flux in nanofluids. *Applied physics letters, 91*(1), 014104.

Kim, K. M., Jeong, Y. S., Kim, I. G., & Bang, I. C. (2015). Comparison of thermal performances of water-filled, SiC nanofluid-filled and SiC nanoparticles-coated heat pipes. *International Journal of Heat and Mass Transfer, 88*, 862-871.

Kiseev, V., & Sazhin, O. (2019). Heat transfer enhancement in a loop thermosyphon using nanoparticles/water nanofluid. *International Journal of Heat and Mass Transfer, 132*, 557-564.

Koito, Y., Imura, H., Mochizuki, M., Saito, Y., & Torii, S. (2006). Numerical analysis and experimental verification on thermal fluid phenomena in a vapor chamber. *Applied Thermal Engineering, 26*(14-15), 1669-1676.

Kole, M., & Dey, T. (2013). Thermal performance of screen mesh wick heat pipes using water-based copper nanofluids. *Applied Thermal Engineering, 50*(1), 763-770.

Kumaresan, G., Venkatachalapathy, S., Asirvatham, L. G., & Wongwises, S. (2014). Comparative study on heat transfer characteristics of sintered and mesh wick heat pipes using CuO nanofluids. *International Communications in Heat and Mass Transfer, 57*, 208-215.

Layeghi, M., & Nouri-Borujerdi, A. (2004). Vapor flow analysis in partially-heated concentric annular heat pipes. *International Journal of Computational Engineering Science, 5*(01), 235-244.

Li, Y., He, H.-f., & Zeng, Z.-x. (2013). Evaporation and condensation heat transfer in a heat pipe with a sintered-grooved composite wick. *Applied Thermal Engineering, 50*(1), 342-351.

Li, Y., Zhou, W., He, J., Yan, Y., Li, B., & Zeng, Z. (2016). Thermal performance of ultra-thin flattened heat pipes with composite wick structure. *Applied Thermal Engineering, 102*, 487-499.

Lin, Y.-H., Kang, S.-W., & Chen, H.-L. (2008). Effect of silver nano-fluid on pulsating heat pipe thermal performance. *Applied Thermal Engineering, 28*(11-12), 1312-1317.

Liu, Z.-H., & Li, Y.-Y. (2012). A new frontier of nanofluid research–application of nanofluids in heat pipes. *International Journal of Heat and Mass Transfer, 55*(23-24), 6786-6797.

Liu, Z.-H., Li, Y.-Y., & Bao, R. (2010). Thermal performance of inclined grooved heat pipes using nanofluids. *International journal of thermal sciences, 49*(9), 1680-1687.

Lohrasbi, S., Gorji-Bandpy, M., & Ganji, D. D. (2017). Thermal penetration depth enhancement in latent heat thermal energy storage system in the presence of heat pipe based on both charging and discharging processes. *Energy Conversion and Management, 148*, 646-667.

Ma, H., Wilson, C., Borgmeyer, B., Park, K., Yu, Q., Choi, S., & Tirumala, M. (2006). Effect of nanofluid on the heat transport capability in an oscillating heat pipe. *Applied physics letters, 88*(14), 143116.

Mahdavi, M. (2016). *Numerical and experimental analysis of heat pipes with application in concentrated solar power systems*: Temple University.

Maheshkumar, P., & Muraleedharan, C. (2011). Minimization of entropy generation in flat heat pipe. *International Journal of Heat and Mass Transfer, 54*(1-3), 645-648.

Mangal, D., Lamba, D. K., Gupta, T., & Jhamb, K. (2010). Acknowledgement of evacuated tube solar water heater over flat plate solar water heater. *International Journal of Engineering (IJE), 4*(4), 279.

Mehrali, M., Sadeghinezhad, E., Latibari, S. T., Kazi, S. N., Mehrali, M., Zubir, M. N. B. M., & Metselaar, H. S. C. (2014). Investigation of thermal conductivity and rheological properties of nanofluids containing graphene nanoplatelets. *Nanoscale research letters, 9*(1), 15.

Menlik, T., Sözen, A., Gürü, M., & Öztaş, S. (2015). Heat transfer enhancement using MgO/water nanofluid in heat pipe. *Journal of the Energy Institute, 88*(3), 247-257.

Min, D., Hwang, G., & Kaviany, M. (2009). Multi-artery, heat-pipe spreader. *International Journal of Heat and Mass Transfer, 52*(3-4), 629-635.

Moradgholi, M., Nowee, S. M., & Farzaneh, A. (2018). Experimental study of using Al2O3/methanol nanofluid in a two phase closed thermosyphon (TPCT) array as a novel photovoltaic/thermal system. *Solar Energy, 164*, 243-250.

Mousa, M. (2011). Effect of nanofluid concentration on the performance of circular heat pipe. *Ain Shams Engineering Journal, 2*(1), 63-69.

Mousavi Ajarostaghi, S. S., Shirzad, M., Rashidi, S., & Li, L. K. (2020). Heat transfer performance of a nanofluid-filled tube with wall corrugations and center-cleared twisted-tape inserts. *Energy Sources, Part A: Recovery, Utilization, and Environmental Effects*, 1-21.

Naemsai, T., Kammuang-lue, N., Terdtoon, P., & Sakulchangsatjatai, P. (2019). Numerical model of heat transfer characteristics for sintered-grooved wick heat pipes under non-uniform heat loads. *Applied Thermal Engineering, 148*, 886-896.

Naphon, P., Assadamongkol, P., & Borirak, T. (2008). Experimental investigation of titanium nanofluids on the heat pipe thermal efficiency. *International Communications in Heat and Mass Transfer, 35*(10), 1316-1319.

Noh, H. K., & Song, K. S. (1998). Temperature distribution of a low temperature heat pipe with multiple heaters for electronic cooling. *ETRI journal, 20*(4), 380-394.

Ooijen, H. v., & Hoogendoorn, C. (1979). Vapor flow calculations in a flat-plate heat pipe. *AIAA Journal, 17*(11), 1251-1259.

Park, J. H. (1997). A study on thermal performance of heat pipe for optimum placement of satellite equipment. *ETRI journal, 19*(2), 59-70.

Peyghambarzadeh, S., Shahpouri, S., Aslanzadeh, N., & Rahimnejad, M. (2013). Thermal performance of different working fluids in a dual diameter circular heat pipe. *Ain Shams Engineering Journal, 4*(4), 855-861.

Plawsky, J., Fedorov, A., Garimella, S., Ma, H., Maroo, S., Chen, L., & Nam, Y. (2014). Nano-and microstructures for thin-film evaporation—A review. *Nanoscale and microscale thermophysical engineering, 18*(3), 251-269.

Pooyoo, N., Kumar, S., Charoensuk, J., & Suksangpanomrung, A. (2014). Numerical simulation of cylindrical heat pipe considering non-Darcian transport for liquid flow inside wick and mass flow rate at liquid–vapor interface. *International Journal of Heat and Mass Transfer, 70*, 965-978.

Quan, X., Wang, D., & Cheng, P. (2017). An experimental investigation on wettability effects of nanoparticles in pool boiling of a nanofluid. *International Journal of Heat and Mass Transfer, 108*, 32-40.

Ramezanizadeh, M., Alhuyi Nazari, M., Ahmadi, M. H., & Chau, K.-w. (2019). Experimental and numerical analysis of a nanofluidic thermosyphon heat exchanger. *Engineering Applications of Computational Fluid Mechanics, 13*(1), 40-47.

Ranjan, R., Garimella, S. V., Murthy, J. Y., & Yazawa, K. (2011). Assessment of nanostructured capillary wicks for passive two-phase heat transport. *Nanoscale and microscale thermophysical engineering, 15*(3), 179-194.

Ranjan, R., Murthy, J. Y., Garimella, S. V., & Vadakkan, U. (2011). A numerical model for transport in flat heat pipes considering wick microstructure effects. *International Journal of Heat and Mass Transfer, 54*(1-3), 153-168.

Ranjan, R., Patel, A., Garimella, S. V., & Murthy, J. Y. (2012). Wicking and thermal characteristics of micropillared structures for use in passive heat spreaders. *International Journal of Heat and Mass Transfer, 55*(4), 586-596.

Reilly, S. (2013). *Optimization of Phase Change Heat Transfer in Biporous Media.* UCLA.

Sadeghinezhad, E., Akhiani, A. R., Metselaar, H. S. C., Latibari, S. T., Mehrali, M., & Mehrali, M. (2020). Parametric study on the thermal performance enhancement of a thermosyphon heat pipe using covalent functionalized graphene nanofluids. *Applied Thermal Engineering, 175*, 115385.

Sadeghinezhad, E., Mehrali, M., Saidur, R., Mehrali, M., Latibari, S. T., Akhiani, A. R., & Metselaar, H. S. C. (2016). A comprehensive review on graphene nanofluids: recent research, development and applications. *Energy Conversion and Management, 111*, 466-487.

Sadri, R., Ahmadi, G., Togun, H., Dahari, M., Kazi, S. N., Sadeghinezhad, E., & Zubir, N. (2014). An experimental study on thermal conductivity and viscosity of nanofluids containing carbon nanotubes. *Nanoscale research letters, 9*(1), 151.

Schonberg, J., DasGupta, S., & Wayner Jr, P. (1995). An augmented Young-Laplace model of an evaporating meniscus in a microchannel with high heat flux. *Experimental thermal and fluid science, 10*(2), 163-170.

Semenic, T., & Catton, I. (2009). Experimental study of biporous wicks for high heat flux applications. *International Journal of Heat and Mass Transfer, 52*(21-22), 5113-5121.

Senthilkumar, R., Vaidyanathan, S., & Sivaraman, B. (2012). Effect of inclination angle in heat pipe performance using copper nanofluid. *Procedia engineering, 38*, 3715-3721.

Seo, J., Bang, I.-C., & Lee, J.-Y. (2016). Length effect on entrainment limit of large-L/D vertical heat pipe. *International Journal of Heat and Mass Transfer, 97*, 751-759.

Septiadi, W., Putra, N., Juarsa, M., Putra, I., & Sahmura, R. (2013). Characteristics of screen mesh wick heat pipe with nano-fluid as passive cooling system. *Atom Indonesia, 39*(1), 24-31.

Shabgard, H., & Faghri, A. (2011). Performance characteristics of cylindrical heat pipes with multiple heat sources. *Applied Thermal Engineering, 31*(16), 3410-3419.

Shafieian, A., Khiadani, M., & Nosrati, A. (2019). Thermal performance of an evacuated tube heat pipe solar water heating system in cold season. *Applied Thermal Engineering, 149*, 644-657.

Sharifi, N., Bergman, T. L., Allen, M. J., & Faghri, A. (2014). Melting and solidification enhancement using a combined heat pipe, foil approach. *International Journal of Heat and Mass Transfer, 78*, 930-941.

Sobhan, C., Garimella, S., & Unnikrishnan, V. (2000). *A computational model for the transient analysis of flat heat pipes.* Paper presented at the ITHERM 2000. The Seventh Intersociety Conference on Thermal and Thermomechanical Phenomena in Electronic Systems (Cat. No. 00CH37069).

Soleymaniha, M., Amiri, A., Shanbedi, M., Chew, B. T., & Wongwises, S. (2018). Water-based graphene quantum dots dispersion as a high-performance long-term stable nanofluid for two-phased closed thermosyphons. *International Communications in Heat and Mass Transfer, 95*, 147-154.

Solomon, A. B., Ramachandran, K., & Pillai, B. (2012). Thermal performance of a heat pipe with nanoparticles coated wick. *Applied Thermal Engineering, 36*, 106-112.

Stephan, P., & Busse, C. (1992). Analysis of the heat transfer coefficient of grooved heat pipe evaporator walls. *International Journal of Heat and Mass Transfer, 35*(2), 383-391.

Sureshkumar, R., Mohideen, S. T., & Nethaji, N. (2013). Heat transfer characteristics of nanofluids in heat pipes: a review. *Renewable and Sustainable Energy Reviews, 20*, 397-410.

Teng, T.-P., Hsu, H.-G., Mo, H.-E., & Chen, C.-C. (2010). Thermal efficiency of heat pipe with alumina nanofluid. *Journal of alloys and compounds, 504*, S380-S384.

Thompson, S., Ma, H., & Wilson, C. (2011). Investigation of a flat-plate oscillating heat pipe with Tesla-type check valves. *Experimental Thermal and Fluid Science, 35*(7), 1265-1273.

Thuchayapong, N., Nakano, A., Sakulchangsatjatai, P., & Terdtoon, P. (2012). Effect of capillary pressure on performance of a heat pipe: Numerical approach with FEM. *Applied Thermal Engineering, 32*, 93-99.

Tournier, J.-M., & El-Genk, M. S. (2003). Startup of a horizontal lithium–molybdenum heat pipe from a frozen state. *International Journal of Heat and Mass Transfer, 46*(4), 671-685.

Tsai, C., Chien, H., Ding, P., Chan, B., Luh, T., & Chen, P. (2004). Effect of structural character of gold nanoparticles in nanofluid on heat pipe thermal performance. *Materials Letters, 58*(9), 1461-1465.

Vadakkan, U., Garimella, S. V., & Murthy, J. Y. (2004). Transport in flat heat pipes at high heat fluxes from multiple discrete sources.

Vadnjal, A., & Catton, I. (2006). *Heat Removal Model for a Thin Bi-Porous Wick.* Paper presented at the International Heat Transfer Conference 13.

Vafal, K., Zhu, N., & Wang, W. (1995). Analysis of asymmetric disk-shaped and flat-plate heat pipes. *Journal of Heat Transfer, 117*(1), 209-218.

Vasil'ev, L., Grakovich, L., Rabetskii, M., & Tulin, D. (2012). Investigation of heat transfer by evaporation in capillary grooves with a porous coating. *Journal of Engineering Physics and Thermophysics, 85*(2), 407-414.

Venkatachalapathy, S., Kumaresan, G., & Suresh, S. (2015). Performance analysis of cylindrical heat pipe using nanofluids–an experimental study. *International Journal of Multiphase Flow, 72*, 188-197.

Vijayakumar, M., Navaneethakrishnan, P., & Kumaresan, G. (2016). Thermal characteristics studies on sintered wick heat pipe using CuO and Al2O3 nanofluids. *Experimental thermal and fluid science, 79*, 25-35.

Wan, Z., Deng, J., Li, B., Xu, Y., Wang, X., & Tang, Y. (2015). Thermal performance of a miniature loop heat pipe using water–copper nanofluid. *Applied Thermal Engineering, 78*, 712-719.

Wang, C., Guo, Z., Zhang, D., Qiu, S., Tian, W., Wu, Y., & Su, G. (2013). Transient behavior of the sodium–potassium alloy heat pipe in passive residual heat removal system of molten salt reactor. *Progress in Nuclear Energy, 68*, 142-152.

Wang, H., Garimella, S. V., & Murthy, J. Y. (2007). Characteristics of an evaporating thin film in a microchannel. *International Journal of Heat and Mass Transfer, 50*(19-20), 3933-3942.

Wang, H., Qu, J., Sun, Q., Kang, Z., & Han, X. (2020). Thermal characteristic comparison of three-dimensional oscillating heat pipes with/without sintered copper particles inside flat-plate evaporator for concentrating photovoltaic cooling. *Applied Thermal Engineering, 167*, 114815.

Wang, J., & Catton, I. (2001). Enhanced evaporation heat transfer in triangular grooves covered with a thin fine porous layer. *Applied Thermal Engineering, 21*(17), 1721-1737.

Wang, P.-Y., Chen, X.-J., Liu, Z.-H., & Liu, Y.-P. (2012). Application of nanofluid in an inclined mesh wicked heat pipes. *Thermochimica acta, 539*, 100-108.

Wang, Y., & Vafai, K. (2000). Transient characterization of flat plate heat pipes during startup and shutdown operations. *International Journal of Heat and Mass Transfer, 43*(15), 2641-2655.

Weibel, J. A., Kim, S. S., Fisher, T. S., & Garimella, S. V. (2013). Experimental characterization of capillary-fed carbon nanotube vapor chamber wicks. *Journal of Heat Transfer, 135*(2), 021501.

Weng, Y.-C., Cho, H.-P., Chang, C.-C., & Chen, S.-L. (2011). Heat pipe with PCM for electronic cooling. *Applied energy, 88*(5), 1825-1833.

Wu, J., & Zhao, J. (2013). A review of nanofluid heat transfer and critical heat flux enhancement—research gap to engineering application. *Progress in Nuclear Energy, 66*, 13-24.

Xiao, B., & Faghri, A. (2008). A three-dimensional thermal-fluid analysis of flat heat pipes. *International Journal of Heat and Mass Transfer, 51*(11-12), 3113-3126.

Yang, X. F., Liu, Z.-H., & Zhao, J. (2008). Heat transfer performance of a horizontal micro-grooved heat pipe using CuO nanofluid. *Journal of Micromechanics and Microengineering, 18*(3), 035038.

Yousefi, T., Shojaeizadeh, E., Veysi, F., & Zinadini, S. (2012). An experimental investigation on the effect of pH variation of MWCNT–H2O nanofluid on the efficiency of a flat-plate solar collector. *Solar Energy, 86*(2), 771-779.

Zohuri, B. (2011). Heat pipe design and technology. *Boca Raton, FL*, 33487-32742.